



Forschungszentrum Karlsruhe
in der Helmholtz-Gemeinschaft

Wissenschaftliche Berichte
FZKA 7490

**Numerical Investigation and
Analytical Modeling of Liquid
Phase Residence Time
Distribution for Bubble Train
Flow in a Square Mini-Channel**

S. Erdogan, M. Wörner

Institut für Kern- und Energietechnik
Programm Rationelle Energieumwandlung und Nutzung

August 2009

Forschungszentrum Karlsruhe

in der Helmholtz-Gemeinschaft

Wissenschaftliche Berichte

FZKA 7490

**Numerical Investigation and Analytical
Modeling of Liquid Phase Residence Time
Distribution for Bubble Train Flow in a Square
Mini-Channel**

S. Erdogan, M. Wörner

Institut für Kern- und Energietechnik

Programm Rationelle Energieumwandlung und Nutzung

Forschungszentrum Karlsruhe GmbH, Karlsruhe

2009

Für diesen Bericht behalten wir uns alle Rechte vor

Forschungszentrum Karlsruhe GmbH
Postfach 3640, 76021 Karlsruhe

Mitglied der Hermann von Helmholtz-Gemeinschaft
Deutscher Forschungszentren (HGF)

ISSN 0947-8620

urn:nbn:de:0005-074901

Abstract

Bubble train flow (or Taylor flow) is a common flow pattern in gas-liquid flows through narrow channels. It consists of a sequence of elongated bubbles that fill almost the entire channel cross section, move with similar axial velocity and are separated by liquid slugs. Bubble train flow is of practical importance, e.g. for micro bubble columns and multiphase monolith reactors. For both devices, the knowledge of the liquid phase residence time distribution (RTD) is of great importance since the RTD provides information about the flow and mixing behaviour of reaction components and thus determines the yield and selectivity of the chemical reactor.

In the present study, the liquid phase RTD in laminar bubble train flow through a square mini-channel driven by a pressure gradient and buoyancy is evaluated from numerical simulations. The simulations with the volume-of-fluid method consider perfect bubble train flow where the hydrodynamics is fully described by a single unit cell consisting of one bubble and one liquid slug. The numerically evaluated unit cell RTD is approximated by an analytical model which has been proposed recently but is improved here to be valid for both co-current upward and co-current downward flow. The model RTD for n identical unit cells in series is obtained from the unit cell RTD model by an $(n-1)$ -fold convolution procedure. While the developed model reasonably fits the numerically evaluated RTD curve of a single unit cell for different flow conditions, the agreement of the convolution-based model for multiple unit cells is less satisfactory and should be improved in future.

Zusammenfassung

Numerische Untersuchung und analytische Modellierung der Verweilzeitverteilung der Flüssigkeit bei Taylorströmung in einem quadratischen Minikanal

Die Zweiphasenströmung eines Gases und einer Flüssigkeit in kleinen Kanälen erfolgt häufig in Form der sogenannten Taylor-Strömung. Diese Strömungsform ist charakterisiert durch eine Folge langgestreckter Blasen, die den Querschnitt des Kanals nahezu ausfüllen, sich mit ähnlicher Geschwindigkeit entlang des Kanals bewegen und durch Flüssigkeitspropfen getrennt sind. Von praktischer Bedeutung ist die Taylor-Strömung z.B. für Mikro-Blasensäulen und Monolith-Reaktoren mit Gas-Flüssig-Strömung. Für beide Apparate ist die Verweilzeitverteilung der Flüssigkeit von Interesse. Die Verweilzeitverteilung liefert Informationen über das Mischungsverhalten von Reaktionskomponenten und ist von großer Bedeutung für den Umsatz und die Selektivität des Reaktionsapparates.

In der vorliegenden Studie wird die Verweilzeitverteilung der flüssigen Phase aus numerischen Simulationen der laminaren Taylor-Strömung in einem vertikalen Mini-Kanal ausgewertet. Die numerischen Simulationen mit der Volume-of-Fluid Methode erfolgen für eine perfekte Taylor-Strömung, bei der die Hydrodynamik vollständig durch eine Einheitszelle bestehend aus einer Blase und einem Flüssigkeitspropfen beschrieben ist. Die aus den numerischen Simulationen ausgewertete Verweilzeitverteilung einer Einheitszelle wird analytisch durch ein für aufwärts gerichtete Taylor-Strömung vorgeschlagenes Modell beschrieben, das hier verbessert und für abwärts gerichtete Strömung erweitert wird. Die Verweilzeitverteilung von n identischen Einheitszellen in Serie wird über die $(n-1)$ -fache Faltung der Verweilzeitverteilung der Einheitszelle modelliert. Während das entwickelte analytische Modell die numerisch bestimmte Verweilzeitverteilung für eine Einheitszelle gut approximiert, ist das auf der Faltungsoperation basierende Modell für mehrere Einheitszellen in Serie nicht voll zufriedenstellend und sollte zukünftig weiter verbessert werden.

TABLE OF CONTENTS

Abstract	i
Zusammenfassung	ii
Nomenclature	vii
1. Introduction.....	1
2. Fundamentals of residence time theory	7
2.1. The residence time distribution.....	7
2.2. Measurement of the RTD	8
2.3. RTD of ideal reactors.....	9
2.4. Non-dimensional RTD	10
2.5. Definitions for the unit cell RTD in bubble train flow	11
3. Numerical simulation of bubble train flow	13
3.1. Numerical method.....	13
3.2. Simulation set-up	14
3.3. Simulation parameters.....	14
3.4. Procedure for numerical evaluation of the RTD from DNS data.....	16
3.5. Analysis of local residence time field	18
4. Modelling the RTD for bubble train flow	21
4.1. The RTD for a single unit cell	21
4.1.1. The WGO model.....	21
4.1.2. The PD and PDD model	24
4.1.3. Steps to determine the parameters of the PD and PDD model	38
4.2. The RTD for multiple unit cells.....	39
4.2.1. Convolution procedure.....	39
4.2.2. PD model and PDD model for multiple unit cells	40
5. Conclusions.....	47

References	49
Appendix A. Integral evaluations for PD model	54
Appendix B. Integral evaluations for the PDD model.....	60
Appendix C. Evaluations by Laplace transformation.....	66

LIST OF TABLES

Tab. 1:	Numerical parameters of the simulations	16
Tab. 2:	Terminal values of velocities, bubble dimensions, mean hydrodynamic residence time, bubble Reynolds number and capillary number for the different cases.	16
Tab. 3:	Values of parameters for unit cell RTD models.	23
Tab. 4:	Values of τ_F and α for the PDD model.	35
Tab. 5:	Binomial coefficients $B_{n,k}$ for $n = 1-4$ and $k = 0-4$.	69
Tab. 6:	Functions $F_{n,k}(s)$ for $n = 1-4$ and $k = 0-4$.	70
Tab. 7:	Inverse Laplace transforms. In the reference column the numbers refer to those in McCollum and Brown (1965), CB, and Roberts and Kaufman (1966), RK, respectively.	71

LIST OF FIGURES

Fig. 1:	Sketch of computational domain and co-ordinate system.	15
Fig. 2:	a) Illustrations of influence of Δt_{class} on the numerically evaluated RTD curve. b) Comparison of RTD curves for two unit cells, obtained from case A1 with $N_{\text{cross}}=2$ and from case A2 with $N_{\text{cross}}=1$.	19
Fig. 3:	Visualization of the bubble shape and contour plot of the local non-dimensional residence time t/t_{ref} in two different planes for case B1.	20

-
- Fig. 4: Compartment representation of the WGO model. Q_L is the volumetric flow rate of the liquid phase and V_{PFR} and V_{CSTR} are the volume of the plug flow reactor and the continuous stirred tank reactor, respectively. 22
- Fig. 5: Comparison of numerically evaluated unit cell RTD with the WGO model for (a) case A1 and (b) case C. The dashed vertical line indicates the bubble break-through time for each case. 25
- Fig. 6: Computed bubble shape and velocity field in vertical mid-plane $z = 1$ mm for fixed frame of reference (left half) and for frame of reference linked to the bubble (right half) for (a) co-current upward flow (case G in Wörner et al., 2007) and (b) co-current downward flow (case C). 26
- Fig. 7: Wall-normal profiles of magnitude of axial velocity in a horizontal cross-section through the middle of the liquid slug for case A1, B1, and C. For each case the velocity profile is normalized by the respective bubble velocity. The horizontal lines denote the normalized maximum velocity of a fully developed Poiseuille profile for each case. 27
- Fig. 8: Compartment representation of the PDD model. Q_L is the volumetric flow rate of the liquid. V_{PFR} is the volume of the plug flow reactor while V_S and V_F denote that of the continuous stirred tank reactor, respectively. The subscripts 'S' and 'F' correspond to the liquid slug and the liquid film / corner flow, respectively. 31
- Fig. 9: Comparison of numerically evaluated RTD for case C with the PD model and the PDD model for $\beta = 1$ and $\beta = 0.97$. 36
- Fig. 10: Comparison of numerically evaluated RTD curves for case A1 (a) and B1 (b) with the PD model and the PDD model for $\beta = 1$ and $\beta = 0.97$. 37
- Fig. 11: Schematic representation of convolution procedure for a general case (top) and for a unit cell of bubble train flow (bottom). 39
- Fig. 12: Comparison of numerically evaluated RTD curves for case A2 (a) and B2 (b) with the PD model and the PDD model. The dashed vertical lines correspond to the delay time for each case. 43

Fig. 13: Comparison of numerically evaluated RTD curves for $N_{\text{cross}}=3$ with convolutions of the PD model and PDD model for (a) case A1 and (b) case B1. The dashed vertical lines correspond to the delay time for each case. 45

Nomenclature

Bo	Bodenstein number
C	Tracer concentration, mol/m ³
C_{cs}	Ratio between mean and maximum velocity in laminar flow through a channel
Ca	Capillary number
d_B	Bubble diameter at a certain axial position of the bubble, m
D_B	Maximum bubble diameter, m
d_{film}	Thickness of liquid film between gas bubble and channel wall, m
D_h	Hydraulic diameter of channel, m
\mathcal{D}_{tracer}	Molecular diffusion coefficient of tracer in liquid phase, m ² /s
E	Residence time distribution (RTD), 1/s
E_θ	Non-dimensional RTD
E_{UC}^α	Unit cell RTD for PDD model, 1/s
F	Cumulative residence time distribution function
f	Liquid volumetric fraction in a mesh cell
J	Total superficial velocity, m/s
J_G	Superficial velocity of gas phase, m/s
J_L	Superficial velocity of liquid phase, m/s
L_{ax}	Axial length of computational domain, m
L_{ref}	Reference length scale, m
L_S	Liquid slug length, m
L_{travel}	Axial travelling distance of particles to determine the RTD, m
L_{UC}	Length of unit cell, m
L_x, L_y, L_z	Physicals dimensions of computational domain, m
n	Number of CSTRs or unit cells in series
N_{cross}	Number of times virtual particles must cross the domain to obtain the RTD
N_p	Number of particles
N_t	Number of time steps

N_{UC}	Number of unit cells
Q	Volumetric flow rate, m ³ /s
Re_B	Bubble Reynolds number
t	Time, s
t_{ref}	Reference time scale, s
\bar{t}	Mean residence time, s
Δt	Time step width, s
Δt_{class}	Time interval of classes in the RTD, s
U_B	Bubble velocity, m/s
U_F	Mean velocity in liquid film and corner flow region in PDD model, m/s
U_L	Mean liquid velocity in the computational domain, m/s
$U_{L, film}$	Mean velocity in the liquid film at a certain axial position, m/s
$U_{L, max}^{act}$	Actual maximum axial velocity in the liquid slug, m/s
$U_{L, max}^{th}$	Maximum axial velocity in fully developed Poiseuille flow, m/s
U_{ref}	Reference velocity scale, m/s
V	Volume, m ³

Greek symbols

α	Weighting factor in PDD model
β	Pre-factor of bubble diameter for computation of U_F in PDD model
δ	Dirac delta function
ε	Gas volume fraction in the unit cell
θ	Dimensionless time, $\theta \equiv t / \bar{t}$
λ	Ratio $U_{L, max}^{act} / U_{L, max}^{th}$
μ	Dynamic viscosity, Pa s
ρ	Density, kg/m ³
σ	Coefficient of surface tension, N/m
σ^2	Variance of RTD, s ²

σ_{θ}^2	Non-dimensional variance of RTD
τ	Mean residence time, s
τ_B	Bubble break through time, s
τ_D	Delay time, s
τ_F	Mean residence time for liquid film and corner region in PDD model, s
τ_h	Mean hydrodynamic residence time, s
τ_S	Mean residence time for liquid slug, s

Subscripts

B	Bubble
F	Liquid film
G	Gas phase
L	Liquid phase
p	Particle
ref	Reference value
S	Liquid slug
UC	Unit cell

Abbreviations

BTF	Bubble Train Flow
CSTR	Continuous Stirred Tank Reactor
PD	Peak-Decay
PDD	Peak-Decay-Decay
PFR	Plug Flow Reactor
RTD	Residence Time Distribution
UC	Unit cell
WGO	RTD model of <u>W</u> örner, <u>G</u> hidersa, <u>O</u> nea (2007)

1. Introduction

Segmented gas-liquid flow is a common two-phase flow pattern in narrow channels. It is also denoted as Taylor flow or bubble train flow (BTF) and consists of a sequence of elongated bubbles which almost fill the entire channel cross section (Taylor bubbles). The individual bubbles move along the channel while they are separated by liquid slugs. Bubble train flow is of technical relevance, e.g. for miniaturized multiphase reactors (Jähnisch et al., 2000; Burns & Ramshaw, 2001; Günther et al., 2004, Haverkamp et al., 2006) and for multiphase monolith reactors (Roy et al., 2004; Kreutzer et al., 2005b, Bauer et al., 2005). While in an industrial scale monolith reactors with Taylor flow are only used for production of H_2O_2 (Edvinson Albers et al., 2001) they find increasing interest for potential use for Fischer-Tropsch synthesis (De Deugd et al., 2003; Bradford et al., 2005; Güttel et al., 2008, Liu et al., 2009).

In real Taylor flow, the length of the liquid slugs and the size of individual bubbles underlies variations. The variation of the bubble size results in a variation of the translational velocity of individual bubbles. This may lead to coalescence and thus a further change of the bubble size and slug length distribution. A useful abstraction of real bubble train flow is *perfect bubble train flow*, where the bubbles are assumed to have identical size, shape and velocity and where the length of all liquid slugs is the same. Then, the hydrodynamics of BTF is fully described by a unit cell (UC) which consists of one bubble and one liquid slug.

An important characteristic of any chemical reactor is its residence time distribution (RTD), since the RTD provides information about the flow and mixing behaviour of reaction components (Levenspiel, 1999; Martin, 2000; Nauman, 2008). The knowledge of the RTD and the kinetics of the chemical reaction is the basis for the design of any chemical reactor since both determine the yield and selectivity of the reactor. This gives the motivation to develop simple but yet reliable models that are able to predict the RTD in bubble train flow from fluid properties and known integral flow parameters such as the superficial velocities of the phases. Of major interest is the RTD of the continuous liquid phase, since the variation of the residence time of the gas phase is small and its mean value can be computed by dividing

Introduction

the length of the channel by the bubble velocity. Desirable is a plug flow behaviour of the liquid phase with a narrow RTD.

For the design and optimization of micro-structured reactors for process intensification the ability to reliably predict the RTD is of great importance. Sun et al. (2008) recently investigated the influence of the RTD on the synthesis of biodiesel in capillary micro-reactors operated with Taylor flow. They found that the RTD in the micro-channel reactor was remarkably decreased compared to the RTD which is required in batch systems to obtain a high yield under the same reaction conditions. However, the RTD of the micro-reactors had to be controlled to avoid the saponification of the biodiesel. Though this example demonstrates the practical importance of the RTD, there are, unfortunately, only very few experimental data on the liquid phase RTD available in literature for multiphase micro-structured reactors such as monolith reactors. This may be attributed on one hand to the difficulties of performing local measurements of the RTD in narrow channels and on the other hand to the only recently increasing interest in this topic. As a consequence, reliable and validated general models for the RTD in micro-structured reactors are missing. This is in particular true for channels of non-circular cross-section, which are quite common in monoliths and other micro-structured reactors. In rectangular channels, the film thickness at the circumference of the bubble is not constant. As a consequence, a so-called corner flow exists which makes the application of RTD models for circular channels invalid and requires the development of refined models.

In experiments the residence time distribution is often measured by a stimulus-response technique, where a specific quantity of a tracer (e.g. fluorescent substance, radionuclide, solution of salt, etc.) is introduced at the system inlet as a short duration pulse or a step function and where the time variation of the tracer concentration is recorded at the outlet. The tracer particles injected at the inlet are assumed to follow the same paths through the system as the original fluid particles they replaced. Thus, the tracer particles will have the same distribution of residence times as the original fluid particles. By recording the times when particles leave a histogram can be constructed. For a large sampling size this

histogram converges to the differential residence time distribution function. This single-phase flow approach can be applied to gas-liquid two-phase flows as well. The main difference is that the system has now usually two inlets (one for the gas phase and one for the liquid phase), while there is still one common outlet. To measure the residence time distribution of the liquid phase in a gas-liquid flow, the tracer pulse is injected at the liquid inlet only.

The stimulus-response measurement technique is well suited for macro-reactors, where the reactor volume is much larger than the volume of the tracer measurement device. However, for micro-structured reactors, the reactor volume is usually smaller than the volume of the measuring unit. This means that the residence time response of the tracer may already be influenced by the measurement configuration itself. Measurements of liquid phase RTD for two-phase flow through narrow channels are reported by Thulasidas et al. (1999) for bubble-train flow in single straight channels (using a conductimetric technique), by Patrick et al. (1995) for a monolith froth reactor (measuring the tracer concentration at the outlet with a spectrometer), by Heibel et al. (2005) for film flow in a monolith reactor (using a dye tracer and a spectrometer), by Yawalkar et al. (2005) and Kreutzer et al. (2005a) for bubble-train flow in a monolith reactor (using a dye tracer and a spectrometer), by Bakker et al. (2005) for a novel 'open wall' monolith reactor, by Kulkarni et al. (2005) for Taylor flow in a monolith reactor (using a KCl tracer solution and a conductivity probe), and by Günther et al. (2004) and Trachsel et al. (2005) for bubble-train flow in micro-fluidic channel networks of rectangular cross-section (using a fluorescently labelled tracer pulse and a fluorescence microscope). The latter authors showed that the residence time distribution of bubble-train flow is very narrow as compared to single phase flow, which is a distinct advantage. Just recently, Lohse et al. (2008) presented a novel method for determining the RTD in an intricately structured micro-reactor, which employs a tracer 'injection' using the optical activation of a caged fluorescent dye.

An alternative way to determine the RTD is by means of computational fluid dynamics (CFD). There exist in principle two options to determine the residence time distribution from CFD methods. The first one is the numerical simulation of the stimulus-response experiment,

Introduction

i.e. setting a short concentration pulse at the inlet of the computational domain, computing the unsteady concentration field of the tracer within the computational domain and evaluating it at the outlet. This approach has been used in a modified form by Salman et al. (2005, 2007) to determine the reactor residence time for Taylor flow in a circular micro-channel from the residence time distribution of a single unit cell by using a convolution procedure. The second possibility is the particle tracking method. Here, virtual particles are released at the inlet and their trajectories are computed from the known velocity field of the CFD calculation. A notable difference between the two methods is that in the particle method convective properties of the flow are only monitored, while by evaluation of the unsteady concentration field diffusive transport is additionally taken into account. The relative importance of convective and diffusive transport is characterized by the Bodenstein number. For bubble-train flow, it can be defined as $Bo \equiv U_B D_h / \mathcal{D}_{\text{tracer}}$, where U_B is the bubble velocity, D_h is the hydraulic diameter of the channel and $\mathcal{D}_{\text{tracer}}$ is the molecular diffusion coefficient of the tracer in the liquid phase. For a particle tracking method, no diffusion of the tracer is taken into account. The RTD obtained by a particle tracking method is therefore representative for an infinite value of the Bodenstein number.

To predict the residence time distribution for Taylor flow, Salman et al. (2004) developed a numerical model valid for low values of the Bodenstein number. This model does not account for the direction of gravity and assumes liquid slugs of uniform concentration and liquid films around the bubble that can be adequately described by a one-dimensional convection-diffusion equation. For large values of the Bodenstein number ($Bo > 10$) the model can be simplified and an analytical solution is derived, which corresponds to the representation of a unit cell by a tank-in-series model, consisting of a plug flow reactor (PFR) and a continuous stirred tank reactor (CSTR). In a more recent paper, Salman et al. (2007) numerically evaluated RTDs for a wide range of Bodenstein numbers (respectively Peclet numbers) and compared it with predictions from three literature models (CSTR-PFR model, two-region model of Pedersen & Horvath (1981), and the model of Thulasidas et al. (1999)). They found that the shape of the RTD and the performance of the different models depend

strongly on the parameter $U_B d_{\text{film}} / \mathcal{D}_{\text{tracer}}$, where d_{film} is the thickness of the liquid film between the gas bubble and the channel wall.

Recently, Wörner et al. (2007) developed a new CFD-based method for evaluating the liquid phase residence time distribution of bubble-train flow using data from direct numerical simulations (DNS). The numerical simulations are performed for perfect bubble-train flow. The method developed for evaluation of the RTD is a particle method and relies on the uniform introduction of virtual particles in the volume occupied by the liquid phase within a single flow unit cell. The residence time distribution is obtained by statistical evaluation of the time required by virtual particles to travel axially the length of the unit cell, and by an appropriate weighting procedure which takes into account the axial velocity at the initial particle position. Residence time curves have been evaluated from DNS data of co-current upward bubble-train flow in a square mini-channel of $2 \text{ mm} \times 2 \text{ mm}$ cross section for values of the capillary number in the range $Ca \equiv U_B \mu_L / \sigma = 0.2 - 0.25$, where μ_L is the liquid viscosity and σ is the coefficient of surface tension. The RTD curves obtained can be fitted well by a simple exponential relationship, which has been developed on the basis of a compartment model consisting of two tanks in series, the first tank being a plug flow reactor and the second being a continuous stirred tank reactor. This model may be considered as generalization of the model of Salman et al. (2004) which was developed for circular channels, but cannot be applied adequately for square channels because of the corner flow.

Both, the model of Salman et al. (2004) and of Wörner et al. (2007) are derived for the RTD of a unit cell. In practice, a single channel with bubble-train flow contains tens or hundreds of unit cells depending on the length of the unit cell and the length of the channel. Salman et al. (2007) computed the residence time of the capillary from the residence time of the unit cell by means of a convolution method. Usually, a micro-structured reactor consists of a large number of parallel channels. If the flow is evenly distributed across the different channels, the RTD of the reactor is equal to that of a single channel. However, in practice the flow rates through the different channels of the monolith reactor differ (Mantle et al., 2002),

Introduction

so that it is necessary to take this maldistribution effect into account when estimating the reactor RTD from the single channel RTD.

The objective of the present report is twofold. First, we want to refine the unit cell RTD model of Wörner, Ghidersa, Onea (2007) (the WGO model) for co-current upward bubble train flow and develop a more general unit cell RTD model which is also valid for co-current downward bubble train flow. Second, we want to develop a procedure to predict the RTD of an arbitrary number of unit cells in series (i.e. the RTD of a single channel with perfect bubble train flow) from the RTD of a single unit cell. In this report we investigate in how far this can be done by a convolution procedure.

This report is organized as follows. In section 2 we introduce some fundamental aspects and definitions of RTD theory. In section 3 we discuss issues related to the numerical simulation of bubble train flow and to the numerical evaluation of the RTD. Section 4 is devoted to the analytical modelling of the RTD for bubble train flow, namely the development of a refined unit cell model and a model for multiple unit cells. In section 5 we present the conclusions.

2. Fundamentals of residence time theory

In this section we give a short introduction into fundamental aspects and definitions related to the concept of residence time distribution. Some passages in this section are adopted from the English Wikipedia page for “residence time distribution” (accessed June, 2009). For further details we refer to text books, e.g. Fogler (1986) and Levenspiel (1999).

2.1. The residence time distribution

The residence time distribution (RTD) of a chemical reactor is a probability distribution function that describes the amount of time that fluid elements spend inside the reactor. The distribution of residence times is represented by an exit age distribution $E(t)$. The function $E(t)$ has unit of time^{-1} and underlies the restriction

$$\int_0^{\infty} E(t) dt = 1 \quad (1)$$

The fraction of the fluid that spends a given duration t inside the reactor is given by $E(t)dt$, while the fraction of fluid that leaves the reactor with an age less than t_1 is

$$\int_0^{t_1} E(t) dt \quad (2)$$

The mean or average residence time is given by the first moment of the age distribution

$$\bar{t} \equiv \int_0^{\infty} t \cdot E(t) dt \quad (3)$$

If there are no stagnant zones within the reactor then \bar{t} will be equal to the mean hydrodynamic residence time τ_h , which is the residence time calculated from the total reactor volume V and the volumetric flow rate Q of the fluid

$$\tau_h \equiv \frac{V}{Q} \quad (4)$$

The second central moment indicates the variance of the RTD and is given by

$$\sigma^2 \equiv \int_0^{\infty} (t - \bar{t})^2 E(t) dt \quad (5)$$

The variance represents the square of the spread of the distribution as it passes the vessel exit and has units of (time)². It is particularly useful for matching experimental curves to one of a family of theoretical curves (Levenspiel, 1999).

2.2. Measurement of the RTD

As discussed in the introduction of this report, residence time distributions are measured by introducing a non-reactive tracer signal at the inlet and by measuring the time-dependent tracer concentration at the outlet. The selected tracer should not modify the physical characteristics of the fluid (equal density, equal viscosity) and the introduction of the tracer should not modify the hydrodynamic conditions. In general, the tracer signal at the inlet will either be a *pulse* or a *step*. Other functions are possible, but they require additional calculations to deconvolute the RTD curve, $E(t)$.

The pulse method requires the introduction of a very small volume of concentrated tracer at the inlet of the reactor, such that it approaches the Dirac delta function. Although an infinitely short injection cannot be produced, it can be made much smaller than the mean residence time of the reactor. In the pulse method the RTD curve can be computed from the measured time dependent tracer concentration $C(t)$ at the reactor outlet by the relation

$$E(t) = \frac{C(t)}{\int_0^{\infty} C(t) dt} \quad (6)$$

In the step method, the concentration of tracer at the reactor inlet is changed abruptly from 0 to C_0 . The concentration of tracer at the outlet is normalized to obtain the non-dimensional curve

$$F(t) = \frac{C(t)}{C_0} \quad (7)$$

which increases monotonically from 0 to 1. The value of the mean residence time and the variance can be computed from the function $F(t)$ by relations

$$\tau = \bar{t} = \int_0^{\infty} [1 - F(t)] dt \quad (8)$$

$$\sigma^2 = 2 \int_0^{\infty} t [1 - F(t)] dt - \bar{t}^2 \quad (9)$$

The step- and pulse-responses of a reactor are related due to

$$F(t) = \int_0^t E(t) dt \quad (10)$$

and

$$E(t) = \frac{dF(t)}{dt} \quad (11)$$

A step experiment is often easier to perform than a pulse experiment, but it tends to smooth over some of the details that a pulse response could show. It is easy to numerically integrate an experimental pulse response to obtain a very high-quality estimate of the step response, but the reverse is not the case because any noise in the concentration measurement will be amplified by numeric differentiation.

2.3. RTD of ideal reactors

The residence time distribution of a real reactor can be used to compare its behavior to that of two ideal reactor models: the plug-flow reactor (PFR) and the continuous stirred-tank reactor (CSTR). In an ideal PFR there is no mixing and the fluid elements leave in the same order they arrived. Therefore, fluid entering the reactor at time t will exit the reactor at time $t + \tau_{\text{PFR}}$, where $\tau_{\text{PFR}} = \bar{t}_{\text{PFR}}$ is the mean residence time of the plug-flow reactor. The residence time distribution function is therefore a Dirac delta function

$$E(t) = \delta(t - \tau_{\text{PFR}}) \quad (12)$$

The variance of an ideal plug-flow reactor is zero.

An ideal CSTR is based on the assumption that the flow at the inlet is completely and instantly mixed into the bulk of the reactor. The reactor and the outlet fluid have identical

Fundamentals of residence time theory

homogeneous compositions at all times. An ideal CSTR has an exponential residence time distribution

$$E_{\text{CSTR}}(t) = \frac{1}{\tau_{\text{CSTR}}} \exp\left(-\frac{t}{\tau_{\text{CSTR}}}\right) \quad (13)$$

Here, $\tau_{\text{CSTR}} = \bar{t}_{\text{CSTR}}$ is the mean residence time of the continuous stirred-tank reactor. The variance of the CSTR is $\sigma_{\text{CSTR}}^2 = \tau_{\text{CSTR}}^2$. The RTD for a cascade consisting of $n \in \mathbb{N}$ identical CSTRs in series is

$$E_{n\text{CSTR}}(t) = \frac{t^{n-1}}{(n-1)! \tau_{\text{CSTR}}^n} \exp\left(-\frac{t}{\tau_{\text{CSTR}}}\right) \quad (14)$$

2.4. Non-dimensional RTD

For comparing different reactors it is useful to introduce a non-dimensional RTD curve

$$E_{\theta}(\theta) \equiv \bar{t} \cdot E(t) \quad (15)$$

which is a function of a dimensionless time

$$\theta \equiv \frac{t}{\bar{t}} \quad (16)$$

The non-dimensional mean value of E_{θ} is then

$$\bar{\theta} \equiv \int_0^{\infty} \theta \cdot E_{\theta}(\theta) d\theta = \int_0^{\infty} \frac{t}{\bar{t}} \cdot \bar{t} \cdot E(t) \frac{1}{\bar{t}} dt = \frac{1}{\bar{t}} \int_0^{\infty} t \cdot E(t) dt = 1 \quad (17)$$

while the non-dimensional variance is $\sigma_{\theta}^2 = \sigma^2 / \bar{t}^2$.

For a single CSTR it is

$$E_{\text{CSTR}}(\theta) = \exp(-\theta) \quad (18)$$

and $\sigma_{\theta, \text{CSTR}}^2 = 1$. The mean residence time for a series of n identical CSTRs is $\tau_{n\text{CSTR}} = n\tau_{\text{CSTR}}$. With definition of the non-dimensional time

$$\theta_{n\text{CSTR}} \equiv \frac{t}{\tau_{n\text{CSTR}}} = \frac{t}{n\tau_{\text{CSTR}}} \quad (19)$$

we can write Eq. (14) in the non-dimensional form

$$E_{nCSTR}(\theta_{nCSTR}) = \frac{n(n\theta_{nCSTR})^{n-1}}{(n-1)!} \exp(-n\theta_{nCSTR}) \quad (20)$$

The non-dimensional variance of a series of n identical CSTRs is

$$\sigma_{\theta}^2 = \frac{1}{n} \quad (21)$$

For real reactors, often the mean residence time τ and the variance σ^2 are measured and the reactor RTD is modelled as a series of n CSTRs, where n is computed from Eq. (22)

$$n = \frac{1}{\sigma_{\theta}^2} = \frac{\tau^2}{\sigma^2} \quad (22)$$

2.5. Definitions for the unit cell RTD in bubble train flow

We now introduce some definitions for the RTD in bubble train flow, which we will need later in this report. We consider a perfect bubble train flow consisting of a cascade of n identical unit cells in series featuring RTD $E_{nUC}(t)$. The mean residence time of this RTD is

$$\tau_{nUC} \equiv \bar{t}_{nUC} = \int_0^{\infty} t \cdot E_{nUC}(t) dt \quad (23)$$

and the variance is

$$\sigma_{nUC}^2 = \int_0^{\infty} (t - \bar{t}_{nUC})^2 E_{nUC}(t) dt \quad (24)$$

We define the non-dimensional time

$$\theta_{nUC} \equiv \frac{t - n\tau_D}{\tau_{nUC}} = \frac{t - n\tau_D}{n\tau_{UC}} \quad (25)$$

Here, τ_D is the delay time which will be defined later and τ_{UC} is the mean residence time of a single unit cell. We define the non-dimensional form of the RTD $E_{nUC}(t)$ as

$$E_{\theta,nUC}(\theta_{nUC}) \equiv n\tau_{UC} E_{nUC}(t) \quad (26)$$

The mean hydrodynamic residence time for a series of n unit cells in bubble train flow is

$$\tau_{nh} = \frac{V_{nUC}}{Q_L} \quad (27)$$

Fundamentals of residence time theory

Here, $V_{nUC} = nL_{UC}A_{ch}$ is the volume of a domain with n unit cells of length L_{UC} , $Q_L = J_L A_{ch}$ is the liquid volumetric flow rate, J_L is the liquid superficial velocity and A_{ch} is the cross-sectional area of the channel. Therefore, Eq. (27) gives

$$\tau_{nh} = \frac{nL_{UC}}{J_L} \quad (28)$$

3. Numerical simulation of bubble train flow

In this section, we first give a short overview on the numerical method and the computer code used to perform the direct numerical simulations of the bubble-train flow. We then describe the simulation set-up and give the physical and numerical parameters of the simulations. Finally, we shortly present the method for evaluation of the RTD from the DNS data and present some visualizations of the local residence time field.

3.1. Numerical method

The direct numerical simulations are performed with the in-house computer code TURBIT-VOF (Sabisch 2000, Sabisch et al. 2001), which solves the single-field Navier-Stokes equations with surface tension term for two incompressible immiscible fluids under assumption of constant fluid properties (i.e. density, viscosity, surface tension). The single-field formulation automatically accounts for the proper momentum jump conditions across the gas-liquid interface. The governing equations are written in non-dimensional form, see Ghidersa et al. (2004) and Öztaskin et al. (2009). For normalization, a reference length scale L_{ref} and reference velocity scale U_{ref} are used, which need to be specified. The solution strategy is based on a projection method, where the resulting Poisson equation for the pressure is solved by a conjugate gradient solver. Time integration of the single field Navier-Stokes equation is done by an explicit third order Runge-Kutta method. Discretization in space is based on a finite volume method, where a regular Cartesian staggered grid is used. All derivatives in space are approximated by second order central differences.

For computing the evolution of the deformable interface, which separates the two immiscible fluids, the volume-of-fluid (VOF) method is used. In any mesh cell that instantaneously contains both phases, the interface is locally approximated by a plane. The orientation and location of the plane is reconstructed from the discrete distribution of the volumetric fraction f of the continuous fluid. Note that - for a certain instant in time - we have $f = 1$ for mesh cells entirely filled with liquid, $f = 0$ for mesh cells entirely filled with gas, and $0 < f < 1$ for mesh cells that contain both phases. The evolution of f is governed

by an advection equation, which expresses the mass conservation of the continuous phase. To avoid any smearing of the interface, this f -equation is not solved by a difference scheme. Instead, the flux of f across the faces of any interface mesh cell is calculated in a geometrical manner, depending on the location and orientation of the plane representing the interface. For further details about the numerical method we refer to Sabisch et al. (2001) and Öztaskin et al. (2009). We also note that a comprehensive code-to-code comparison exercise of TURBIT-VOF with three major commercial CFD codes was performed for bubble-train flow in a square mini-channel, see Özkan et al. (2007).

3.2. Simulation set-up

The set-up of the simulations is described in detail in Ghidersa et al. (2004) and Wörner et al. (2007) and is therefore only shortly repeated here. We consider a computational domain and co-ordinate system as displayed in Fig. 1. No-slip boundary conditions are applied at the four side walls of the square channel, while in (vertical) axial direction (y) periodic boundary conditions are used. The length of the computational domain in axial direction is L_{ax} . This length may represent one unit cell as displayed in Fig. 1, or may represent N_{uc} unit cells, where N_{uc} is a positive integer. The flow can be co-current upward or downward, depending on the sign of the specified driving axial pressure drop across the computational domain. The simulations start from fluid at rest with a bubble placed in the centre of the computational domain. They are continued in time until the bubble velocity and the mean liquid velocity within the computational domain obey constant terminal values.

3.3. Simulation parameters

In the present report five different cases are considered. For all cases the following parameters are used: $D_h = L_x = L_z = L_{ref} = 2 \text{ mm}$, liquid density $\rho_L = 957 \text{ kg/m}^3$, gas density $\rho_G = 11.7 \text{ kg/m}^3$, liquid viscosity $\mu_L = 0.048 \text{ Pa}\cdot\text{s}$, gas viscosity $\mu_G = 0.184 \text{ mPa}\cdot\text{s}$, coefficient of surface tension $\sigma = 0.02218 \text{ N/m}$, reference velocity $U_{ref} = 0.0264 \text{ m/s}$, reference time scale $t_{ref} \equiv L_{ref} / U_{ref} = 0.0757 \text{ s}$ and gas holdup in the computational domain $\varepsilon \approx 33\%$.

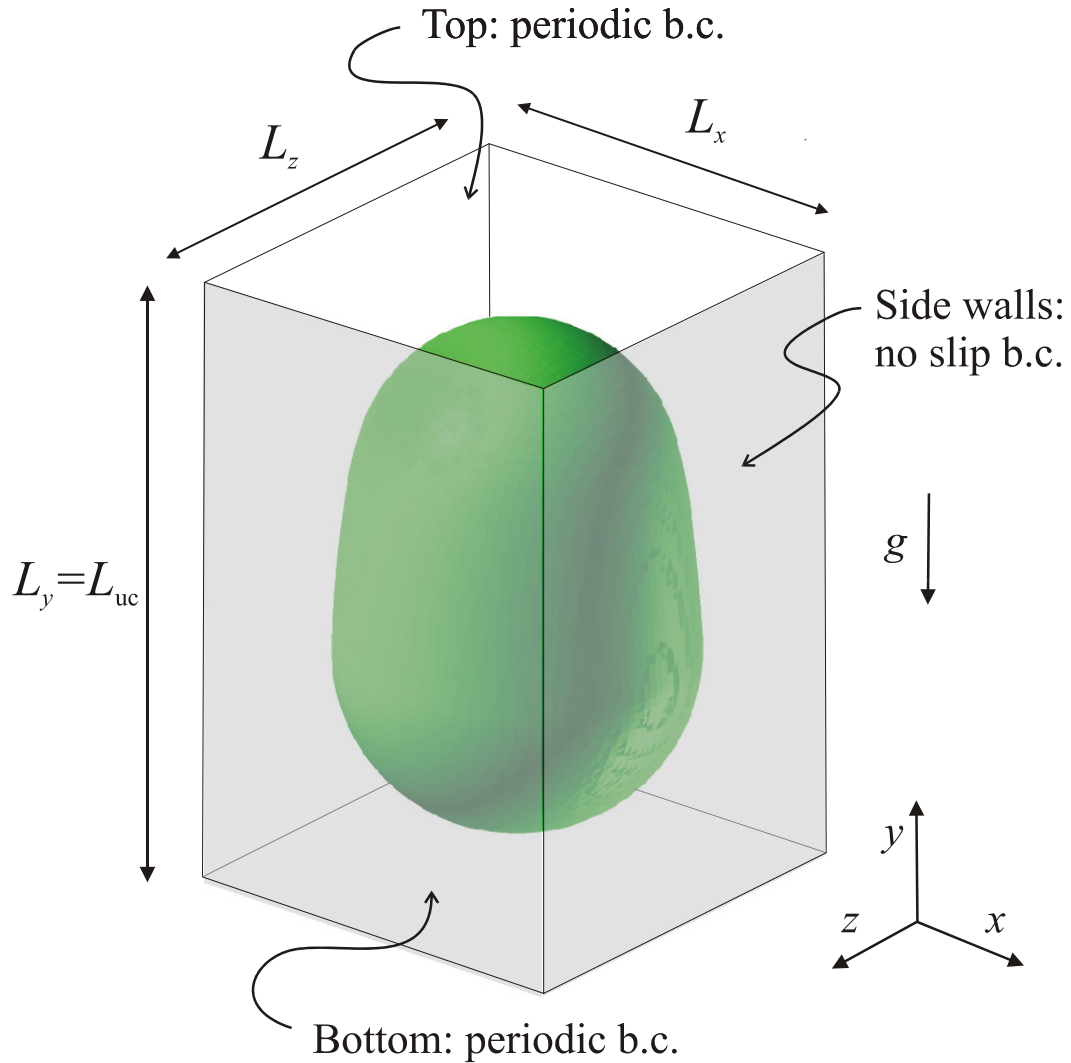


Fig. 1: Sketch of computational domain and co-ordinate system.

The cases differ with respect to the length of the unit cell, L_{uc} , the number of unit cells in the domain, N_{uc} , and the flow direction, see Tab. 1. For cases A1, B1 and C the computational domain contains one unit cell only, while it contains two unit cells for cases A2 and B2. Case A1 and B1 correspond to case A2 and E, respectively, in Wörner et al. (2007). Cases A2 and B2 correspond to case A1 and B1, respectively, in Öztaskein et al. (2009). While in all these cases the flow is co-current upward, it is co-current downward for case C, which is otherwise similar to case G in Wörner et al. (2007). Further data given in Tab. 1 are the time step width Δt and the number of computes times steps N_t . In all cases a uniform grid of mesh size $\Delta x = \Delta y = \Delta z = L_{ref} / 48$ is used.

Tab. 1: Numerical parameters of the simulations

Case	Domain	Grid	L_{ax} / L_{ref}	N_{UC}	ε	N_t	$\Delta t / t_{ref}$
A1	1×1×1	48×48×48	1.0	1	0.3307	40 000	2.5×10^{-5}
A2	1×2×1	48×96×48	2.0	2	0.3307	50 000	2.5×10^{-5}
B1	1×1.5×1	48×72×48	1.5	1	0.3303	50 000	2.5×10^{-5}
B2	1×3×1	48×144×48	3.0	2	0.3303	70 000	2.5×10^{-5}
C	1×1.75×1	48×84×48	1.75	1	0.3303	45 000	1.5×10^{-5}

In Tab. 2 for each case terminal values of characteristic velocities and bubble dimensions as well as the bubble Reynolds number $Re_B \equiv \rho_L D_h U_B / \mu_L$ and capillary number $Ca \equiv \mu_L U_B / \sigma$ are given. For all cases the bubble is axi-symmetric, i.e. its cross-section at any axial position is circular.

Tab. 2: Terminal values of velocities, bubble dimensions, mean hydrodynamic residence time, bubble Reynolds number and capillary number for the different cases.

Case	U_B / U_{ref}	U_L / U_{ref}	J / U_{ref}	D_B / D_h	L_S / D_h	τ_h / t_{ref}	Re_B	Ca
A1	3.66	1.20	2.02	0.809	0.064	1.245	3.86	0.21
A2	3.66	1.20	2.02	0.809	0.064	1.245	3.86	0.21
B1	3.86	1.37	2.19	0.849	0.292	1.635	4.06	0.22
B2	3.96	1.37	2.22	0.843	0.280	1.635	4.17	0.23
C	-3.25	-1.53	-2.09	0.891	0.480	1.708	3.42	0.19

3.4. Procedure for numerical evaluation of the RTD from DNS data

The procedure for the numerical evaluation of the RTD of the liquid phase within a unit cell of the bubble train flow is described in detail in Wörner et al. (2007). Here, we give a short overview on key issues of this evaluation procedure. The method relies on data for the instantaneous three-dimensional velocity and volume fraction field within a unit cell which have to be obtained in advance by a direct numerical simulation (DNS). The evaluation

procedure is only useful for fully developed bubble train flow, where the translational velocity of the bubble is constant and the bubble shape is steady. The method to evaluate the RTD from the DNS data is a particle tracking method and relies on the uniformly spaced introduction of virtual particles in the volume occupied by the liquid phase within a single flow unit cell. The position of each particle within the given flow field is tracked by a first order Euler scheme, in which the velocity field at the particle position is obtained from linear interpolation from the staggered DNS grid. The residence time distribution is obtained by a statistical evaluation of the time needed by virtual particles to travel an axial distance equivalent to the length of the unit cell, and by an appropriate weighting procedure which takes into account the axial velocity at the particle's initial position.

There exist three numerical parameters for evaluation of the RTD. The first one is the particle Courant-Friedrich-Levy (CFL) number

$$CFL_p \equiv \frac{\Delta t_p |\mathbf{u}_p|}{\Delta x} \quad (29)$$

which is used to determine the time step width Δt_p for the particle tracking. Here, the CFL number is 0.2 for all cases. The second parameter is the number of particles per unit length N_p . This parameter defines the initial positions of the particle set, as it constitutes the distance between neighbouring particles in the three coordinate directions. Here, we use $N_p = 48$ for all cases. The third parameter is Δt_{class} . It is used to subdivide the time axis in certain intervals of size Δt_{class} . Each time interval is denoted as a class. The RTD is obtained by sorting the residence time of all particles in classes and by subsequent normalization of the resulting histogram. In Fig. 2 a) we illustrate the influence of the choice of Δt_{class} on the numerically evaluated RTD. Three different values of Δt_{class} are used for evaluation of the RTD for case C, namely $\Delta t_{\text{class}} = \tau_D / 3$, $\tau_D / 2$ and τ_D . It appears that values of Δt_{class} may result in quite different values of E in neighbouring classes while large values of Δt_{class} lead to smoother curves but have a coarser resolution. In Fig. 2 a) one may also recognise that the area of the first three classes with $\Delta t_{\text{class}} = \tau_D / 3$, the area of the first two classes with $\Delta t_{\text{class}} = \tau_D / 2$ and the area of the first class for $\Delta t_{\text{class}} = \tau_D$ are all equal. However, the choice

of Δt_{class} has a large influence on the height of the peak of the RTD at $t \approx \tau_D$. This makes a comparison of models for the RTD with the numerical evaluated RTD difficult.

A particle that leaves the computational domain through one of its two faces with periodic boundary conditions re-enters it through the opposite face. Thus a particle may travel an axial distance that is larger than the axial size of the computational domain L_{ax} . We denote the axial distance that any virtual particle must travel before its residence time is recorded by L_{travel} and define $N_{\text{cross}} \equiv L_{\text{travel}} / L_{\text{ax}}$. Thus, N_{cross} allows evaluating the RTD of a series of multiple virtual unit cells. To test if this procedure is adequate to determine the RTD of multiple unit cells we applied it to cases A1 and A2. Both cases have an identical unit cell. However, in case A1 the computational domain contains one unit cell while it contains two unit cells in case A2. In Fig. 2 b) we compare the RTD for case A1 and $N_{\text{cross}} = 2$ with the RTD for case A2 and $N_{\text{cross}} = 1$. The differences between both RTDs are very small. Therefore we conclude that the RTD for a number of n unit cells in series can be determined from simulation results with one unit cell in the computational domain by setting N_{cross} equal to n .

3.5. Analysis of local residence time field

From evaluation of the three-dimensional direct numerical simulation data the three-dimensional field of the local residence time in the liquid phase of the bubble train flow is obtained. Fig. 3 shows a visualization of this field for case B1 and also displays the computed bubble shape (note the periodic boundary conditions in axial direction). In this figure, the local residence time in the computational domain is shown for two different planes, once for a mid-plane in vertical axial direction (y) and once for a horizontal channel cross-section. The different values of the residence time are represented by a colour code. The figure indicates that fluid elements in the central region of the liquid slug have the shortest residence time, i.e. travel fastest along the channel. In general, the residence time is small for liquid fluid elements close to the bubble and is large for liquid fluid elements close to the solid walls. As expected, the highest values of the residence time are found in the four corners of channel.

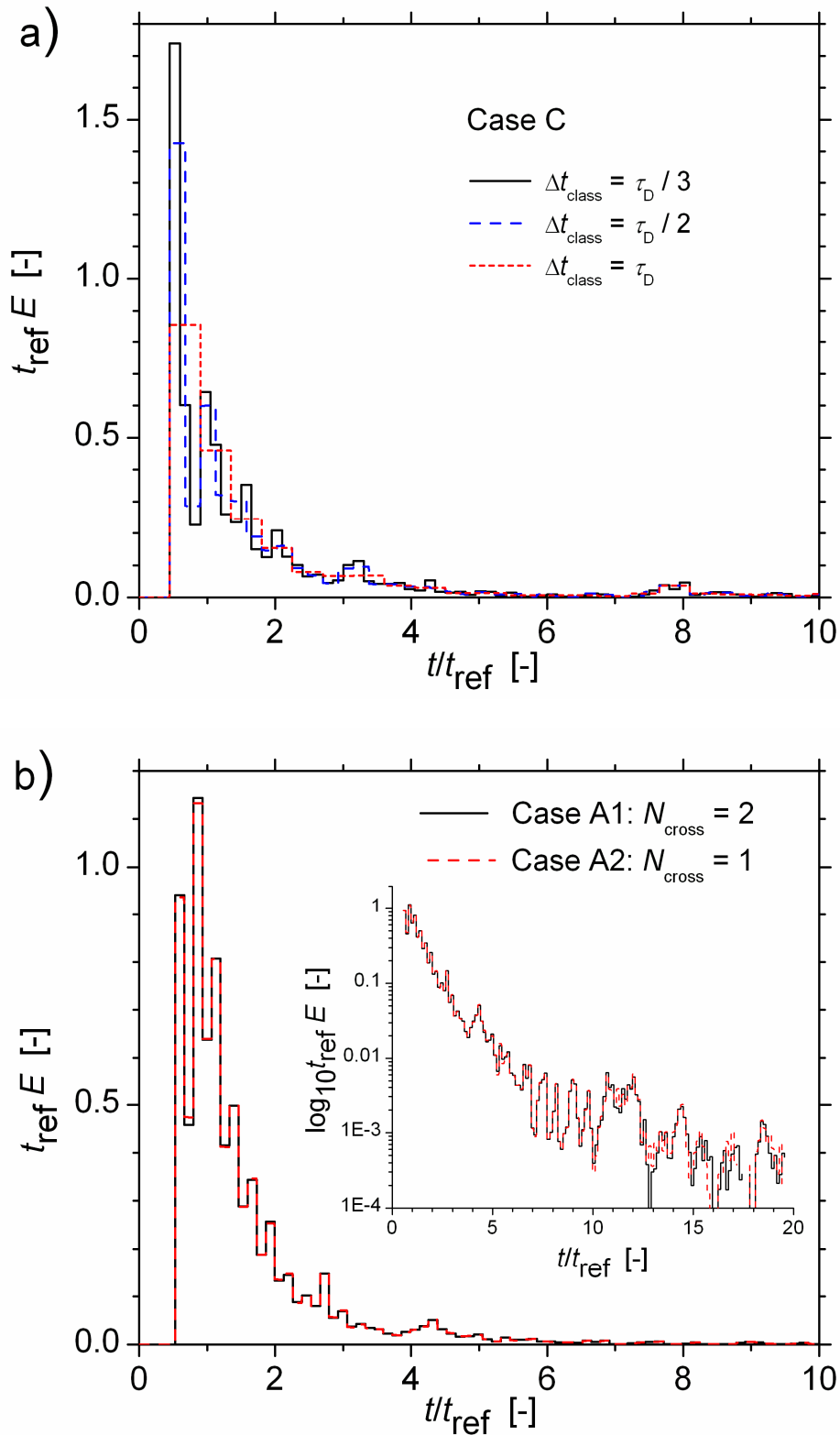


Fig. 2: a) Illustrations of influence of Δt_{class} on the numerically evaluated RTD curve. b) Comparison of RTD curves for two unit cells, obtained from case A1 with $N_{\text{cross}}=2$ and from case A2 with $N_{\text{cross}}=1$.

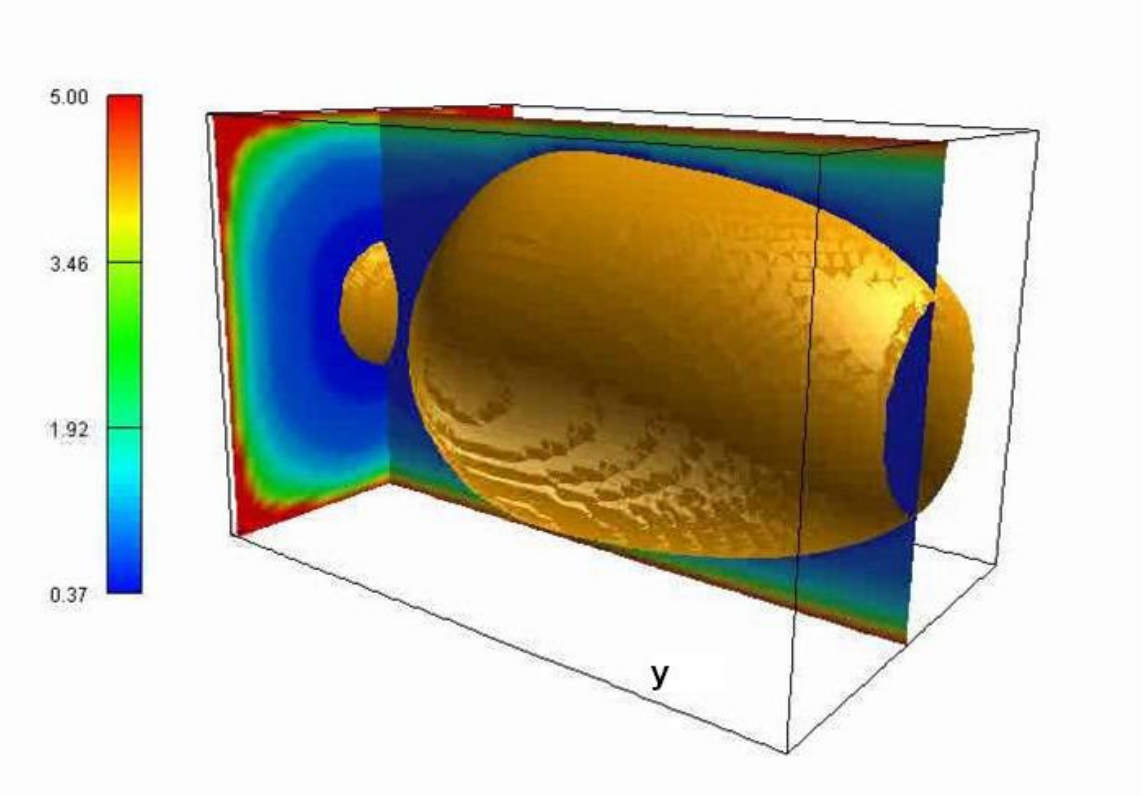


Fig. 3: Visualization of the bubble shape and contour plot of the local non-dimensional residence time t/t_{ref} in two different planes for case B1.

4. Modelling the RTD for bubble train flow

4.1. The RTD for a single unit cell

4.1.1. The WGO model

The RTD curves in Fig. 2 show a characteristic behaviour. For small values of t the RTD is zero. At the so called “delay time” τ_D the RTD becomes positive. The delay time of the RTD may thus be modelled by a plug flow reactor. For $t > \tau_D$ the RTD strongly increases to the highest value and then slowly decays. The sudden increase of the RTD from zero to the highest value corresponds to the residence time of the fastest fluid particles, i.e. the liquid slug region in Fig. 3. The semi-logarithmic scale of the inset graphics shows that the slope of the RTD at small and medium time is almost constant. This suggests that this part of the RTD curve may be approximated by an exponential relationship. Thus, the RTD curve may be approximated by a (single-phase flow) compartment model consisting of two tanks in series. The first tank is a plug flow reactor (PFR) which represents the delay time and the second tank is a continuous stirred tank reactor (CSTR) which represents the exponential decay, see Fig. 4. The delay time is determined by the minimum time of fluid elements to pass the channel, whereas the height of the peak and the slope of the exponential decay are determined by the ratio of flow rate to tank volume Q/V (see Fig. 12.1 in Levenspiel, 1999). This PFR-CSTR in series concept has already been adopted by Salman et al. (2004) to develop an analytical model for predicting axial mixing during Taylor flow in micro-channels at low Bodenstein numbers. However, this model was developed for circular channels where the film thickness is uniform and showed deficiencies for non-circular channels where the film thickness is not uniform (Wörner et al., 2007).

For co-current upward bubble train flow in a square channel, Wörner et al. (2007) proposed two slightly different models. The first model denoted as E_J is given by

$$E_J = E_{UC}(t) = \begin{cases} 0 & \text{for } t < L_{UC}/U_B \\ \frac{J}{L_{UC}} \exp\left[\frac{J}{L_{UC}}\left(\frac{L_{UC}}{U_B} - t\right)\right] & \text{for } t \geq L_{UC}/U_B \end{cases} \quad (30)$$

Modelling the RTD for bubble train flow

In this model, the CSTR corresponds to the liquid slug region, which is well mixed because of the fluids recirculating motion (Thulasidas et al., 1997). The mean velocity in the liquid slug is equal to the total superficial velocity J which is given by $J \equiv J_G + J_L = \varepsilon U_B + (1 - \varepsilon) U_L$. Here, U_L is the mean liquid velocity and ε is the gas volume fraction in the unit cell. The mean residence time of the CSTR is, therefore, in this model given by $\tau_{\text{CSTR}} = \tau_s = L_{\text{UC}} / J$. The model E_{U_L} is obtained from Eq. (30) by replacing the superficial velocity J by the mean liquid velocity U_L . In the following we will consider only model E_J and denote it as WGO model (Wörner, Ghidersa, Onea 2007).

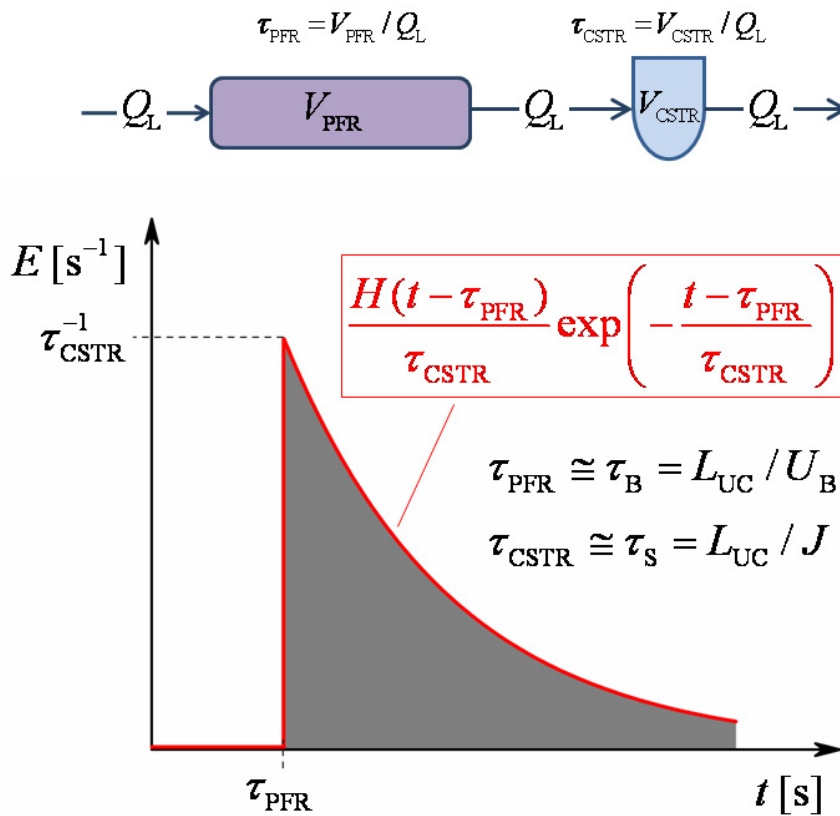


Fig. 4: Compartment representation of the WGO model. Q_L is the volumetric flow rate of the liquid phase and V_{PFR} and V_{CSTR} are the volume of the plug flow reactor and the continuous stirred tank reactor, respectively.

In the WGO model, the delay time is taken to be the bubble break-through time $\tau_B \equiv L_{UC} / U_B$, which is the time the bubble needs to move an axial distance equivalent to L_{UC} . The mean residence time of the CSTR representing the liquid slug is $\tau_S \equiv L_{UC} / J$. With these definitions one can write Eq. (30) in the compact form

$$E_J = E_{UC}(t) = \frac{H(t - \tau_B)}{\tau_S} \exp\left(-\frac{t - \tau_B}{\tau_S}\right) \quad (31)$$

Here,

$$H(x) = \begin{cases} 0 & \text{for } x < 0 \\ 1 & \text{for } x \geq 0 \end{cases} \quad (32)$$

is the Heaviside step function. The argument of this discontinuous function determines the delay time of the RTD, i.e. the time needed by the fastest particles to cross the reactor. The integral of Eq. (31) from zero to infinity is unity and thus satisfies the necessary conditions of any RTD, see Appendix A.1.1.

In Tab. 3 we list the values of τ_B and τ_S which are used in the WGO model for the different cases. Also given are the values for $\Delta t_{\text{class}} / t_{\text{ref}}$ that will be used for each case.

Tab. 3: Values of parameters for unit cell RTD models.

Case	τ_B / t_{ref}	τ_S / t_{ref}	$U_{L,\text{max}}^{\text{act}} / U_{\text{ref}}$	$U_{L,\text{max}}^{\text{th}} / U_{\text{ref}}$	λ	τ_D / t_{ref}	$\Delta t_{\text{class}} / t_{\text{ref}}$
A1	0.273	0.497	3.66	4.22	0.867	0.273	0.133
A2	0.273	0.497	3.64	4.22	0.863	0.275	0.133
B1	0.389	0.684	4.02	4.59	0.876	0.373	0.186
B2	0.379	0.674	4.08	4.66	0.876	0.367	0.183
C	0.539	0.836	-3.89	-4.39	0.879	0.450	0.225

4.1.2. The PD and PDD model

In this section, we develop two improved models for the RTD of a unit cell. The new models will refine the WGO model with respect to the delay time and with respect to the slope of the RTD at high values of t (i.e. the “tail” of the RTD).

4.1.2.1. Delay time

In Fig. 5 we compare the unit cell RTD model with the numerically evaluated RTD curves for case A1 and case C. In the figure, the shaded area represents the numerically evaluated RTD and the solid line the approximation by the WGO model. The dashed vertical lines denote the bubble break-through time. From Fig. 5 (a), where the dashed line agrees with the delay time of the RTD, we see that no fluid particles are moving faster than the bubble and most of the fluid particles are moving with a velocity that is only slightly smaller than the bubble velocity. However, for downward flow we see from Fig. 5 (b) that some particles need less time than the bubble to pass the channel. This means that the velocity of some fluid particles is higher than the bubble velocity. To investigate the reason for this we analyze next the local flow field in upward and downward bubble train flow.

Fig. 6 shows visualisations of the computed bubble shape and velocity fields for co-current upward flow (case G in Wörner et al., 2007) and for co-current downward flow (present case C). In the left half of the figure the velocity field in the vertical axial mid-plane is shown in the fixed frame of reference, while in the right half it is displayed in the frame of reference moving with the bubble (i.e. U_B is subtracted from the vertical velocity component). For both cases, the velocity in the liquid film region is almost zero as indicated in the fixed frame of reference. In the moving frame of reference, the velocity is almost zero in the rear part of the bubble for the upward case. These blank regions, which are visible in the right half of Fig. 6 a), indicate that part of the liquid slug that is moving approximately with the bubble velocity U_B . Hence, to consider the bubble velocity as representative for the fastest tracer particles and to use the bubble break-through time in the unit cell RTD model is reasonable for this upward flow case.

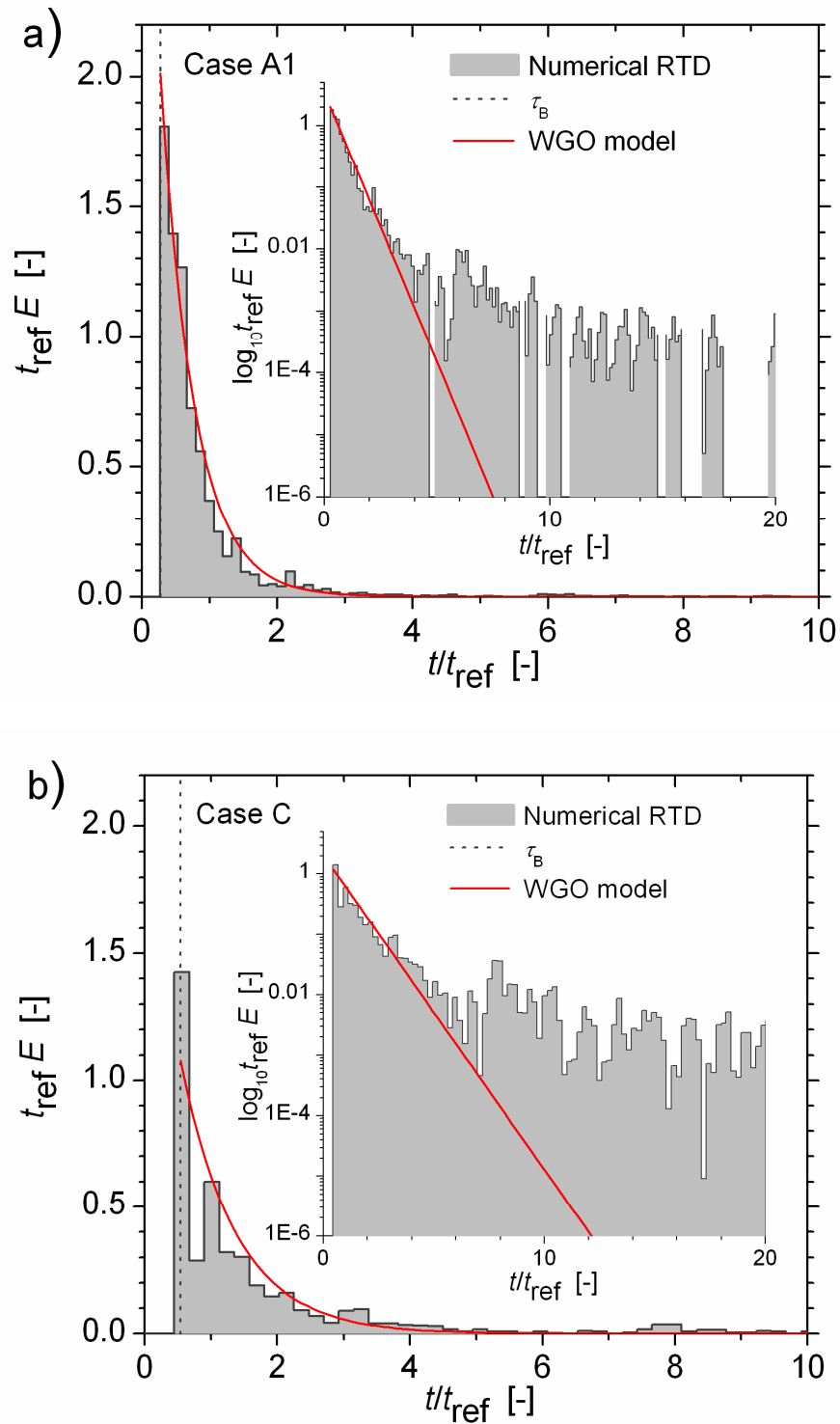


Fig. 5: Comparison of numerically evaluated unit cell RTD with the WGO model for (a) case A1 and (b) case C. The dashed vertical line indicates the bubble break-through time for each case.

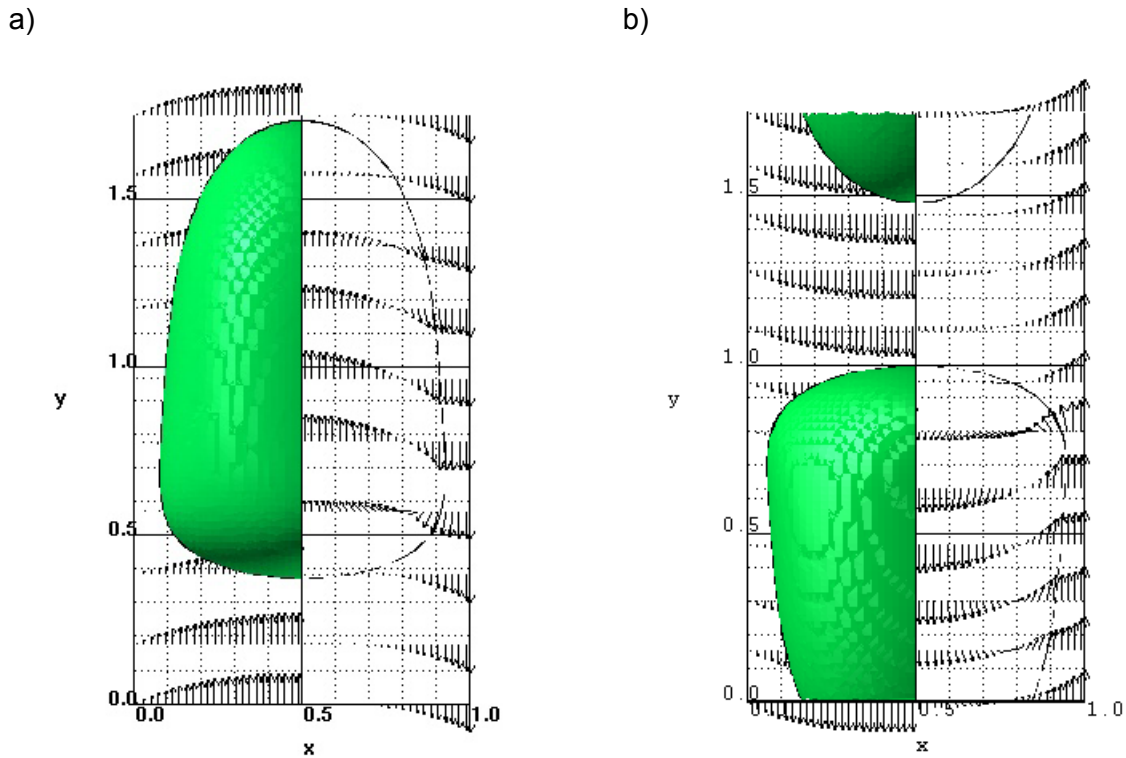


Fig. 6: Computed bubble shape and velocity field in vertical mid-plane $z = 1$ mm for fixed frame of reference (left half) and for frame of reference linked to the bubble (right half) for (a) co-current upward flow (case G in Wörner et al., 2007) and (b) co-current downward flow (case C).

However, for the downward case C the velocity vectors in the liquid slug behind the bubble have a finite length in the moving frame of reference; see the right half of Fig. 6 b). This indicates that the velocity of that part of the liquid slug is higher than the bubble velocity, which is consistent with the RTD displayed in Fig. 5 (b). This behaviour can be explained by the buoyancy force, which accelerates the bubble relative to the liquid for co-current upward flow but retards it for co-current downward flow. Thus, in the downward flow regime liquid fluid elements may be faster than the bubble. In the RTD model, therefore, in Eq. (30) the bubble velocity should be replaced by the maximum velocity in the liquid slug in order to obtain a more general model which is also valid for downward flow.

For any fully developed laminar flow through a straight channel there exists a linear relationship between the mean and maximum velocity, i.e. $U_{\text{mean}} = C_{\text{cs}} U_{\text{max}}$. The value of the constant C_{cs} depends only on the shape of the channel cross-section and is $C_{\text{cs}} = 0.5$ for a circular channel and $C_{\text{cs}} = 1/2.0962 = 0.477$ for a square channel (Shah and London, 1978). In bubble train flow, the mean liquid velocity within the liquid slug is given by $U_{L,\text{mean}} = J$. Thus, if the liquid slug is long enough to be fully developed, we have $U_{L,\text{max}}^{\text{th}} = J / C_{\text{cs}}$. For shorter liquid slugs the actual maximum velocity in the liquid slug may be smaller, say $U_{L,\text{max}}^{\text{act}} = \lambda U_{L,\text{max}}^{\text{th}}$ where λ is in the range $0 < \lambda \leq 1$.

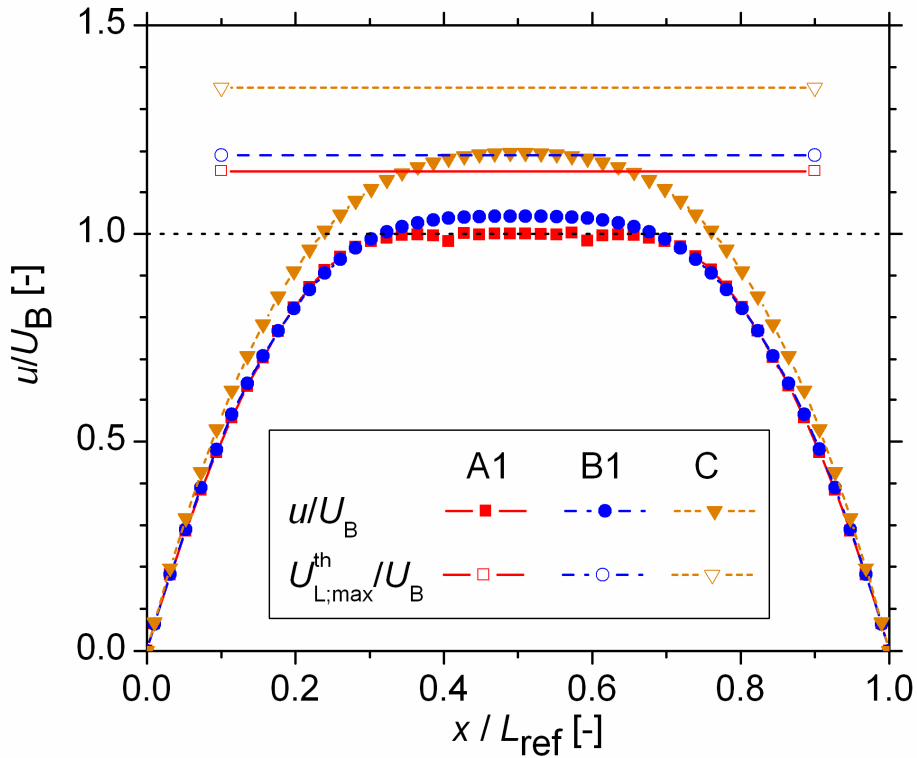


Fig. 7: Wall-normal profiles of magnitude of axial velocity in a horizontal cross-section through the middle of the liquid slug for case A1, B1, and C. For each case the velocity profile is normalized by the respective bubble velocity. The horizontal lines denote the normalized maximum velocity of a fully developed Poiseuille profile for each case.

In Fig. 7 we show the profile of the magnitude of the axial velocity in the middle of the liquid slug for case A1, B1 and C. In this figure, the horizontal lines denote the maximum velocity in a fully developed laminar flow with the same flow rate for each case. Fig. 7 shows that in the present simulations the liquid slug is too short to become fully developed. I.e. the profiles are not parabolic but rather flat for all cases. This supports the experimental finding of Thulasidas et al. (1997) and Tsoligkas et al (2007). The latter authors investigated the liquid velocity profiles in the centre of the liquid slug of a co-current downward Taylor flow in a square mini-channel and found that short liquid slugs with $L_S < D_h$ exhibited a flat axial velocity profile while long slugs with $L_S > D_h$ have a parabolic one. Obviously, in short slugs the velocity field is not fully developed. Thulasidas et al. (1997) found that in their experiments the Poiseuille profile within the liquid slug is fully developed for $L_S / D_h \geq 1.5$. Therefore, λ must increase with increasing slug length and asymptotically approach unity when the flow is fully developed. The values of $\lambda = U_{L,\max}^{\text{act}} / U_{L,\max}^{\text{th}}$ in the present simulations are given in Tab. 3. For all cases λ is in the range 0.86–0.88.

Fig. 7 also shows that for case A1, by incident, the maximum velocity $U_{L,\max}^{\text{act}}$ just equals the bubble velocity. For case B1, where the liquid slug is somewhat longer than in case A1, the maximum velocity $U_{L,\max}^{\text{act}}$ is somewhat larger than U_B . For case C with a co-current downward flow, $U_{L,\max}^{\text{act}}$ is clearly higher than U_B . Additionally, the velocity profile tends to become more parabolic. These results also elucidate the relation between the bubble break-through time and the delay time. To use the bubble break-through time as delay time may be reasonable only for upward flow with very short liquid slug lengths like case A1 and A2, where $U_{L,\max}^{\text{act}} \approx U_B$. This is, however, not valid for case C, where $U_{L,\max}^{\text{act}}$ is much larger than U_B , and therefore τ_B is larger than τ_D . Thus, it is necessary to refine the WGO model with respect to the delay time, to yield a more general and consistent model for any flow direction and any length of the liquid slug.

To refine the WGO model for co-current downward bubble train flow with an arbitrary length of the liquid slug we replace in Eq. (30) the bubble velocity U_B by $U_{L,\max}^{\text{act}} = \lambda U_{L,\max}^{\text{th}} = \lambda J / C_{cs}$. This yields the following model:

$$E_{UC}(t) = \begin{cases} 0 & \text{for } t < C_{cs}L_{UC} / (\lambda J) \\ \frac{J}{L_{UC}} \exp\left(\frac{C_{cs}}{\lambda} - t \frac{L_{UC}}{J}\right) & \text{for } t \geq C_{cs}L_{UC} / (\lambda J) \end{cases} \quad (33)$$

This revised WGO model is more general since it takes the velocity of the fastest fluid particles to compute the delay time instead of the bubble velocity. Here, the delay time is

$$\tau_D \equiv \frac{L_{uc}}{U_{L,max}^{act}} = \frac{L_{uc}}{\lambda U_{L,max}^{th}} = \frac{C_{cs}}{\lambda} \frac{L_{uc}}{J} = \frac{C_{cs}}{\lambda} \tau_S \quad (34)$$

The revised WGO model for a single unit cell can then be written in the compact form

$$E_{UC}(t) = \frac{H(t - \tau_D)}{\tau_S} \exp\left(-\frac{t - \tau_D}{\tau_S}\right) = \frac{H(t - \tau_D)}{\tau_S} \exp\left(\frac{C_{cs}}{\lambda} - \frac{t}{\tau_S}\right) \quad (35)$$

In the following, we denote this model as **PD model**. Here P stands for “peak” and D for “decay”. This name reflects that the RTD consists of one peak followed by an exponential decay. In the PD model λ is unknown yet. However, λ is a function of L_S / D_h and should approach unity for large values of L_S / D_h . Here, we take the values of λ as given in Tab. 3 while the development of a suitable relationship for $\lambda = \lambda(L_S / D_h)$ will be a future task for us.

For the mean residence time of the RTD in Eq. (35), we obtain the result

$$\tau_{UC} \equiv \bar{t}_{UC} = \int_0^{\infty} t E_{UC}(t) dt = \tau_D + \tau_S = \tau_S \left(\frac{C_{cs}}{\lambda} + 1 \right) \quad (36)$$

(see Appendix A.1.2). The variance is given by

$$\sigma_{UC}^2 = \tau_S^2 \quad (37)$$

(see Appendix A.1.3). Introducing the non-dimensional time

$$\theta_{UC} \equiv \frac{t - \tau_D}{\tau_{UC}} \quad (38)$$

we can write Eq. (35) in the compact non-dimensional form

$$\begin{aligned} E_{\theta,UC} \equiv \tau_{UC} E_{UC}(t) &= H(\tau_{UC} \theta_{UC}) \frac{\tau_{UC}}{\tau_S} \exp\left(-\theta_{UC} \frac{\tau_{UC}}{\tau_S}\right) \\ &= H((\tau_D + \tau_S) \theta_{UC}) \frac{\tau_D + \tau_S}{\tau_S} \exp\left(-\theta_{UC} \frac{\tau_D + \tau_S}{\tau_S}\right) \end{aligned} \quad (39)$$

4.1.2.2. Tail of the RTD

The tails of the RTDs in Fig. 5 correspond to the flow in the liquid film which is almost stagnant (see velocity profiles in the left half of Fig. 6). The inset graphic in Fig. 5 shows the numerical and modelled RTD in a semi-logarithmic representation. This allows for an easy visual comparison of the slopes of both RTDs. The numerical RTD shows two slopes, a steeper one for $t/t_{\text{ref}} < 4$ and flatter one for $t/t_{\text{ref}} > 4$. In contrast, the slope of the WGO model is constant and the tail of the RTD is not accurately represented by this model. In Wörner et al. (2007), the steeper RTD slope for $t/t_{\text{ref}} < 4$ is better fitted by model E_J since residence times $t/t_{\text{ref}} < 4$ correspond mainly to fluid elements in the liquid slug, where the mean velocity is equal to J . However, the flatter slope for $t/t_{\text{ref}} > 4$ is better approximated by model E_{U_L} . This is because residence times $t/t_{\text{ref}} > 4$ correspond to fluid elements in the four corners of the channel. There, the mean liquid velocity is smaller than J and may be approximated by the mean liquid velocity in the unit cell U_L . Though E_{U_L} is a better approximation for $t/t_{\text{ref}} > 4$, the slope of this model is still too steep for high residence times (see Fig. 8 a in Wörner et al., 2007). Hence, an even lower mean liquid velocity should be chosen for the corner flow to cause a flatter slope for high residence times.

Considering these ideas, the WGO model respectively the PD model shall be developed further towards a model which yields two different slopes for small and large times in order to represent the tail of the RTD more accurately. For this purpose, Wörner et al. (2007) suggested the three tank compartment model as displayed in Fig. 8. This model consists of a PFR that is in series with two CSTRs in parallel. The RTD of this compartment model is characterized by a peak which is followed by the superposition of two exponential decays with different slopes (see Fig. 12.1 in Levenspiel, 1999). We will, therefore, denote this model as **PDD model** (peak-decay-decay). In the PDD model one CSTR corresponds to the liquid slug, while the second corresponds to the flow in the liquid film and the corners. Since both CSTRs are in parallel, the resulting RTD is the sum of two exponentials. The slopes of both exponentials are determined by the mean residence time of the liquid slug τ_s and by the mean residence time of the CSTR representing the liquid film /corner flow, respectively.

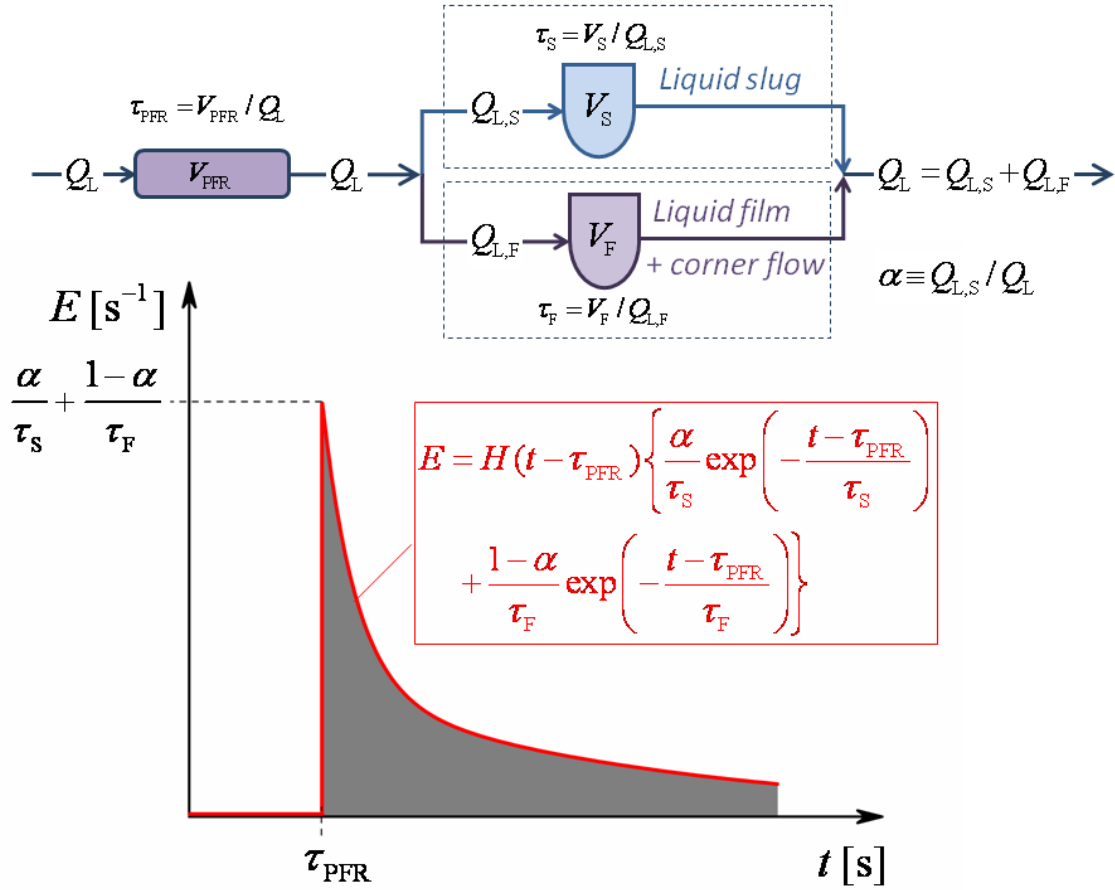


Fig. 8: Compartment representation of the PDD model. Q_L is the volumetric flow rate of the liquid. V_{PFR} is the volume of the plug flow reactor while V_S and V_F denote that of the continuous stirred tank reactor, respectively. The subscripts 'S' and 'F' correspond to the liquid slug and the liquid film / corner flow, respectively.

A relation for $Q_{L,F}$ can be obtained from a liquid mass balance in a frame of reference moving with the bubble. We consider a control volume that consists of an axial portion of the channel where one end is in the liquid slug and the other end is in the bubble region. Then a balance of the liquid inflow and outflow flow rates yields

$$(J - U_B) A_{ch} = (U_{L, \text{film}} - U_B)(A_{ch} - A_B) \quad (40)$$

so that

$$U_{L, \text{film}} = U_B - (U_B - J) \frac{A_{ch}}{A_{ch} - A_B} \quad (41)$$

Modelling the RTD for bubble train flow

In this equation, $U_{L,\text{film}} = U_{L,\text{film}}(y)$ and $A_B = A_B(y)$ represent the mean axial liquid velocity and bubble cross-sectional area, respectively. The position y denotes the control volume outlet and is variable. The liquid volumetric flow rate in the outflow cross-section of the control volume is then given by

$$Q_{L,\text{film}} = U_{L,\text{film}} (A_{\text{ch}} - A_B) = \left[U_B - (U_B - J) \frac{A_{\text{ch}}}{A_{\text{ch}} - A_B} \right] (A_{\text{ch}} - A_B) = JA_{\text{ch}} - U_B A_B \quad (42)$$

As pointed out by Abiev (2008), the sign of $U_{L,\text{film}}$ and $Q_{L,f}$ can be positive or negative.

For an axi-symmetric bubble with local cross-sectional diameter $d_B(y)$ one obtains from Eq. (41) the result

$$U_{L,\text{film}} \equiv U_B - (U_B - J) \left[1 - \frac{\pi \left(\frac{d_B}{D_h} \right)^2}{4} \right]^{-1} \quad (43)$$

This relation is very sensitive to the value of d_B . Here, we are interested in the mean liquid velocity in the axial cross-section where the bubble diameter is largest. Thus, we take $d_B = \beta D_B$ and compute the mean liquid velocity in the liquid film / corner region from relation

$$U_F \equiv U_B - (U_B - J) \left[1 - \frac{\pi \left(\frac{\beta D_B}{D_h} \right)^2}{4} \right]^{-1} \quad (44)$$

In the sequel, we consider two different values for β , namely $\beta = 1$ and $\beta = 0.97$. In Tab. 4 we list the values of U_F that are obtained from this equation for the different cases for both values of β . Our RTD model is only reasonable if U_F has the same sign as J , i.e. is positive for upward flow and negative for downward flow. Then, the mean residence time of the CSTR representing the liquid film is computed from $\tau_F \equiv L_{\text{UC}} / |U_F|$ while that of the CSTR representing the liquid slug is the same as in the WGO and PD model, namely $\tau_S \equiv L_{\text{UC}} / J$.

For the moment, we define the relation between the flow rates $Q_{L,S}$ and $Q_{L,F}$ in the two CSTRs by a weighting factor $\alpha = Q_{L,S} / (Q_{L,S} + Q_{L,F})$. This weighting factor is in the range $0 < \alpha \leq 1$ and will be determined later. In section 4.2 where we consider multiple unit cells, we always assume that all unit cells are identical so that the value of α is the same.

The RTD of the three tank compartment model is then given by

$$E_{UC}^{\alpha}(t) = 0 \quad (45)$$

for $t < L_{UC} / U_{L,max}^{act}$, and by

$$E_{UC}^{\alpha}(t) = \alpha \frac{J}{L_{UC}} \exp\left[\frac{J}{L_{UC}} \left(\frac{L_{UC}}{U_{L,max}^{act}} - t\right)\right] + (1-\alpha) \frac{U_F}{L_{UC}} \exp\left[\frac{U_F}{L_{UC}} \left(\frac{L_{UC}}{U_{L,max}^{act}} - t\right)\right] \quad (46)$$

for $t \geq L_{UC} / U_{L,max}^{act}$. Introducing the delay time $\tau_D \equiv L_{uc} / |U_{L,max}^{act}|$ according to Eq. (34), as well as τ_F and τ_S we can write the PDD model in the compact form

$$E_{UC}^{\alpha}(t) = H(t - \tau_D) \left[\frac{\alpha}{\tau_S} \exp\left(-\frac{t - \tau_D}{\tau_S}\right) + \frac{1-\alpha}{\tau_F} \exp\left(-\frac{t - \tau_D}{\tau_F}\right) \right] \quad (47)$$

As required, the integral of Eq. (47) from zero to infinity is unity, see Appendix B.1.1.

For the mean residence time we obtain the result

$$\tau_{UC}^{\alpha} \equiv \bar{t}_{UC}^{\alpha} = \int_0^{\infty} t E_{UC}^{\alpha}(t) dt = \tau_D + \alpha \tau_S + (1-\alpha) \tau_F, \quad (48)$$

see Appendix B.1.2., and for the variance

$$\sigma_{\alpha UC}^2 = 2\alpha \tau_S^2 + 2(1-\alpha) \tau_F^2 - [\alpha \tau_S + (1-\alpha) \tau_F]^2, \quad (49)$$

see Appendix B.1.3. Introducing the non-dimensional time

$$\theta_{UC}^{\alpha} \equiv \frac{t - \tau_D}{\tau_{UC}^{\alpha}} = \frac{t - \tau_D}{\tau_D + \alpha \tau_S + (1-\alpha) \tau_F} \quad (50)$$

we can write the PDD model in the form

$$E_{\theta,UC}^{\alpha}(\theta) = \tau_{UC}^{\alpha} E_{UC}^{\alpha}(t) = \left[\alpha \frac{\tau_{UC}^{\alpha}}{\tau_S} \exp\left(-\theta_{UC}^{\alpha} \frac{\tau_{UC}^{\alpha}}{\tau_S}\right) + (1-\alpha) \frac{\tau_{UC}^{\alpha}}{\tau_F} \exp\left(-\theta_{UC}^{\alpha} \frac{\tau_{UC}^{\alpha}}{\tau_F}\right) \right] H(\tau_{UC}^{\alpha} \theta_{UC}^{\alpha}) \quad (51)$$

When the flow rate of the liquid film region is zero we have $\alpha = 1$ and the PDD model of Eq. (47) becomes equal to the PD model in Eq. (35). Furthermore, the right hand sides of Eq. (48), Eq. (49) and Eq. (51) reduce to those of Eq. (36), Eq. (37) and Eq. (39), respectively.

Modelling the RTD for bubble train flow

We now determine a suitable value for α and consider two possible choices. In the first one, we compute α from relation

$$\alpha = \alpha_Q \equiv \frac{Q_{L,tot} - Q_{L,filn}}{Q_{L,tot}} \quad (52)$$

With $Q_{L,tot} = J_L A_{ch}$ and Eq. (42) we obtain from Eq. (52) the result

$$\alpha_Q = \frac{J_L A_{ch} - J A_{ch} + U_B A_B}{J_L A_{ch}} = \frac{-J_G A_{ch} + U_B A_B}{J_L A_{ch}} = \frac{-\varepsilon U_B A_{ch} + U_B A_B}{J_L A_{ch}} = \frac{U_B}{J_L} \left(\frac{A_B}{A_{ch}} - \varepsilon \right) \quad (53)$$

From the mean residence time of the RTD model given by Eq. (48) we obtain

$$\begin{aligned} \tau_{UC}^\alpha &= \tau_D + \alpha \tau_S + (1 - \alpha) \tau_F = \frac{C_{cs}}{\lambda} \tau_S + \frac{U_B}{J_L} \left(\frac{A_B}{A_{ch}} - \varepsilon \right) \tau_S + \left[1 - \frac{U_B}{J_L} \left(\frac{A_B}{A_{ch}} - \varepsilon \right) \right] \tau_F \\ &= \left[\frac{C_{cs}}{\lambda} + \frac{U_B}{J_L} \left(\frac{A_B}{A_{ch}} - \varepsilon \right) \right] \frac{L_{UC}}{J} + \left[1 - \frac{U_B}{J_L} \left(\frac{A_B}{A_{ch}} - \varepsilon \right) \right] \frac{L_{UC}}{U_F} \end{aligned} \quad (54)$$

where U_F is given by Eq. (41). The problem of this choice for α is that in general the mean residence time according to Eq. (54) differs from the hydrodynamic residence time of the unit cell given by Eq. (28). In Tab. 4 we list the values of α_Q for both values of β . Also given are values of the relative deviation of the mean residence time from the hydrodynamic residence time. For $\beta = 1$ the relative error is typically about 4 - 9%, whereas it is only about 1 - 7% for $\beta = 0.97$. For both values of β , the relative error is larger for the downward flow case C than for the cases with upward flow. While a relative error in the mean residence time below 7% may be acceptable for some cases, we nevertheless disregard this approach for determining α .

In the second approach to determine α , we demand instead that the mean residence time of the model is equal to the mean hydrodynamic residence time. Thus, we set $\tau_{UC}^\alpha = \tau_h$ and obtain from Eq. (48) the following relation

$$\alpha = \alpha_h \equiv \frac{\tau_D + \tau_F - \tau_h}{\tau_F - \tau_S} \quad (55)$$

The corresponding values of α_h for all cases are listed in Tab. 4. We note that for all cases the differences in the values of α_h and α_Q are small in general.

In Fig. 9 and Fig. 10 a) and b), we compare the PD and PDD model with the numerically evaluated RTD curves for case C, A1 and B1. In these figures, the shaded area represents the numerical evaluated RTD curve (with the values of Δt_{class} as given in Tab. 3) while the lines represent the PD model and the PDD model for two different values of β , respectively. The linear plots in Fig. 9 and Fig. 10 b) show that for case C and B1 the peaks of the models are clearly lower than the peak of the numerically evaluated RTD. However, as noted before the peak of the numerically evaluated RTD may change depending on Δt_{class} , see the discussion of Fig. 2 a) above.

Tab. 4: Values of τ_F and α for the PDD model.

Case	$\beta = 1$					$\beta = 0.97$				
	$\frac{U_F}{U_{\text{ref}}}$	$\frac{\tau_F}{t_{\text{ref}}}$	α_Q	$\frac{\tau_{\text{UC}}^{\alpha_Q} - \tau_h}{\tau_h}$	α_h	$\frac{U_F}{U_{\text{ref}}}$	$\frac{\tau_F}{t_{\text{ref}}}$	α_Q	$\frac{\tau_{\text{UC}}^{\alpha_Q} - \tau_h}{\tau_h}$	α_h
A1	0.274	3.65	0.834	3.8%	0.849	0.473	2.12	0.696	1.4%	0.706
A2	0.274	3.65	0.834	4.0%	0.850	0.473	2.12	0.696	1.5%	0.707
B1	0.019	78.0	0.991	7.7%	0.993	0.294	5.10	0.850	5.2%	0.869
B2	0.037	40.6	0.982	7.2%	0.985	0.309	4.85	0.840	4.6%	0.858
C	-0.193	9.07	0.929	9.4%	0.949	-0.465	3.76	0.812	7.4%	0.855

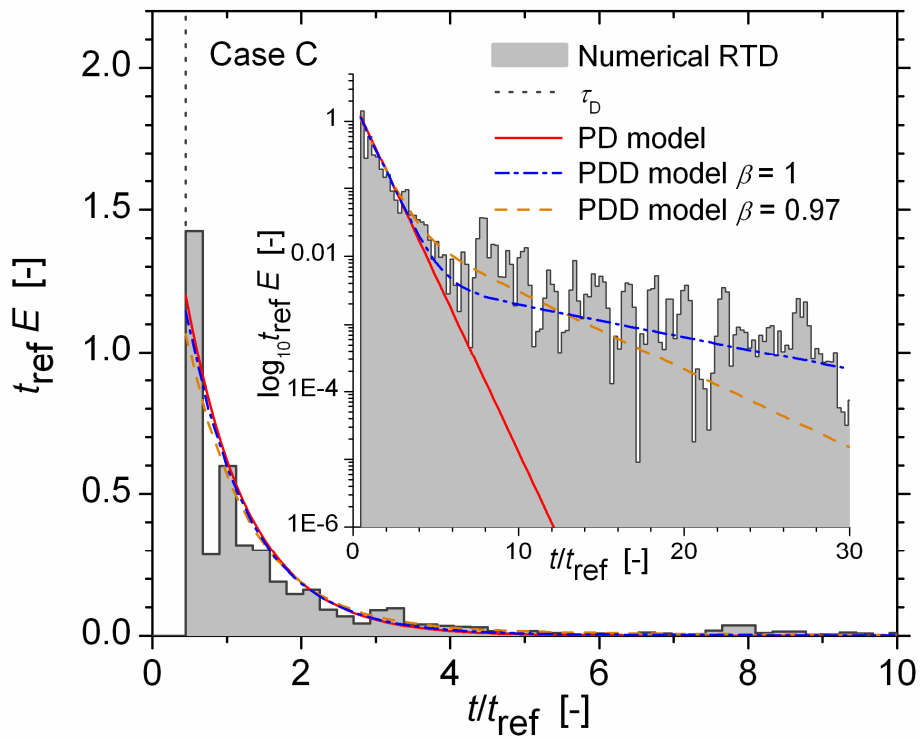


Fig. 9: Comparison of numerically evaluated RTD for case C with the PD model and the PDD model for $\beta = 1$ and $\beta = 0.97$.

For all three cases, the curves of the PDD model intersect that of the PD model and exhibit a flatter slope at high residence times. This can be seen more clearly in the inset graphics with semi-logarithmic representation of the data. Fig. 9 and Fig. 10 a) and b) show that the slope of the PDD model changes at $t/t_{\text{ref}} \approx 4$. For larger residence times the slope becomes less steep. The figures show that the slope of the PDD model at large values of t depends on the value of β . For case C and A1 $\beta = 1$ seems to give better results, while for case B1 it appears that $\beta = 0.97$ may be more appropriate. With the present PDD model the slope of the RTD at large values of t is also much better approximated than by the model E_{U_L} of Wörner et al. (2007). In conclusion the present PDD model with the delay time computed from Eq. (34) and U_F computed from Eq. (44) with $0.97 \leq \beta \leq 1$ is a reasonably good fit to the numerically evaluated RTD, both at small and large residence times, and both, for co-current upward and downward Taylor flow.

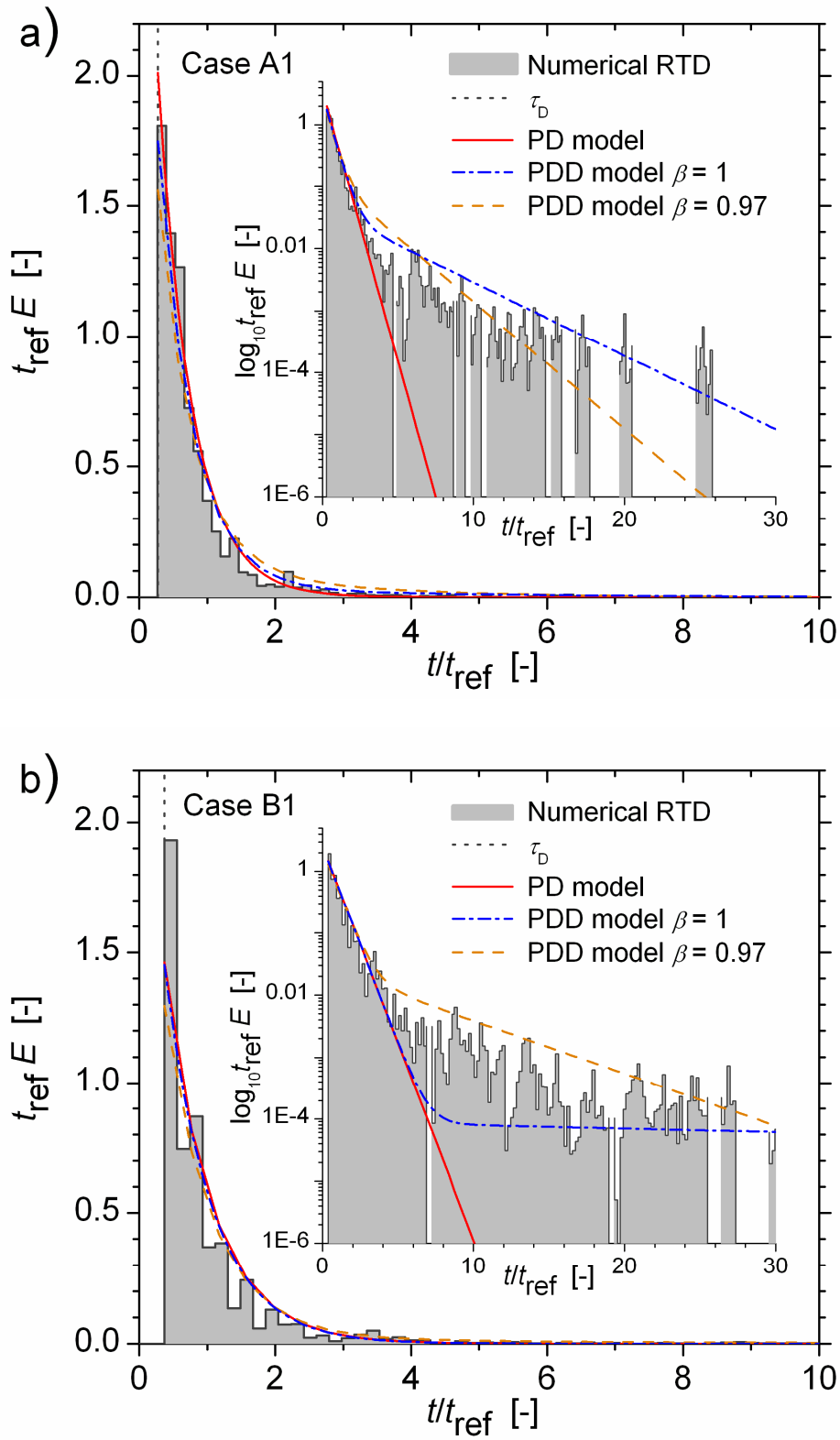


Fig. 10: Comparison of numerically evaluated RTD curves for case A1 (a) and B1 (b) with the PD model and the PDD model for $\beta = 1$ and $\beta = 0.97$.

4.1.3. Steps to determine the parameters of the PD and PDD model

In this subsection we list the sequence of steps which are necessary to determine the parameters of our RTD model. We assume that the following quantities are given:

- Viscosity of continuous phase μ_L
- Interfacial tension σ
- Superficial liquid velocity $J_L = Q_L / A_{ch}$
- Superficial gas velocity $J_G = Q_G / A_{ch}$

The individual steps to determine the RTD are then as follows:

1. Compute the capillary number $Ca_J = \mu_L J / \sigma$ where $J = J_G + J_L$
2. Compute the bubble velocity U_B from an empirical correlation, e.g. of drift flux model type or of the form $U_B = U_B(Ca_J)$, see e.g. Angeli and Gavriilidis (2008).
3. Compute the capillary number $Ca = \mu_L U_B / \sigma$
4. Compute the bubble diameter from an empirical correlation $D_B = D_B(Ca)$, see e.g. the review by Angeli and Gavriilidis (2008).
5. Estimate the length of the unit cell L_{UC} and the length of the liquid slug L_S either from experimental data or from empirical correlations, see e.g. Angeli and Gavriilidis (2008) and Fries and von Rohr (2009).
6. Determine $\tau_S = L_{UC} / J$
7. Determine $C_{cs} = U_{mean} / U_{max}$, estimate an appropriate value for λ and compute the delay time $\tau_D = C_{cs} \tau_S / \lambda$. This defines all parameters of the PD model. The PDD model requires additionally the following two steps.
8. Estimate U_F from Eq. (44) (with an appropriate value for β , e.g. 0.98) and determine $\tau_F = L_{UC} / U_F$.
9. Determine the hydrodynamic residence time of one unit cell from relation $\tau_h = L_{UC} / J_L$ and compute the values of α from Eq. (55).

4.2. The RTD for multiple unit cells

In section 4.1 we developed the PD and PDD model for the RTD of a single unit cell. Since Taylor flow consists of a sequence of a large number of unit cells, the single unit cell RTD model is at first of limited practical value. The overall goal is, therefore, to develop a model for the RTD of Taylor flow consisting of n identical unit cells. In this section we investigate in how far this multiple unit cell RTD model can be obtained from the single unit cell RTD model by a convolution procedure.

4.2.1. Convolution procedure

The RTD has the property to transfer any reactor input signal $C_{in}(t)$ into a unique output signal $C_{out}(t)$. Mathematically, this transfer is described by the convolution integral

$$C_{out}(t) = \int_0^t C_{in}(t-t')E(t')dt' \quad (56)$$

(see e.g. Levenspiel 1999). Eq. (56) can be written symbolically as

$$C_{out} = C_{in} * E \quad (57)$$

Here C_{out} is the convolution of E with C_{in} . Thus, in passing through the vessel the input signal is modified to give an output signal C_{out} , see Fig. 11 top. The kind of this modification is determined by the RTD.

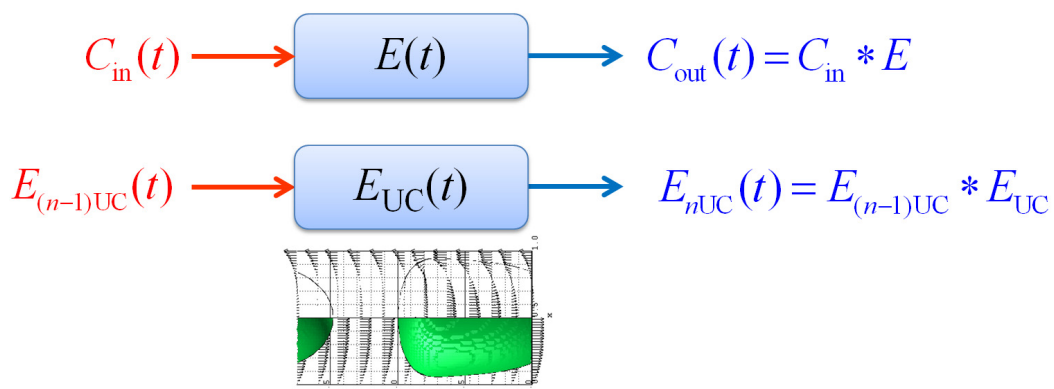


Fig. 11: Schematic representation of convolution procedure for a general case (top) and for a unit cell of bubble train flow (bottom).

We now consider a bubble train flow consisting of n identical unit cells and assume that the input signal for the first unit cell is an ideal Dirac delta pulse. In this case the output signal of the first unit cell is equal to $E_{UC}(t)$. Since this RTD is the input signal for the second unit cell, the output signal for the second unit cell is given by the convolution $E_{UC} * E_{UC}$. Since the input signal for this convolution is an RTD, the output signal has also the properties of an RTD. It can be considered as an approximation for the residence time distribution of unit cell 2, i.e. $E_{2UC} = E_{UC} * E_{UC}$. Assuming that the RTD of the unit cell can be described by the PDD model E_{UC}^α , we obtain for unit cell n the result

$$E_{nUC}^\alpha(t) = E_{(n-1)UC}^\alpha(t) * E_{UC}^\alpha(t) = \int_0^t E_{(n-1)UC}^\alpha(t-t')E_{UC}^\alpha(t')dt' \quad (58)$$

(see Fig. 11 bottom). Therefore, we can compute the RTD for a series of n unit cells from the RTD of a single unit cell by successive evaluation of $n-1$ convolutions integrals. Next we present the results of these convolutions both for the PD model and for the PDD model and refer to the Appendices for mathematical details.

4.2.2. PD model and PDD model for multiple unit cells

4.2.2.1. RTD for two unit cells

To evaluate Eq. (58) for $n = 2$ we have to solve the convolution integral

$$E_{2UC}^\alpha(t) = E_{UC}^\alpha(t) * E_{UC}^\alpha(t) = \int_0^t E_{UC}^\alpha(t-t')E_{UC}^\alpha(t')dt' \quad (59)$$

As shown in Appendix B.2.1.1, this yields the result

$$E_{2UC}^\alpha(t) = H(t-2\tau_D) \left\{ (t-2\tau_D) \left[\left(\frac{\alpha}{\tau_S} \right)^2 \exp\left(-\frac{t-2\tau_D}{\tau_S}\right) + \left(\frac{1-\alpha}{\tau_F} \right)^2 \exp\left(-\frac{t-2\tau_D}{\tau_F}\right) \right] + \frac{2\alpha(1-\alpha)}{\tau_S - \tau_F} \left[\exp\left(-\frac{t-2\tau_D}{\tau_S}\right) - \exp\left(-\frac{t-2\tau_D}{\tau_F}\right) \right] \right\} \quad (60)$$

By setting $\alpha = 1$ we obtain from Eq. (60) the RTD for two unit cells of the PD model

$$E_{2UC}(t) = \frac{t - 2\tau_D}{\tau_S^2} \exp\left(-\frac{t - 2\tau_D}{\tau_S}\right) H(t - 2\tau_D) \quad (61)$$

(see also Appendix A.2.1.1).

As shown in Appendix B.2.1.2, the mean residence time for two unit cells is

$$\tau_{2UC}^\alpha \equiv \bar{t}_{2UC}^\alpha = \int_0^\infty t E_{2UC}^\alpha(t) dt = 2\left[\tau_D + \alpha\tau_S + (1-\alpha)\tau_F\right] = 2\tau_{UC}^\alpha \quad (62)$$

For $\alpha = 1$ we obtain the result (see also Appendix A.2.1.2)

$$\tau_{2UC} = 2(\tau_D + \tau_S) \quad (63)$$

The non-dimensional time for two unit cells is defined as

$$\theta_{2UC}^\alpha \equiv \frac{t - 2\tau_D}{2\tau_{UC}^\alpha} \quad (64)$$

Then, the RTD for two unit cells can be written in the non-dimensional form

$$\begin{aligned} E_{\theta,2UC}^\alpha(\theta) &= 2\tau_{UC}^\alpha E_{2UC}^\alpha(t) \\ &= \left\{ \theta_{2UC}^\alpha \left[\left(\alpha \frac{2\tau_{UC}^\alpha}{\tau_S} \right)^2 \exp\left(-\theta_{2UC}^\alpha \frac{2\tau_{UC}^\alpha}{\tau_S}\right) + \left((1-\alpha) \frac{2\tau_{UC}^\alpha}{\tau_F} \right)^2 \exp\left(-\theta_{2UC}^\alpha \frac{2\tau_{UC}^\alpha}{\tau_F}\right) \right] \right. \\ &\quad \left. + \alpha(1-\alpha) \frac{4\tau_{UC}^\alpha}{\tau_S - \tau_F} \left[\exp\left(-\theta_{2UC}^\alpha \frac{2\tau_{UC}^\alpha}{\tau_S}\right) - \exp\left(-\theta_{2UC}^\alpha \frac{2\tau_{UC}^\alpha}{\tau_F}\right) \right] \right\} H(2\tau_{UC}^\alpha \theta_{2UC}^\alpha) \end{aligned} \quad (65)$$

For $\alpha = 1$ we obtain

$$E_{\theta,2UC}(\theta) = \theta_{2UC} \left(\frac{2\tau_{UC}}{\tau_S} \right)^2 \exp\left(-\theta_{2UC} \frac{2\tau_{UC}}{\tau_S}\right) H(2\tau_{UC} \theta_{2UC}) \quad (66)$$

We now compare the RTD for two unit cells obtained by this convolution procedure with the numerically evaluated RTD curves. Fig. 12 a) and b) show the results for cases A2 and B2 both for the PD model and the PDD model (for two different values of β). Comparing the model RTDs for two unit cells in Fig. 12 a) and b) with those in Fig. 10 a) and b) for one unit cell shows one apparent difference. Namely, for one unit cell the RTD is zero for $t < \tau_D$, jumps to its maximum value at $t = \tau_D$ and decreased monotonically to zero for values $t > \tau_D$.

Modelling the RTD for bubble train flow

Instead, for two unit cells the model RTD is zero for $t \leq \tau_D$, increases till a maximum value is obtained and finally decreases toward zero. The maximum value of the RTD is always higher for the PD model than for the PDD model, both for the single unit cell and for two unit cells. Fig. 12 a) and b) show that for the PDD model the maximum value of the RTD is very sensitive to the value of β . We recall, as noted before, that the maximum value of the numerically evaluated RTD is sensitive to the value of Δt_{class} . In all cases, the RTD curve of the PDD model intersects that of the PD model, giving lower values of the RTD at low values of t and higher values of the RTD at large values of t as compared to the PD model. Due to this behaviour the PDD model provides a better fit to the long tails of the numerical RTD for two unit cells, see Fig. 12 a) and b). Interestingly, in the numerical RTD there appears a second peak at $t/t_{\text{ref}} \approx 4.3$ for case A2 and for $t/t_{\text{ref}} \approx 6$ for case B2. The inset graphics in Fig. 12 a) and b) show, that at high values of t the slope of the numerical RTD is well approximated by the PDD model with a value of $\beta = 1$ for case A2, and $\beta = 0.97$ for case B2.

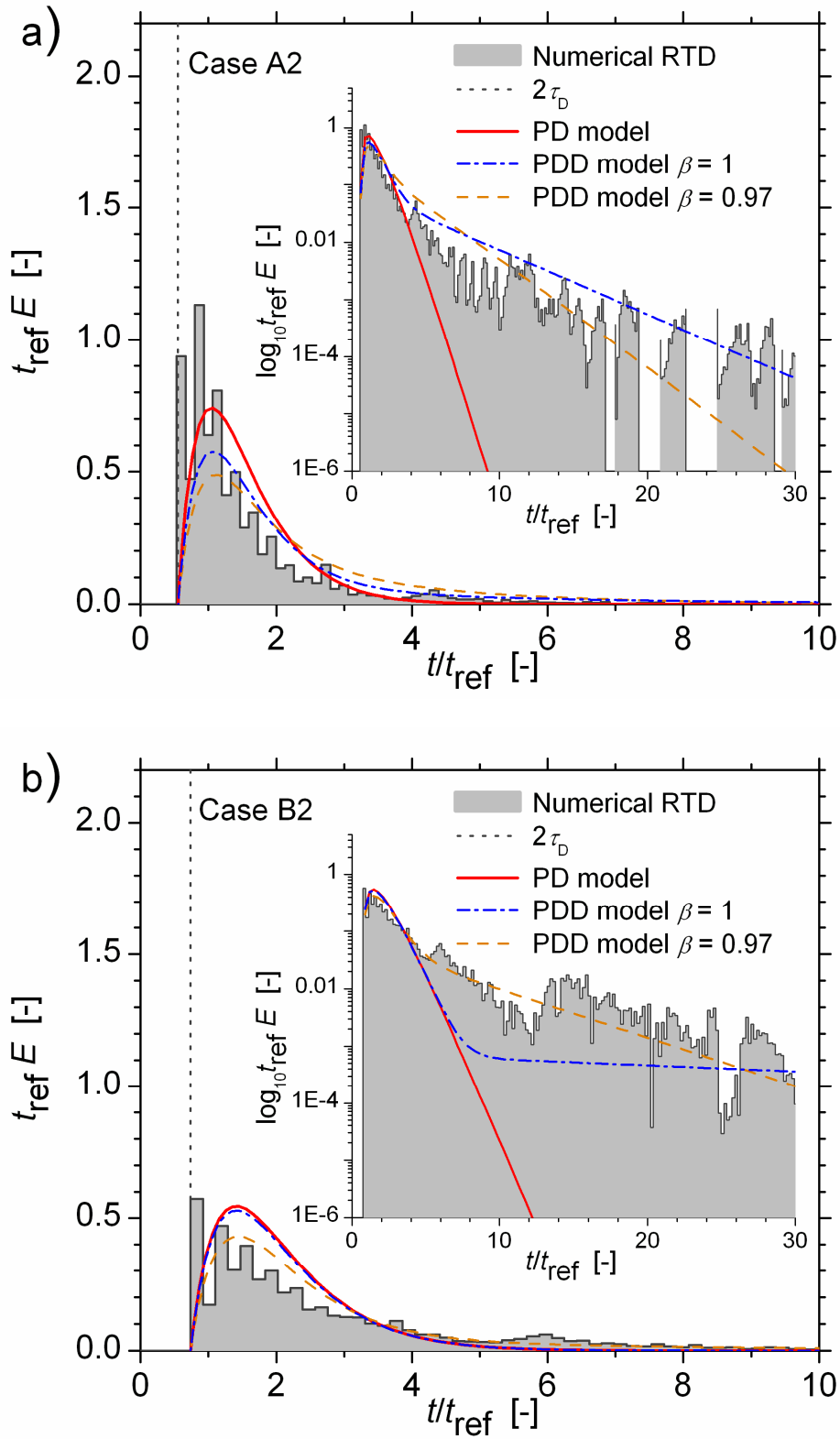


Fig. 12: Comparison of numerically evaluated RTD curves for case A2 (a) and B2 (b) with the PD model and the PDD model. The dashed vertical lines correspond to the delay time for each case.

Modelling the RTD for bubble train flow

4.2.2.2. RTD for three unit cells

For the PD model, the output signal for three unit cells is given by

$$E_{3UC}(t) = E_{2UC}(t) * E_{UC}(t) = \int_0^t E_{2UC}(t-t')E_{UC}(t')dt' \quad (67)$$

The evaluation of this convolution integral yields the result

$$E_{3UC}(t) = \frac{(t-3\tau_D)^2}{2\tau_S^3} \exp\left(-\frac{t-3\tau_D}{\tau_S}\right) H(t-3\tau_D), \quad (68)$$

see Appendix A.2.2.1. The mean residence time is

$$\tau_{3UC} \equiv \bar{t}_{3UC} = \int_0^{\infty} tE_{3UC}(t)dt = 3(\tau_S + \tau_D) = 3\tau_{UC}, \quad (69)$$

see Appendix A.2.2.2. The non-dimensional time for three unit cells is defined as

$$\theta_{3UC} \equiv \frac{t-3\tau_D}{3\tau_{UC}} \quad (70)$$

so that Eq. (68) can be written in the following non-dimensional form

$$E_{\theta,3UC} \equiv 3\tau_{UC}E_{3UC}(t) = \frac{\theta_{3UC}^2}{2} \left(3\frac{\tau_{UC}}{\tau_S}\right)^3 \exp\left(-3\theta_{3UC}\frac{\tau_{UC}}{\tau_S}\right) H(3\tau_{UC}\theta_{3UC}) \quad (71)$$

For the PDD model, the RTD $E_{3UC}^{\alpha}(t)$ for three unit cells becomes very complicated so that the convolution integral is evaluated by Laplace transformation. The result can be found at the end of Appendix C and is not repeated here.

In Fig. 13 we compare the RTD of the PD and PDD model for three unit cells with the numerically evaluated RTD curves for case A1 and B1. Similar as for two unit cells, there is a notable difference between the heights of the peaks. Higher residence times are not accurately represented by the PD model but are reasonably represented by the PDD model. However both for the PD model and the PDD model, the location of the maximum of the RTD is shifted to larger times as compared to the numerically evaluated RTD. It is expected that this discrepancy will even increase for larger numbers of unit cells in series.

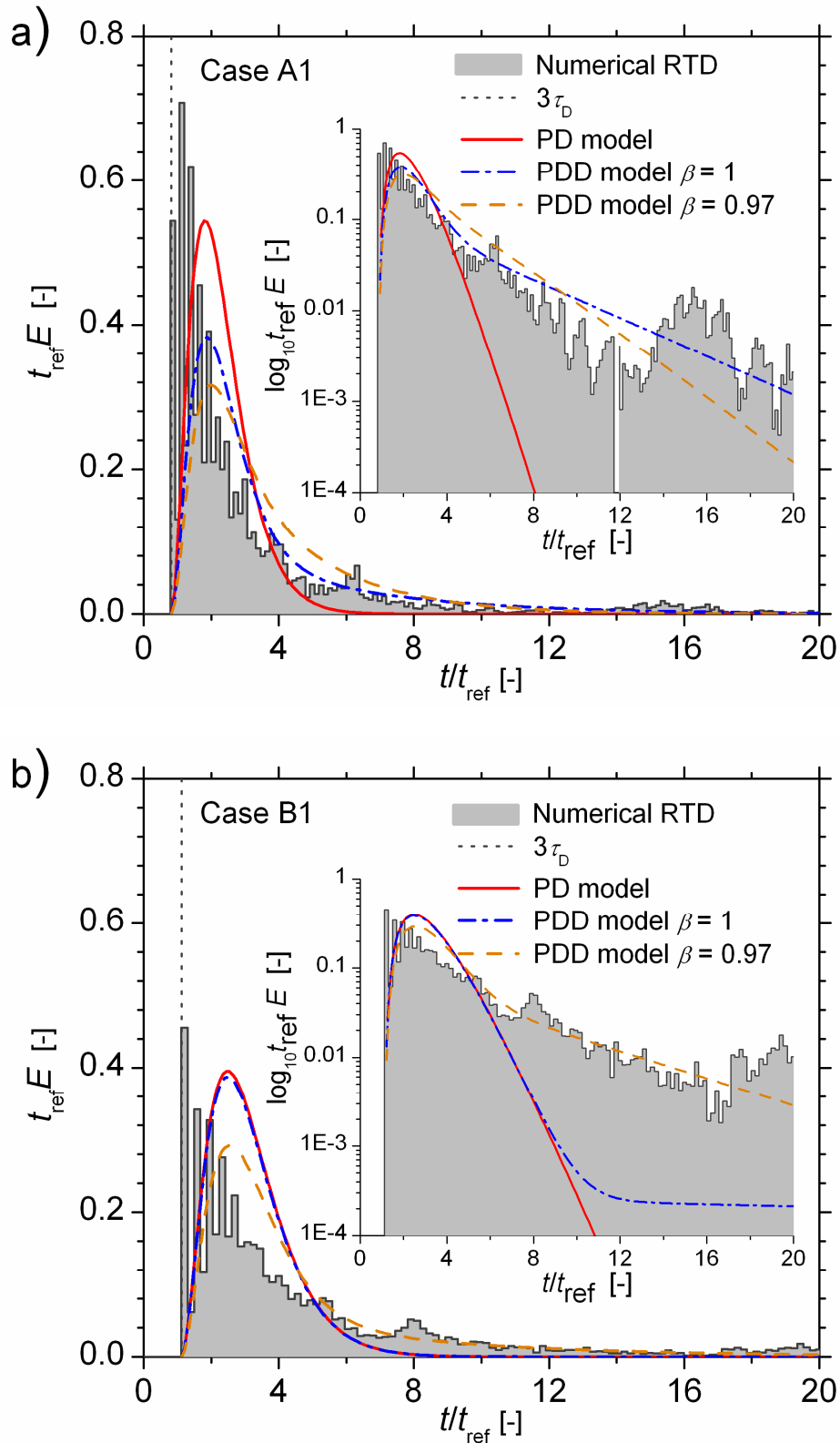


Fig. 13: Comparison of numerically evaluated RTD curves for $N_{\text{cross}}=3$ with convolutions of the PD model and PDD model for (a) case A1 and (b) case B1. The dashed vertical lines correspond to the delay time for each case.

4.2.2.3. General RTD model

The RTD of the PD model for four unit cells is

$$E_{4UC}(t) = \frac{(t-4\tau_D)^3}{6\tau_S^4} \exp\left(-\frac{t-4\tau_D}{\tau_S}\right) H(t-4\tau_D) \quad (72)$$

see Appendix A.2.3. The mean residence time is

$$\tau_{4UC} \equiv \bar{t}_{4UC} = \int_0^{\infty} t E_{4UC}(t) dt = 4(\tau_S + \tau_D) = 4\tau_{UC} \quad (73)$$

As shown in Appendix C, the PD model for n identical unit cells in series is

$$E_{nUC}(t) = \frac{(t-n\tau_D)^{n-1}}{(n-1)!\tau_S^n} \exp\left(-\frac{t-n\tau_D}{\tau_S}\right) H(t-n\tau_D) \quad (74)$$

The mean residence time of this RTD is

$$\tau_{nUC} = n(\tau_S + \tau_D) \quad (75)$$

With the non-dimensional time defined in Eq. (25), the RTD of the PD model for n unit cells can be written in the general form

$$E_{\theta, nUC}(\theta) = n\tau_{UC} E_{nUC}(t) = \frac{\theta^{n-1}}{(n-1)!} \left(n \frac{\tau_{UC}}{\tau_S}\right)^n \exp\left(-n\theta \frac{\tau_{UC}}{\tau_S}\right) H(n\tau_{UC}\theta) \quad (76)$$

This RTD for a cascade of n identical unit cells is equivalent to the RTD of a cascade of n identical CSTRs in series given in Eq. (20). For $\tau_D = 0$ we have $\tau_{UC} = \tau_S$ and Eq. (76) becomes identical to Eq. (20).

For the PDD model, the RTD becomes increasingly complex for an increasing number of unit cells, see Appendix C. Therefore, this model is hardly useful for large values of n . Thus, simpler models for a large number of unit cells shall be developed in future, which accurately represent the tail of the RTD, and, even more important, correctly predict both (i) the sharp increase of the RTD for values of t slightly higher than the delay time and (ii) the location of the maximum value of the RTD.

5. Conclusions

In this report, we used results from direct numerical simulations of a bubble train flow in a square vertical mini-channel to develop an analytical model for the prediction of the liquid phase residence time distribution from given integral flow parameters. For this purpose, the unit cell RTD model of Wörner, Ghidersa, Onea (2007) (the WGO model), which was developed for co-current upward flow and can be represented by a compartment model consisting of a plug flow reactor (PFR) and a continuous-stirred-tank reactor (CSTR) in series, was improved with respect to two aspects. First, in the peak-decay (PD) model the delay time of the RTD (which corresponds to the residence time of the PFR) is consistently formulated to be valid in both co-current upward and downward bubble train flow. Second, to account better for the long tails of the RTD, the compartment model was further refined and consists in the peak-decay-decay (PDD) model of a PFR in series with two CSTRs in parallel. The two CSTRs represent the liquid slug and liquid film / corner flow region, respectively. Both CSTRs have a different mean residence time. The resulting RTD consists of the superposition of two decaying exponential terms showing different slopes. It is shown that the PDD model accurately represents the numerically evaluated unit cell RTD for different flow conditions.

In practical applications, not the RTD of the unit cell but that of a bubble train flow consisting of a finite number of unit cells is of interest. In this report, the RTD for n unit cells in series is determined from the unit cell RTD by a $(n-1)$ -fold convolution procedure. For the PD model these convolutions can be evaluated analytically and yield a rather simple and general expression. For the PDD model, however, the analytical evaluation of these convolution integrals is becoming increasingly complex and is - without further approximations - of limited practical use for $n > 4$. The comparison of the convolution based PD and PDD models for $n = 2$ and $n = 3$ with the numerically evaluated RTD has shown, however, that the agreement is not satisfactory. In particular, the models overestimate the residence time for which the RTD has its maximum value. It appears that this discrepancy

Conclusions

even increases with increasing value of n . Thus we conclude that in future the RTD model for multiple unit cells should be further improved.

Concerning the unit cell RTD, further issues that should be investigated in future are the consideration of numerical simulations with longer liquid slugs and the reason for the appearance of a second peak in the numerically evaluated unit cell RTD at the residence time where - in a semi-logarithmic representation - the RTD changes its slope. While measurements of the unit cell RTD are not available in literature, there exist experimental data for a single channel that should be used for validation of the RTD model for multiple unit cells.

Acknowledgement

The authors gratefully acknowledge the supports of EU Erasmus program and of Institute of Science and Technology at Sakarya University. We also acknowledge the support of Dr. Hakan S. Soyhan who was the main supervisor of S.E. at Sakarya University, Turkey, during this research project for master thesis.

References

- Abiev, R. Sh., 2008. Simulation of the slug flow of a gas-liquid system in capillaries. *Theor. Found. Chem. Eng.* 42, 105–127.
- Angeli, P., Gavriilidis, A., 2008. Hydrodynamics of Taylor flow in small channels: a review. *Proc. IMechE Part C: J. Mech. Eng. Sci.* 222, 737–751.
- Bakker, J.J.W., Kreutzer, M., de Lathouder, K., Kapteijn, F., Moulijn, J.A., Wallin, S.A., 2005. Hydrodynamic properties of a novel ‘open wall’ monolith reactor. *Catalysis Today* 105, 385–390.
- Bauer, T., Guettel, R., Roy, S., Schubert, M., Al-Dahhan, M., Lange, R., 2005. Modelling and simulation of the monolithic reactor for gas-liquid-solid reactions. *Chem. Eng. Res. Design* 83, 811–819.
- Bradford, M.C.J., Tem M., Pollack, A., 2005. Monolith loop catalytic membrane reactor for Fischer-Tropsch synthesis. *Applied Catalysis A: General* 283, 39–46.
- Burns, J.R., Ramshaw, C., 2001. The intensification of rapid reactions in multiphase systems using slug flow in capillaries. *Lab Chip* 1, 10-15.
- De Deugd, R.M., Chougule, R.B., Kreutzer, M.T., Meeuse, F.M., Grievink, J., Kapteijn, F., Moulijn, J.A., 2003. Is a monolithic loop reactor a viable option for Fischer-Tropsch synthesis? *Chem. Eng. Sci.* 58, 583–591.
- Edvinsson Albers, R., Nyström, M., Siverström, M., Sellin, A., Dellve, A.-C., Andersson, U., Herrmann, W., Berglin, Th., 2001. Development of a monolith-based process for H₂O₂ production: from idea to large-scale implementation. *Catalysis Today* 69, 247–252.
- Fogler, H.S., 1986. *Elements of Chemical Reaction Engineering*. Prentice Hall.
- Fries, D.M., von Rohr, P.R., 2009. Impact of inlet design on mass transfer in gas-liquid rectangular microchannels. *Microfluid Nanofluid* 6, 27–35.

References

- Ghidersa, B., Wörner, M., Cacuci, D.G., 2004. Exploring the flow of immiscible fluids in a square vertical mini-channel by direct numerical simulation. *Chem. Eng. J.* 101, 285–294.
- Günther, A., Khan, S.A., Thalmann, M., Trachsel, F., Jensen, K.F., 2004. Transport and reaction in microscale segmented gas-liquid flow. *Lab Chip* 4, 278–286.
- Güttel R., Kunz, U., Turek, T., 2008. Reactors for Fischer-Tropsch synthesis. *Chem. Eng. Technol.* 31, 746–754.
- Haverkamp, V., Hessel, V., Löwe, H., Menges, G., Warnier, M.J.F., Rebrov, E.V., de Croon, M.H.J.M., Schouten, J.C., Liauw, M., 2006. Hydrodynamics and mixer-induced bubble formation in microbubble columns with single and multiple channels. *Chem. Eng. Technol.* 29, 1015–1026.
- Heibel, A.K., Lebens, P.J.M., Middelhoff, J.W., Kapteijn, F., Moulijn, J., 2005. Liquid residence time distribution in the film flow monolith reactor. *AIChE J.* 51, 122–133.
- Jähnisch, K., Baerns, M., Hessel, V., Ehrfeld, W., Haverkamp, V., Löwe, H., Wille, Ch., Guber, A., 2000. Direct fluorination of toluene using elemental fluorine in gas/liquid microreactors. *J. Fluor. Chem.* 105, 117–128.
- Kreutzer, M.T., Bakker, J.J.W., Kapteijn, F., Moulijn, J.A., Verheijen, P.J.T., 2005a. Scaling-up multiphase monolith reactors: linking residence time distribution and feed maldistribution. *Ind. Eng. Chem. Res.* 44, 4898–4913.
- Kreutzer, M.T., Kapteijn, F., Moulijn, J.A., Heiszwolf, J.J., 2005b. Multiphase monolith reactors: chemical reaction engineering of segmented flow in microchannels. *Chem. Eng. Sci.* 60, 5895–5916.
- Kulkarni, R., Natividad, R., Wood, J., Stitt, E.H., Winterbottom, J.M., 2005. A comparative study of residence time distribution and selectivity in a monolith CDC reactor and a trickle bed reactor. *Catalysis Today* 105, 455–463.
- Levenspiel, O., 1999. *Chemical Reaction Engineering*, third ed. Wiley, New York.

- Liu, W., Hu, J., Wang, Y., 2009. Fischer-Tropsch synthesis on ceramic monolith-structured catalysts. *Catalysis Today* 140, 142–148.
- Lohse, S., Kohnen, B.T., Janasek, D., Dittrich, P.S., Franzke, J., Agar, D.W., 2008. A novel method for determining the residence time distribution in intricately structured microreactors. *Lab Chip* 8, 431–438.
- Mantle, M.D., Sederman, A.J., Gladden, L.F., Raymahasay, S., Winterbottom, J.M., Stitt, E.H., 2002. Dynamic MRI visualization of two-phase flow in a ceramic monolith. *AIChE J.* 48, 909–912.
- Martin, A.D., 2000. Interpretation of residence time distribution data. *Chem. Eng. Sci.* 55, 5907–5917.
- Mc Collum, P.A., Brown, B.F., 1965. *Laplace Transform Tables and Theorems*. Holt, Rinehart and Winston, New York.
- Nauman, E.B., 2008. Residence time theory. *Ind. Eng. Chem. Res.* 47, 3752–3766.
- Özkan, F., Wörner, M., Wenka, A., Soyhan, H.S., 2007. Critical evaluation of CFD codes for interfacial simulation of bubble-train flow in a narrow channel. *Int. J. Numer. Meth. Fluids* 55, 537–564.
- Öztaskin, M.C., Wörner, M., Soyhan, H.S., 2009. Numerical investigation of the stability of bubble train flow in a square mini-channel. *Phys. Fluids* 21, 042108-1 – 042108-17.
- Patrick, R.H. Jr., Klindera, T., Crynes L.L., Cerro, R.L., Abraham, M.A., 1995. Residence time distribution in three-phase monolith reactor. *AIChE J.* 41, 649–657.
- Pedersen, H., Horvath, C., 1981. Axial dispersion in a segmented gas-liquid flow. *Ind. & Eng. Chem. Fund.* 20, 181–186.
- Roberts, G.E., Kaufman, H., 1966. *Table of Laplace Transforms*. W.B. Saunders Company, Philadelphia and New York.
- Roy, S., Bauer, T., Al-Dahhan, M., Lehner, P., Turek, S., 2004. Monoliths as multiphase reactors: a review. *AIChE J.* 50, 2918–2938.

References

- Sabisch, W., 2000. Dreidimensionale numerische Simulation der Dynamik von aufsteigenden Einzelblasen und Blasenschwärmen mit einer Volume-of-Fluid Methode. Forschungszentrum Karlsruhe, Wissenschaftliche Berichte FZKA 6478, Juni 2000.
- Sabisch, W., Wörner, M., Grötzbach, G., Cacuci, D.G., 2001. 3D volume-of-fluid simulation of a wobbling bubble in a gas–liquid system of low Morton number. In: Proc. 4th Int. Conf. Multiphase Flow, New Orleans, USA, May 27–June 1, 2001.
- Salman, W., Gavriilidis, A., Angeli, P., 2004. A model for predicting axial mixing during gas-liquid Taylor flow in microchannels at low Bodenstein numbers. *Chem. Eng. J.* 101, 391–396.
- Salman, W., Angeli, P., Gavriilidis, A., 2005. Sample pulse broadening in Taylor flow microchannels for screening applications. *Chem. Eng. Technol.* 28, 509–514.
- Salman, W., Gavriilidis, A., Angeli, P., 2007. Axial mass transfer in Taylor flow through circular microchannels. *AIChE J.* 53, 1413–1428.
- Shah, R.K., London, A.L., 1978. *Laminar flow forced convection in ducts*. Academic Press, pg. 198.
- Sun, J., Ju, J., Ji, L., Zhang, L., Xu, N., 2008. Synthesis of biodiesel in capillary microreactors. *Ind. Eng. Chem. Res.* 47, 1398–1403.
- Thulasidas, T.C., Abraham, M.A., Cerro, R.L., 1997. Flow patterns in liquid slugs during bubble-train flow inside capillaries. *Chem. Eng. Sci.* 52, 2947–2962.
- Thulasidas, T.C., Abraham, M.A., Cerro, R.L., 1999. Dispersion during bubble-train flow in capillaries. *Chem. Eng. Sci.* 54, 61–76.
- Trachsel, F., Günther, A., Khan, S., Jensen, K.F., 2005. Measurement of residence time distribution in microfluidic systems. *Chem. Eng. Sci.* 60, 5729–5737.
- Tsoligkas, A.N., Simmons, M.J.H., Wood, J., 2007. Influence of orientation upon the hydrodynamics of gas-liquid flow for square channels in monolith supports. *Chem. Eng. Sci.* 62, 4365–4378.

Wörner, M., Ghidersa, B., Onea, A., 2007. A model for the residence time distribution of bubble-train-flow in a square mini-channel based on direct numerical simulation results. *Int. J. Heat Fluid Flow*, 28, 83–94.

Yawalkar, A.A., Sood, R., Kreutzer, M.T., Kapteijn, F., Moulijn, J.A., 2005. Axial mixing in monolith reactors: effect of channel size. *Ind. Eng. Chem. Res.* 44, 2046–2057.

Appendix A. Integral evaluations for PD model

To evaluate the various integrals in this Appendix and in Appendix B we will - without further notice - take advantage of the identity

$$\int_0^{\infty} z^{n-1} e^{-z/a} dz = (n-1)! a^n$$

A.1. Evaluations for one unit cell

A.1.1. Integral of RTD

The integral of the PD model for one unit cell is

$$\begin{aligned} \int_0^{\infty} E_{UC}(t) dt &= \int_0^{\infty} H(t - \tau_D) \tau_S^{-1} e^{-(t-\tau_D)/\tau_S} dt = \int_{\tau_D}^{\infty} \tau_S^{-1} e^{-(t-\tau_D)/\tau_S} dt = \tau_S^{-1} e^{\tau_D/\tau_S} \int_{\tau_D}^{\infty} e^{-t/\tau_S} dt \\ &= \tau_S^{-1} e^{\tau_D/\tau_S} \left[-\tau_S e^{-t/\tau_S} \right]_{\tau_D}^{\infty} = -e^{\tau_D/\tau_S} \left[e^{-t/\tau_S} \right]_{\tau_D}^{\infty} = -e^{\tau_D/\tau_S} \left[0 - e^{-\tau_D/\tau_S} \right] = e^0 = 1 \end{aligned}$$

A.1.2. Mean residence time

The mean residence time of the PD model for one unit cell is

$$\begin{aligned} \tau_{UC} &= \int_0^{\infty} t E_{UC}(t) dt = \int_0^{\infty} t H(t - \tau_D) \tau_S^{-1} e^{-(t-\tau_D)/\tau_S} dt = \int_{\tau_D}^{\infty} t \tau_S^{-1} e^{-(t-\tau_D)/\tau_S} dt = \tau_S^{-1} e^{\tau_D/\tau_S} \int_{\tau_D}^{\infty} t e^{-t/\tau_S} dt \\ &= \tau_S^{-1} e^{\tau_D/\tau_S} \left[\tau_S^2 (-t\tau_S^{-1} - 1) e^{-t/\tau_S} \right]_{\tau_D}^{\infty} = -\tau_S e^{\tau_D/\tau_S} \left[(t\tau_S^{-1} + 1) e^{-t/\tau_S} \right]_{\tau_D}^{\infty} = -\tau_S e^{\tau_D/\tau_S} \left[t\tau_S^{-1} e^{-t/\tau_S} + e^{-t/\tau_S} \right]_{\tau_D}^{\infty} \\ &= -\tau_S e^{\tau_D/\tau_S} \left[\lim_{t \rightarrow \infty} t\tau_S^{-1} e^{-t/\tau_S} + 0 - (\tau_D\tau_S^{-1} e^{-\tau_D/\tau_S}) - e^{-\tau_D/\tau_S} \right] = -\tau_S e^{\tau_D/\tau_S} \left[\lim_{t \rightarrow \infty} \frac{t}{\tau_S e^{t/\tau_S}} - e^{-\tau_D/\tau_S} (\tau_D\tau_S^{-1} + 1) \right] \\ &= -\tau_S e^{\tau_D/\tau_S} \left[\frac{\lim_{t \rightarrow \infty} 1}{\lim_{t \rightarrow \infty} e^{z/\tau_S}} - e^{-\tau_D/\tau_S} (\tau_D\tau_S^{-1} + 1) \right] = -\tau_S e^{\tau_D/\tau_S} \left[\frac{1}{\infty} - e^{-\tau_D/\tau_S} (\tau_D\tau_S^{-1} + 1) \right] = \tau_D + \tau_S \end{aligned}$$

A.1.3. Variance

The variance of the PD model for one unit cell is

$$\sigma_{UC}^2 = \int_0^{\infty} (t - \bar{t}_{UC})^2 E_{UC}(t) dt = \int_0^{\infty} (t - (\tau_D + \tau_S))^2 H(t - \tau_D) \tau_S^{-1} e^{-(t-\tau_D)/\tau_S} dt$$

We introduce the substitution $z \equiv t - \tau_D$ so that $dz = dt$. This gives

$$\begin{aligned}
 \sigma_{\text{UC}}^2 &= \int_0^{\infty} (t - (\tau_D + \tau_S))^2 H(t - \tau_D) \tau_S^{-1} e^{-(t - \tau_D)/\tau_S} dt = \int_{-\tau_D}^{\infty} (z - \tau_S)^2 H(z) \tau_S^{-1} e^{-z/\tau_S} dz \\
 &= \tau_S^{-1} \int_0^{\infty} (z^2 - 2z\tau_S + \tau_S^2) e^{-z/\tau_S} dz = \tau_S^{-1} \left[\int_0^{\infty} (z^2 e^{-z/\tau_S} - 2\tau_S z e^{-z/\tau_S} + \tau_S^2 e^{-z/\tau_S}) dz \right] \\
 &= \tau_S^{-1} \left\{ \left[(-z^2 \tau_S - 2z\tau_S^2 - 2\tau_S^3) e^{-z/\tau_S} \right]_0^{\infty} - 2\tau_S \left[\tau_S^2 (-z\tau_S^{-1} - 1) e^{-z/\tau_S} \right]_0^{\infty} + \tau_S^2 \left[-\tau_S e^{-z/\tau_S} \right]_0^{\infty} \right\} \\
 &= \tau_S^{-1} \left\{ \left[\left(-\lim_{z \rightarrow \infty} (z^2 \tau_S e^{-z/\tau_S}) - \lim_{z \rightarrow \infty} (2z\tau_S^2 e^{-z/\tau_S}) \right) + 2\tau_S^3 \right] + 2\tau_S^3 \left[\lim_{z \rightarrow \infty} z\tau_S^{-1} e^{-z/\tau_S} - 1 \right] - \tau_S^3 [0 - 1] \right\} \\
 &= \tau_S^{-1} \left[\left(2\tau_S^3 - \lim_{z \rightarrow \infty} \frac{2z\tau_S}{\tau_S^{-1} e^{z/\tau_S}} - \frac{\lim_{z \rightarrow \infty} 2\tau_S^2}{\lim_{z \rightarrow \infty} \tau_S^{-1} e^{z/\tau_S}} \right) + 2\tau_S^3 \left(\lim_{z \rightarrow \infty} \frac{z}{\tau_S e^{z/\tau_S}} - 1 \right) + \tau_S^3 \right] \\
 &= \tau_S^{-1} \left[\left(2\tau_S^3 - \frac{\lim_{z \rightarrow \infty} 2\tau_S}{\lim_{z \rightarrow \infty} \tau_S^{-2} e^{z/\tau_S}} - \frac{2\tau_S^2}{\infty} \right) + 2\tau_S^3 \left(\frac{\lim_{z \rightarrow \infty} 1}{\lim_{z \rightarrow \infty} e^{z/\tau_S}} - 1 \right) + \tau_S^3 \right] \\
 &= \tau_S^{-1} \left[\left(2\tau_S^3 - \frac{2\tau_S}{\infty} \right) + 2\tau_S^3 (0 - 1) + \tau_S^3 \right] = \tau_S^{-1} (2\tau_S^3 - 2\tau_S^3 + \tau_S^3) = \tau_S^2
 \end{aligned}$$

A.2. Evaluations for multiple unit cells

A.2.1. Evaluations for two unit cells

A.2.1.1. Convolution integral for two unit cells

The convolution integral of the PD model for two unit cells is

$$E_{2\text{UC}}(t) = E_{\text{UC}}(t) * E_{\text{UC}}(t) = \int_0^t E_{\text{UC}}(t - t') E_{\text{UC}}(t') dt'$$

This integral is given by

$$\begin{aligned}
 E_{2\text{UC}}(t) &= \int_0^t H(t - t' - \tau_D) \tau_S^{-1} e^{-(t - t' - \tau_D)/\tau_S} H(t' - \tau_D) \tau_S^{-1} e^{-(t' - \tau_D)/\tau_S} dt' \\
 &= \int_0^t H(t - t' - \tau_D) H(t' - \tau_D) \tau_S^{-2} e^{-(t - 2\tau_D)/\tau_S} dt' = \tau_S^{-2} e^{-(t - 2\tau_D)/\tau_S} \int_0^t H(t - t' - \tau_D) H(t' - \tau_D) dt'
 \end{aligned}$$

To evaluate the integral with the two Heaviside step functions we introduce the substitution

$u \equiv t' - \tau_D$ so that $du = dt'$. This gives

$$I \equiv \int_0^t H(t - t' - \tau_D) H(t' - \tau_D) dt' = \int_{-\tau_D}^{t - \tau_D} H(t - u - 2\tau_D) H(u) du = \int_0^{t - \tau_D} H(t - u - 2\tau_D) du$$

Next we introduce a second substitution $w \equiv -u + t - 2\tau_D$ so that $dw = -du$. This gives

$$\begin{aligned} I &= \int_0^{t-2\tau_D} H(t-u-2\tau_D) du = - \int_{t-2\tau_D}^{-\tau_D} H(w) dw = \int_{-\tau_D}^{t-2\tau_D} H(w) dw = \int_0^{t-2\tau_D} H(w) dw \\ &= H(t-2\tau_D) \int_0^{t-2\tau_D} dw = H(t-2\tau_D) [w]_0^{t-2\tau_D} = (t-2\tau_D)H(t-2\tau_D) \end{aligned}$$

Thus, we obtain

$$E_{2UC}(t) = H(t-2\tau_D)(t-2\tau_D)\tau_S^{-2} e^{-(t-2\tau_D)/\tau_S}$$

The integral of $E_{2UC}(t)$ is given by

$$\int_0^{\infty} E_{2UC}(t) dt = \int_0^{\infty} H(t-2\tau_D)(t-2\tau_D)\tau_S^{-2} e^{-(t-2\tau_D)/\tau_S} dt$$

We introduce the substitution $z \equiv t - 2\tau_D$ and obtain

$$\begin{aligned} \int_0^{\infty} E_{2UC}(t) dt &= \int_0^{\infty} H(t-2\tau_D)(t-2\tau_D)\tau_S^{-2} e^{-(t-2\tau_D)/\tau_S} dt = \int_{-2\tau_D}^{\infty} H(z)z\tau_S^{-2} e^{-z/\tau_S} dz \\ &= \tau_S^{-2} \int_0^{\infty} z e^{-z/\tau_S} dz = \tau_S^{-2} \left[\tau_S^2 (-z\tau_S^{-1} - 1) e^{-z/\tau_S} \right]_0^{\infty} = - \left[(z\tau_S^{-1} + 1) e^{-z/\tau_S} \right]_0^{\infty} = - \left[z\tau_S^{-1} e^{-z/\tau_S} + e^{-z/\tau_S} \right]_0^{\infty} \\ &= - \lim_{z \rightarrow \infty} z\tau_S^{-1} e^{-z/\tau_S} - 0 + 0 + 1 = 1 - \lim_{z \rightarrow \infty} \frac{z}{\tau_S} e^{z/\tau_S} = 1 - \frac{\lim_{z \rightarrow \infty} 1}{\lim_{z \rightarrow \infty} e^{z/\tau_S}} = 1 - \frac{1}{\infty} = 1 \end{aligned}$$

A.2.1.2. Mean residence time for two unit cells

The mean residence time for a length of two unit cells is

$$\bar{t}_{2UC} = \int_0^{\infty} t E_{2UC}(t) dt = \int_0^{\infty} t H(t-2\tau_D)(t-2\tau_D)\tau_S^{-2} e^{-(t-2\tau_D)/\tau_S} dt$$

We introduce the substitution $z \equiv t - 2\tau_D$ and obtain

$$\begin{aligned} \bar{t}_{2UC} &= \int_0^{\infty} t E_{2UC}(t) dt = \int_0^{\infty} t H(t-2\tau_D)(t-2\tau_D)\tau_S^{-2} e^{-(t-2\tau_D)/\tau_S} dt = \int_{-2\tau_D}^{\infty} (z+2\tau_D)H(z)z\tau_S^{-2} e^{-z/\tau_S} dz \\ &= \int_0^{\infty} (z+2\tau_D)z\tau_S^{-2} e^{-z/\tau_S} dz = \tau_S^{-2} \int_0^{\infty} \left[z^2 e^{-z/\tau_S} + 2\tau_D z e^{-z/\tau_S} \right] dz \end{aligned}$$

and thus

$$\begin{aligned}\bar{t}_{2UC} &= \tau_S^{-2} \left\{ \left[(-z^2 \tau_S - 2z\tau_S^2 - 2\tau_S^3) e^{-z/\tau_S} \right]_0^\infty + 2\tau_D \left[\tau_S^2 (-z\tau_S^{-1} - 1) e^{-z/\tau_S} \right]_0^\infty \right\} \\ &= \tau_S^{-2} \left[2\tau_S^3 + 2\tau_D \tau_S^2 \right] = 2(\tau_S + \tau_D)\end{aligned}$$

A.2.2. Evaluations for three unit cells

A.2.2.1. Convolution integral for three unit cells

The convolution integral of the PD model for three unit cells is

$$E_{3UC}(t) = E_{2UC}(t) * E_{UC}(t) = \int_0^t E_{2UC}(t-t') E_{UC}(t') dt'$$

This integral is given by

$$\begin{aligned}E_{3UC}(t) &= \int_0^t H(t-t'-2\tau_D)(t-t'-2\tau_D) \tau_S^{-2} e^{-(t-t'-2\tau_D)/\tau_S} H(t'-\tau_D) \tau_S^{-1} e^{-(t'-\tau_D)/\tau_S} dt' \\ &= \int_0^t H(t-t'-2\tau_D) H(t'-\tau_D) (t-t'-2\tau_D) \tau_S^{-3} e^{-(t-3\tau_D)/\tau_S} dt' \\ &= \tau_S^{-3} e^{-(t-3\tau_D)/\tau_S} \int_0^t (t-t'-2\tau_D) H(t-t'-2\tau_D) H(t'-\tau_D) dt'\end{aligned}$$

To evaluate the integral with the two Heaviside step functions we introduce the substitution

$u \equiv t' - \tau_D$ so that $du = dt'$. This gives

$$\begin{aligned}I &\equiv \int_0^t (t-t'-2\tau_D) H(t-t'-2\tau_D) H(t'-\tau_D) dt' = \int_{-\tau_D}^{t-\tau_D} (t-u-3\tau_D) H(t-u-3\tau_D) H(u) du \\ &= \int_0^{t-\tau_D} (t-u-3\tau_D) H(t-u-3\tau_D) du\end{aligned}$$

Next we introduce a second substitution $w \equiv -u + t - 3\tau_D$ so that $dw = -du$. This gives

$$\begin{aligned}I &= \int_0^{t-\tau_D} (t-u-3\tau_D) H(t-u-3\tau_D) du = - \int_{t-3\tau_D}^{-2\tau_D} w H(w) dw = \int_{-2\tau_D}^{t-3\tau_D} w H(w) dw = \int_0^{t-3\tau_D} w H(w) dw \\ &= H(t-3\tau_D) \int_0^{t-3\tau_D} w dw = H(t-3\tau_D) \left[\frac{w^2}{2} \right]_0^{t-3\tau_D} = \frac{1}{2} (t-3\tau_D)^2 H(t-3\tau_D)\end{aligned}$$

Thus, we obtain

$$E_{3UC}(t) = H(t - 3\tau_D) \frac{1}{2} (t - 3\tau_D)^2 \tau_S^{-3} e^{-(t-3\tau_D)/\tau_S}$$

The integral of $E_{3UC}(t)$ is given by

$$\int_0^{\infty} E_{3UC}(t) dt = \int_0^{\infty} \frac{1}{2} H(t - 3\tau_D) (t - 3\tau_D)^2 \tau_S^{-3} e^{-(t-3\tau_D)/\tau_S} dt$$

We introduce the substitution $z \equiv t - 3\tau_D$ and obtain

$$\begin{aligned} \int_0^{\infty} E_{3UC}(t) dt &= \int_0^{\infty} \frac{1}{2} H(t - 3\tau_D) (t - 3\tau_D)^2 \tau_S^{-3} e^{-(t-3\tau_D)/\tau_S} dt = \int_{-3\tau_D}^{\infty} \frac{1}{2} H(z) z^2 \tau_S^{-3} e^{-z/\tau_S} dz \\ &= \frac{1}{2} \tau_S^{-3} \int_0^{\infty} z^2 e^{-z/\tau_S} dz = \frac{1}{2} \tau_S^{-3} \left[(-z^2 \tau_S - 2z\tau_S^2 - 2\tau_S^3) e^{-z/\tau_S} \right]_0^{\infty} \\ &= \frac{1}{2} \tau_S^{-3} \left[-z^2 \tau_S e^{-z/\tau_S} - 2z\tau_S^2 e^{-z/\tau_S} - 2\tau_S^3 e^{-z/\tau_S} \right]_0^{\infty} \\ &= \frac{1}{2} \tau_S^{-3} \left[\left(-\lim_{z \rightarrow \infty} (z^2 \tau_S e^{-z/\tau_S}) - \lim_{z \rightarrow \infty} (2z\tau_S^2 e^{-z/\tau_S}) - 0 \right) + 0 + 0 + 2\tau_S^3 \right] \\ &= \frac{1}{2} \tau_S^{-3} \left(2\tau_S^3 - \lim_{z \rightarrow \infty} \frac{z^2 \tau_S}{e^{z/\tau_S}} - \lim_{z \rightarrow \infty} \frac{2z\tau_S^2}{e^{z/\tau_S}} \right) = \frac{1}{2} \tau_S^{-3} \left(2\tau_S^3 - \lim_{z \rightarrow \infty} \frac{2z\tau_S}{\tau_S^{-1} e^{z/\tau_S}} - \frac{\lim_{z \rightarrow \infty} 2\tau_S^2}{\lim_{z \rightarrow \infty} \tau_S^{-1} e^{z/\tau_S}} \right) \\ &= \frac{1}{2} \tau_S^{-3} \left(2\tau_S^3 - \frac{\lim_{z \rightarrow \infty} 2\tau_S}{\lim_{z \rightarrow \infty} \tau_S^{-2} e^{z/\tau_S}} - \frac{2\tau_S^2}{\infty} \right) = \frac{1}{2} \tau_S^{-3} \left(2\tau_S^3 - \frac{2\tau_S}{\infty} \right) = 1 \end{aligned}$$

A.2.2.2. Mean residence time for three unit cells

The mean residence time for three unit cells is

$$\bar{t}_{3UC} = \int_0^{\infty} t E_{3UC}(t) dt = \int_0^{\infty} t \frac{1}{2} H(t - 3\tau_D) (t - 3\tau_D)^2 \tau_S^{-3} e^{-(t-3\tau_D)/\tau_S} dt$$

We introduce the substitution $z \equiv t - 3\tau_D$ and obtain

$$\begin{aligned} \bar{t}_{3UC} &= \int_0^{\infty} t E_{3UC}(t) dt = \int_0^{\infty} t \frac{1}{2} H(t - 3\tau_D) (t - 3\tau_D)^2 \tau_S^{-3} e^{-(t-3\tau_D)/\tau_S} dt = \int_{-3\tau_D}^{\infty} \frac{1}{2} (z + 3\tau_D) H(z) z^2 \tau_S^{-3} e^{-z/\tau_S} dz \\ &= \frac{1}{2} \tau_S^{-3} \int_0^{\infty} (z + 3\tau_D) z^2 e^{-z/\tau_S} dz = \frac{1}{2} \tau_S^{-3} \int_0^{\infty} [z^3 e^{-z/\tau_S} + 3\tau_D z^2 e^{-z/\tau_S}] dz \end{aligned}$$

and thus

$$\begin{aligned}\bar{t}_{3UC} &= \frac{1}{2} \tau_S^{-3} \left\{ \left[-\tau_S z^3 e^{-z/\tau_S} \right]_0^\infty - \left(-3\tau_S \int_0^\infty z^2 e^{-z/\tau_S} du \right) \right\} + 3\tau_D \left[\left(-z^2 \tau_S - 2z\tau_S^2 - 2\tau_S^3 \right) e^{-z/\tau_S} \right]_0^\infty \Big\} \\ &= \frac{1}{2} \tau_S^{-3} (6\tau_S^4 + 3\tau_D 2\tau_S^3) = 3(\tau_S + \tau_D)\end{aligned}$$

A.2.3. Evaluations for four unit cells

The convolution integral for four unit cells is

$$E_{4UC}(t) = E_{3UC}(t) * E_{UC}(t) = \int_0^t E_{3UC}(t-t') E_{UC}(t') dt'$$

This integral is given by

$$\begin{aligned}E_{4UC}(t) &= \int_0^t \frac{1}{2} H(t-t'-3\tau_D) (t-t'-3\tau_D)^2 \tau_S^{-3} e^{-(t-t'-3\tau_D)/\tau_S} H(t'-\tau_D) \tau_S^{-1} e^{-(t'-\tau_D)/\tau_S} dt' \\ &= \int_0^t \frac{1}{2} H(t-t'-3\tau_D) H(t'-\tau_D) (t-t'-3\tau_D)^2 \tau_S^{-4} e^{-(t-4\tau_D)/\tau_S} dt' \\ &= \frac{1}{2} \tau_S^{-4} e^{-(t-4\tau_D)/\tau_S} \int_0^t (t-t'-3\tau_D)^2 H(t-t'-3\tau_D) H(t'-\tau_D) dt'\end{aligned}$$

To evaluate the integral we introduce the substitution $u \equiv t' - \tau_D$ so that $du = dt'$. This gives

$$\begin{aligned}I \equiv \int_0^t (t-t'-3\tau_D)^2 H(t-t'-3\tau_D) H(t'-\tau_D) dt' &= \int_{-\tau_D}^{t-\tau_D} (t-u-4\tau_D)^2 H(t-u-4\tau_D) H(u) du \\ &= \int_0^{t-\tau_D} (t-u-4\tau_D)^2 H(t-u-4\tau_D) du\end{aligned}$$

Next we introduce a second substitution $w \equiv -u + t - 4\tau_D$ so that $dw = -du$. This gives

$$\begin{aligned}I &= \int_0^{t-\tau_D} (t-u-4\tau_D)^2 H(t-u-4\tau_D) du = - \int_{t-4\tau_D}^{-3\tau_D} w^2 H(w) dw = \int_{-3\tau_D}^{t-4\tau_D} w^2 H(w) dw = \int_0^{t-4\tau_D} w^2 H(w) dw \\ &= H(t-4\tau_D) \int_0^{t-4\tau_D} w^2 dw = H(t-4\tau_D) \left[\frac{w^3}{3} \right]_0^{t-4\tau_D} = \frac{1}{3} (t-4\tau_D)^3 H(t-4\tau_D)\end{aligned}$$

Thus, we obtain

$$E_{4UC}(t) = H(t-4\tau_D) \frac{1}{6} (t-4\tau_D)^3 \tau_S^{-4} e^{-(t-4\tau_D)/\tau_S}$$

Appendix B. Integral evaluations for the PDD model

B.1. Evaluations for one unit cell

B.1.1. Integral of the PDD model

The integral of the PDD model is

$$\begin{aligned}
 \int_0^{\infty} E_{UC}^{\alpha}(t) dt &= \int_0^{\infty} H(t - \tau_D) \left[\alpha \tau_S^{-1} e^{-(t-\tau_D)/\tau_S} + (1-\alpha) \tau_F^{-1} e^{-(t-\tau_D)/\tau_F} \right] dt \\
 &= \int_{\tau_D}^{\infty} \left[\alpha \tau_S^{-1} e^{-(t-\tau_D)/\tau_S} + (1-\alpha) \tau_F^{-1} e^{-(t-\tau_D)/\tau_F} \right] dt \\
 &= \alpha \tau_S^{-1} e^{\tau_D/\tau_S} \int_{\tau_D}^{\infty} e^{-t/\tau_S} dt + (1-\alpha) \tau_F^{-1} e^{\tau_D/\tau_F} \int_{\tau_D}^{\infty} e^{-t/\tau_F} dt \\
 &= \alpha \tau_S^{-1} e^{\tau_D/\tau_S} \left[-\tau_S e^{-t/\tau_S} \right]_{\tau_D}^{\infty} + (1-\alpha) \tau_F^{-1} e^{\tau_D/\tau_F} \left[-\tau_F e^{-t/\tau_F} \right]_{\tau_D}^{\infty} \\
 &= -\alpha e^{\tau_D/\tau_S} \left[0 - e^{-\tau_D/\tau_S} \right] - (1-\alpha) e^{\tau_D/\tau_F} \left[0 - e^{-\tau_D/\tau_F} \right] = \alpha + (1-\alpha) = 1
 \end{aligned}$$

B.1.2. Mean residence time

The mean residence time of the PDD model for a single unit cell is

$$\bar{t}_{UC}^{\alpha} = \int_0^{\infty} t E_{UC}^{\alpha}(t) dt = \int_0^{\infty} t H(t - \tau_D) \left[\alpha \tau_S^{-1} e^{-(t-\tau_D)/\tau_S} + (1-\alpha) \tau_F^{-1} e^{-(t-\tau_D)/\tau_F} \right] dt$$

To evaluate the integral we introduce the substitution $z \equiv t - \tau_D$ so that $dz = dt$. This gives

$$\begin{aligned}
 \bar{t}_{UC}^{\alpha} &= \int_0^{\infty} t H(t - \tau_D) \left[\alpha \tau_S^{-1} e^{-(t-\tau_D)/\tau_S} + (1-\alpha) \tau_F^{-1} e^{-(t-\tau_D)/\tau_F} \right] dt \\
 &= \int_{-\tau_D}^{\infty} (z + \tau_D) H(z) \left[\alpha \tau_S^{-1} e^{-z/\tau_S} + (1-\alpha) \tau_F^{-1} e^{-z/\tau_F} \right] dz \\
 &= \int_0^{\infty} (z + \tau_D) \left[\alpha \tau_S^{-1} e^{-z/\tau_S} + (1-\alpha) \tau_F^{-1} e^{-z/\tau_F} \right] dz
 \end{aligned}$$

and

$$\begin{aligned}
 \bar{t}_{UC}^{\alpha} &= \tau_D \int_0^{\infty} \left[\alpha \tau_S^{-1} e^{-z/\tau_S} + (1-\alpha) \tau_F^{-1} e^{-z/\tau_F} \right] dz + \int_0^{\infty} \left[\alpha \tau_S^{-1} z e^{-z/\tau_S} + (1-\alpha) \tau_F^{-1} z e^{-z/\tau_F} \right] dz \\
 &= \tau_D \left[\alpha \tau_S^{-1} \tau_S + (1-\alpha) \tau_F^{-1} \tau_F \right] + \alpha \tau_S^{-1} \tau_S^2 + (1-\alpha) \tau_F^{-1} \tau_F^2 = \tau_D + \alpha \tau_S + (1-\alpha) \tau_F
 \end{aligned}$$

B.1.3. Variance

The variance of the PDD model for a single unit cell can be computed as follows

$$\begin{aligned}\sigma_{\alpha UC}^2 &= \int_0^{\infty} (t - \bar{t}_{UC}^{\alpha})^2 E_{UC}^{\alpha}(t) dt \\ &= \int_0^{\infty} [t - (\tau_D + \alpha\tau_S + (1-\alpha)\tau_F)]^2 H(t - \tau_D) [\alpha\tau_S^{-1} e^{-(t-\tau_D)/\tau_S} + (1-\alpha)\tau_F^{-1} e^{-(t-\tau_D)/\tau_F}] dt\end{aligned}$$

We introduce the substitution $z \equiv t - \tau_D$ so that $dz = dt$. This gives

$$\begin{aligned}\sigma_{\alpha UC}^2 &= \int_0^{\infty} [t - (\tau_D + \alpha\tau_S + (1-\alpha)\tau_F)]^2 H(t - \tau_D) [\alpha\tau_S^{-1} e^{-(t-\tau_D)/\tau_S} + (1-\alpha)\tau_F^{-1} e^{-(t-\tau_D)/\tau_F}] dt \\ &= \int_{-\tau_D}^{\infty} [z - (\alpha\tau_S + (1-\alpha)\tau_F)]^2 H(z) [\alpha\tau_S^{-1} e^{-z/\tau_S} + (1-\alpha)\tau_F^{-1} e^{-z/\tau_F}] dz \\ &= \int_0^{\infty} [z^2 - 2z(\alpha\tau_S + (1-\alpha)\tau_F) + (\alpha\tau_S + (1-\alpha)\tau_F)^2] [\alpha\tau_S^{-1} e^{-z/\tau_S} + (1-\alpha)\tau_F^{-1} e^{-z/\tau_F}] dz \\ &= \int_0^{\infty} [\alpha\tau_S^{-1} z^2 e^{-z/\tau_S} + (1-\alpha)\tau_F^{-1} z^2 e^{-z/\tau_F}] dz \\ &\quad - 2[\alpha\tau_S + (1-\alpha)\tau_F] \int_0^{\infty} [\alpha\tau_S^{-1} z e^{-z/\tau_S} + (1-\alpha)\tau_F^{-1} z e^{-z/\tau_F}] dz \\ &\quad + [\alpha\tau_S + (1-\alpha)\tau_F]^2 \int_0^{\infty} [\alpha\tau_S^{-1} e^{-z/\tau_S} + (1-\alpha)\tau_F^{-1} e^{-z/\tau_F}] dz\end{aligned}$$

We obtain

$$\begin{aligned}\sigma_{\alpha UC}^2 &= \int_0^{\infty} [\alpha\tau_S^{-1} z^2 e^{-z/\tau_S} + (1-\alpha)\tau_F^{-1} z^2 e^{-z/\tau_F}] dz \\ &\quad - 2[\alpha\tau_S + (1-\alpha)\tau_F] \int_0^{\infty} [\alpha\tau_S^{-1} z e^{-z/\tau_S} + (1-\alpha)\tau_F^{-1} z e^{-z/\tau_F}] dz \\ &\quad + [\alpha\tau_S + (1-\alpha)\tau_F]^2 \int_0^{\infty} [\alpha\tau_S^{-1} e^{-z/\tau_S} + (1-\alpha)\tau_F^{-1} e^{-z/\tau_F}] dz \\ &= \alpha\tau_S^{-1} \cdot 2\tau_S^3 + (1-\alpha)\tau_F^{-1} \cdot 2\tau_F^3 - 2[\alpha\tau_S + (1-\alpha)\tau_F] [\alpha\tau_S^{-1} \tau_S^2 + (1-\alpha)\tau_F^{-1} \tau_F^2] \\ &\quad + [\alpha\tau_S + (1-\alpha)\tau_F]^2 [\alpha\tau_S^{-1} \tau_S + (1-\alpha)\tau_F^{-1} \tau_F]\end{aligned}$$

and after simplification

$$\sigma_{\alpha UC}^2 = 2\alpha\tau_S^2 + 2(1-\alpha)\tau_F^2 - [\alpha\tau_S + (1-\alpha)\tau_F]^2$$

B.2. Evaluations for the PDD model and multiple unit cells

B.2.1. Two unit cells

B.2.1.1. Convolution integral

The convolution integral of the PDD model for two unit cells is

$$E_{2\text{UC}}^\alpha(t) = E_{\text{UC}}^\alpha(t) * E_{\text{UC}}^\alpha(t) = \int_0^t E_{\text{UC}}^\alpha(t-t')E_{\text{UC}}^\alpha(t')dt'$$

This integral is given by

$$\begin{aligned} E_{2\text{UC}}^\alpha(t) &= \int_0^t H(t-t'-\tau_D) \left[\alpha \tau_S^{-1} e^{-(t-t'-\tau_D)/\tau_S} + (1-\alpha) \tau_F^{-1} e^{-(t-t'-\tau_D)/\tau_F} \right] \\ &\quad \times H(t'-\tau_D) \left[\alpha \tau_S^{-1} e^{-(t'-\tau_D)/\tau_S} + (1-\alpha) \tau_F^{-1} e^{-(t'-\tau_D)/\tau_F} \right] dt' \\ &= \int_0^t H(t-t'-\tau_D) H(t'-\tau_D) \left[\alpha^2 \tau_S^{-2} e^{-(t-2\tau_D)/\tau_S} + (1-\alpha)^2 \tau_F^{-2} e^{-(t-2\tau_D)/\tau_F} \right. \\ &\quad \left. + \alpha(1-\alpha) \tau_S^{-1} \tau_F^{-1} \left(e^{-(t'-\tau_D)/\tau_S - (t-t'-\tau_D)/\tau_F} + e^{-(t-t'-\tau_D)/\tau_S - (t'-\tau_D)/\tau_F} \right) \right] dt' \end{aligned}$$

To evaluate this integral we introduce the substitution $u \equiv t' - \tau_D$ so that $du = dt'$. This gives

$$\begin{aligned} E_{2\text{UC}}^\alpha(t) &= \int_{-\tau_D}^{t-\tau_D} H(t-u-2\tau_D) H(u) \left[\alpha^2 \tau_S^{-2} e^{-(t-2\tau_D)/\tau_S} + (1-\alpha)^2 \tau_F^{-2} e^{-(t-2\tau_D)/\tau_F} \right. \\ &\quad \left. + \alpha(1-\alpha) \tau_S^{-1} \tau_F^{-1} \left(e^{-u/\tau_S - (t-u-2\tau_D)/\tau_F} + e^{-(t-u-2\tau_D)/\tau_S - u/\tau_F} \right) \right] du \\ &= \int_0^{t-\tau_D} H(t-u-2\tau_D) \left[\alpha^2 \tau_S^{-2} e^{-(t-2\tau_D)/\tau_S} + (1-\alpha)^2 \tau_F^{-2} e^{-(t-2\tau_D)/\tau_F} \right. \\ &\quad \left. + \alpha(1-\alpha) \tau_S^{-1} \tau_F^{-1} \left(e^{-u/\tau_S - (t-u-2\tau_D)/\tau_F} + e^{-(t-u-2\tau_D)/\tau_S - u/\tau_F} \right) \right] du \end{aligned}$$

Next we introduce a second substitution $w \equiv t - u - 2\tau_D$ so that $dw = -du$. This gives

$$\begin{aligned}
 E_{2UC}^\alpha(t) &= - \int_{t-2\tau_D}^{-\tau_D} H(w) \left[\alpha^2 \tau_S^{-2} e^{-(t-2\tau_D)/\tau_S} + (1-\alpha)^2 \tau_F^{-2} e^{-(t-2\tau_D)/\tau_F} \right. \\
 &\quad \left. + \alpha(1-\alpha) \tau_S^{-1} \tau_F^{-1} \left(e^{-(t-w-2\tau_D)/\tau_S - w/\tau_F} + e^{-w/\tau_S - (t-w-2\tau_D)/\tau_F} \right) \right] dw \\
 &= \int_{-\tau_D}^{t-2\tau_D} H(w) \left[\alpha^2 \tau_S^{-2} e^{-(t-2\tau_D)/\tau_S} + (1-\alpha)^2 \tau_F^{-2} e^{-(t-2\tau_D)/\tau_F} \right. \\
 &\quad \left. + \alpha(1-\alpha) \tau_S^{-1} \tau_F^{-1} \left(e^{-(t-w-2\tau_D)/\tau_S - w/\tau_F} + e^{-w/\tau_S - (t-w-2\tau_D)/\tau_F} \right) \right] dw \\
 &= \int_0^{t-2\tau_D} H(w) \left[\alpha^2 \tau_S^{-2} e^{-(t-2\tau_D)/\tau_S} + (1-\alpha)^2 \tau_F^{-2} e^{-(t-2\tau_D)/\tau_F} \right. \\
 &\quad \left. + \alpha(1-\alpha) \tau_S^{-1} \tau_F^{-1} \left(e^{-(t-w-2\tau_D)/\tau_S - w/\tau_F} + e^{-w/\tau_S - (t-w-2\tau_D)/\tau_F} \right) \right] dw \\
 &= H(t-2\tau_D) \underbrace{\int_0^{t-2\tau_D} \left[\alpha^2 \tau_S^{-2} e^{-(t-2\tau_D)/\tau_S} + (1-\alpha)^2 \tau_F^{-2} e^{-(t-2\tau_D)/\tau_F} \right] dw}_{I_1} \\
 &\quad + H(t-2\tau_D) \underbrace{\int_0^{t-2\tau_D} \alpha(1-\alpha) \tau_S^{-1} \tau_F^{-1} \left(e^{-(t-2\tau_D)/\tau_S + w/\tau_S - w/\tau_F} + e^{-(t-2\tau_D)/\tau_F - w/\tau_S + w/\tau_F} \right) dw}_{I_2}
 \end{aligned}$$

For the first integral we obtain

$$\begin{aligned}
 I_1 &= \left[\alpha^2 \tau_S^{-2} e^{-(t-2\tau_D)/\tau_S} + (1-\alpha)^2 \tau_F^{-2} e^{-(t-2\tau_D)/\tau_F} \right] [w]_0^{t-2\tau_D} \\
 &= (t-2\tau_D) \left[\alpha^2 \tau_S^{-2} e^{-(t-2\tau_D)/\tau_S} + (1-\alpha)^2 \tau_F^{-2} e^{-(t-2\tau_D)/\tau_F} \right]
 \end{aligned}$$

and for the second

$$\begin{aligned}
 I_2 &= \alpha(1-\alpha) \tau_S^{-1} \tau_F^{-1} \int_0^{t-2\tau_D} \left(e^{-(t-2\tau_D)/\tau_S + w/\tau_S - w/\tau_F} + e^{-(t-2\tau_D)/\tau_F - w/\tau_S + w/\tau_F} \right) dw \\
 &= \alpha(1-\alpha) \tau_S^{-1} \tau_F^{-1} \left[(\tau_S^{-1} - \tau_F^{-1})^{-1} e^{-(t-2\tau_D)/\tau_S + w/\tau_S - w/\tau_F} - (\tau_S^{-1} - \tau_F^{-1})^{-1} e^{-(t-2\tau_D)/\tau_F - w/\tau_S + w/\tau_F} \right]_0^{t-2\tau_D} \\
 &= \alpha(1-\alpha) \tau_S^{-1} \tau_F^{-1} (\tau_S^{-1} - \tau_F^{-1})^{-1} \left[e^{-(t-2\tau_D)/\tau_S + w/\tau_S - w/\tau_F} - e^{-(t-2\tau_D)/\tau_F - w/\tau_S + w/\tau_F} \right]_0^{t-2\tau_D} \\
 &= \alpha(1-\alpha) \tau_S^{-1} \tau_F^{-1} (\tau_S^{-1} - \tau_F^{-1})^{-1} \\
 &\quad \times \left[e^{-(t-2\tau_D)/\tau_S + (t-2\tau_D)/\tau_S - (t-2\tau_D)/\tau_F} - e^{-(t-2\tau_D)/\tau_F - (t-2\tau_D)/\tau_S + (t-2\tau_D)/\tau_F} - e^{-(t-2\tau_D)/\tau_S} + e^{-(t-2\tau_D)/\tau_F} \right] \\
 &= \alpha(1-\alpha) \tau_S^{-1} \tau_F^{-1} (\tau_S^{-1} - \tau_F^{-1})^{-1} \left[e^{-(t-2\tau_D)/\tau_F} - e^{-(t-2\tau_D)/\tau_S} - e^{-(t-2\tau_D)/\tau_S} + e^{-(t-2\tau_D)/\tau_F} \right] \\
 &= 2\alpha(1-\alpha) \tau_S^{-1} \tau_F^{-1} (\tau_S^{-1} - \tau_F^{-1})^{-1} \left[e^{-(t-2\tau_D)/\tau_F} - e^{-(t-2\tau_D)/\tau_S} \right]
 \end{aligned}$$

Thus we have

$$E_{2UC}^{\alpha}(t) = H(t - 2\tau_D) \left\{ (t - 2\tau_D) \left[\alpha^2 \tau_S^{-2} e^{-(t-2\tau_D)/\tau_S} + (1-\alpha)^2 \tau_F^{-2} e^{-(t-2\tau_D)/\tau_F} \right] \right. \\ \left. + 2\alpha(1-\alpha) \tau_S^{-1} \tau_F^{-1} (\tau_S^{-1} - \tau_F^{-1})^{-1} \left[e^{-(t-2\tau_D)/\tau_F} - e^{-(t-2\tau_D)/\tau_S} \right] \right\}$$

The integral of $E_{2UC}^{\alpha}(t)$ is given by

$$\int_0^{\infty} E_{2UC}^{\alpha}(t) dt = \int_0^{\infty} H(t - 2\tau_D) \left\{ (t - 2\tau_D) \left[\alpha^2 \tau_S^{-2} e^{-(t-2\tau_D)/\tau_S} + (1-\alpha)^2 \tau_F^{-2} e^{-(t-2\tau_D)/\tau_F} \right] \right. \\ \left. + 2\alpha(1-\alpha) \tau_S^{-1} \tau_F^{-1} (\tau_S^{-1} - \tau_F^{-1})^{-1} \left[e^{-(t-2\tau_D)/\tau_F} - e^{-(t-2\tau_D)/\tau_S} \right] \right\} dt$$

We introduce the substitution $z \equiv t - 2\tau_D$ and obtain

$$\int_0^{\infty} E_{2UC}^{\alpha}(t) dt = \int_{-2\tau_D}^{\infty} H(z) \left\{ z \left[\alpha^2 \tau_S^{-2} e^{-z/\tau_S} + (1-\alpha)^2 \tau_F^{-2} e^{-z/\tau_F} \right] \right. \\ \left. + 2\alpha(1-\alpha) \tau_S^{-1} \tau_F^{-1} (\tau_S^{-1} - \tau_F^{-1})^{-1} \left[e^{-z/\tau_F} - e^{-z/\tau_S} \right] \right\} dz \\ = \int_0^{\infty} \left\{ \left[\alpha^2 \tau_S^{-2} z e^{-z/\tau_S} + (1-\alpha)^2 \tau_F^{-2} z e^{-z/\tau_F} \right] + 2\alpha(1-\alpha) \tau_S^{-1} \tau_F^{-1} (\tau_S^{-1} - \tau_F^{-1})^{-1} \left[e^{-z/\tau_F} - e^{-z/\tau_S} \right] \right\} dz \\ = \left[\alpha^2 \tau_S^{-2} \tau_S^2 + (1-\alpha)^2 \tau_F^{-2} \tau_F^2 \right] + 2\alpha(1-\alpha) \tau_S^{-1} \tau_F^{-1} (\tau_S^{-1} - \tau_F^{-1})^{-1} (\tau_F - \tau_S) \\ = \left[\alpha^2 + (1-\alpha)^2 \right] + 2\alpha(1-\alpha) \tau_S^{-1} \tau_F^{-1} (\tau_S^{-1} - \tau_F^{-1})^{-1} (\tau_F - \tau_S) \\ = (\alpha^2 + 1 - 2\alpha + \alpha^2) + 2\alpha(1-\alpha) (\tau_S^{-1} - \tau_F^{-1})^{-1} (\tau_S^{-1} \tau_F^{-1} \tau_F - \tau_S^{-1} \tau_F^{-1} \tau_S) \\ = 1 - 2\alpha + 2\alpha^2 + 2\alpha(1-\alpha) (\tau_S^{-1} - \tau_F^{-1})^{-1} (\tau_S^{-1} - \tau_F^{-1}) \\ = 1 - 2\alpha + 2\alpha^2 + 2\alpha(1-\alpha) = 1$$

B.2.1.2. Mean residence time

The mean residence time of the PDD model for two unit cells is

$$\bar{t}_{2UC}^{\alpha} = \int_0^{\infty} t E_{2UC}^{\alpha}(t) dt = \int_0^{\infty} t H(t - 2\tau_D) \left\{ (t - 2\tau_D) \left[\alpha^2 \tau_S^{-2} e^{-(t-2\tau_D)/\tau_S} + (1-\alpha)^2 \tau_F^{-2} e^{-(t-2\tau_D)/\tau_F} \right] \right. \\ \left. + 2\alpha(1-\alpha) \tau_S^{-1} \tau_F^{-1} (\tau_S^{-1} - \tau_F^{-1})^{-1} \left[e^{-(t-2\tau_D)/\tau_F} - e^{-(t-2\tau_D)/\tau_S} \right] \right\} dt$$

We introduce the substitution $z \equiv t - 2\tau_D$ and obtain

$$\begin{aligned}
 \bar{t}_{2UC}^\alpha &= \int_{-2\tau_D}^{\infty} (z + 2\tau_D)H(z) \left\{ z \left[\alpha^2 \tau_S^{-2} e^{-z/\tau_S} + (1-\alpha)^2 \tau_F^{-2} e^{-z/\tau_F} \right] \right. \\
 &\quad \left. + 2\alpha(1-\alpha)\tau_S^{-1}\tau_F^{-1}(\tau_S^{-1} - \tau_F^{-1})^{-1} \left[e^{-z/\tau_F} - e^{-z/\tau_S} \right] \right\} dz \\
 &= \int_0^{\infty} \left\{ \left[\alpha^2 \tau_S^{-2} (z^2 + 2\tau_D z) e^{-z/\tau_S} + (1-\alpha)^2 \tau_F^{-2} (z^2 + 2\tau_D z) e^{-z/\tau_F} \right] \right. \\
 &\quad \left. + 2\alpha(1-\alpha)\tau_S^{-1}\tau_F^{-1}(\tau_S^{-1} - \tau_F^{-1})^{-1} \left[(z + 2\tau_D) e^{-z/\tau_F} - (z + 2\tau_D) e^{-z/\tau_S} \right] \right\} dz \\
 &= \alpha^2 \tau_S^{-2} (2\tau_S^3 + 2\tau_D \tau_S^2) + (1-\alpha)^2 \tau_F^{-2} (2\tau_F^3 + 2\tau_D \tau_F^2) \\
 &\quad + 2\alpha(1-\alpha)\tau_S^{-1}\tau_F^{-1}(\tau_S^{-1} - \tau_F^{-1})^{-1} (\tau_F^2 + 2\tau_D \tau_F - \tau_S^2 - 2\tau_D \tau_S) \\
 &= 2\alpha^2 (\tau_S + \tau_D) + 2(1-\alpha)^2 (\tau_F + \tau_D) \\
 &\quad + 2\alpha(1-\alpha)(\tau_S^{-1} - \tau_F^{-1})^{-1} (\tau_S^{-1}\tau_F + 2\tau_D \tau_S^{-1} - \tau_S \tau_F^{-1} - 2\tau_D \tau_F^{-1}) \\
 &= 2\alpha^2 \tau_S + 2\alpha^2 \tau_D + 2(1-\alpha)^2 \tau_F + 2(1-\alpha)^2 \tau_D \\
 &\quad + 2\alpha(1-\alpha)(\tau_S^{-1} - \tau_F^{-1})^{-1} \left[\tau_S^{-1}\tau_F - \tau_S \tau_F^{-1} + 2\tau_D (\tau_S^{-1} - \tau_F^{-1}) \right] \\
 &= 2\alpha^2 \tau_S + 2\alpha^2 \tau_D + 2(1-\alpha)^2 \tau_F + 2(1-\alpha)^2 \tau_D \\
 &\quad + 2\alpha(1-\alpha)(\tau_S^{-1} - \tau_F^{-1})^{-1} (\tau_S^{-1}\tau_F - \tau_S \tau_F^{-1}) + 4\alpha(1-\alpha)\tau_D \\
 &= 2\tau_D \left[\alpha^2 + (1-\alpha)^2 + 2\alpha(1-\alpha) \right] + 2\alpha^2 \tau_S + 2(1-\alpha)^2 \tau_F + 2\alpha(1-\alpha) \frac{\tau_S^{-1}\tau_F - \tau_S \tau_F^{-1}}{\tau_S^{-1} - \tau_F^{-1}} \\
 &= 2\tau_D \left[\alpha^2 + 1 - 2\alpha + \alpha^2 + 2\alpha - 2\alpha^2 \right] + 2\alpha^2 \tau_S + 2(1-\alpha)^2 \tau_F + 2\alpha(1-\alpha) \frac{\tau_F^2 - \tau_S^2}{\tau_F - \tau_S} \\
 &= 2\tau_D + 2\alpha^2 \tau_S + 2(1-\alpha)^2 \tau_F + 2\alpha(1-\alpha) \frac{(\tau_F - \tau_S)(\tau_F + \tau_S)}{\tau_F - \tau_S} \\
 &= 2\tau_D + 2\alpha^2 \tau_S + 2(1-2\alpha + \alpha^2)\tau_F + 2\alpha(1-\alpha)(\tau_F + \tau_S) \\
 &= 2\tau_D + 2\alpha^2 \tau_S + 2\tau_F - 4\alpha\tau_F + 2\alpha^2 \tau_F + 2\alpha\tau_F - 2\alpha^2 \tau_F + 2\alpha\tau_S - 2\alpha^2 \tau_S \\
 &= 2\tau_D + 2\alpha\tau_S + 2(1-\alpha)\tau_F = 2 \left\{ \tau_D + \left[\alpha\tau_S + (1-\alpha)\tau_F \right] \right\} = 2\tau_{UC}^\alpha
 \end{aligned}$$

Appendix C. Evaluations by Laplace transformation

The unit cell RTD of the PD model is given by

$$E_{UC}(t) = \frac{H(t - \tau_D)}{\tau_S} \exp\left(-\frac{t - \tau_D}{\tau_S}\right) \quad (77)$$

and that of the PDD model by

$$E_{UC}^\alpha(t) = H(t - \tau_D) \frac{\alpha}{\tau_S} \exp\left(-\frac{t - \tau_D}{\tau_S}\right) + H(t - \tau_D) \frac{1 - \alpha}{\tau_F} \exp\left(-\frac{t - \tau_D}{\tau_F}\right) \quad (78)$$

The Laplace transform of Eq. (77) is

$$\begin{aligned} E_{UC}(s) &= \int_0^\infty \exp(-st) E_{UC}(t) dt = \int_0^\infty \exp(-st) \frac{H(t - \tau_D)}{\tau_S} \exp\left(-\frac{t - \tau_D}{\tau_S}\right) dt \\ &= \int_0^\infty \frac{H(t - \tau_D)}{\tau_S} \exp\left(-\frac{t(1 + s\tau_S) - \tau_D}{\tau_S}\right) dt = \int_{\tau_D}^\infty \frac{1}{\tau_S} \exp\left(-\frac{t(1 + s\tau_S) - \tau_D}{\tau_S}\right) dt \\ &= \frac{1}{\tau_S} \exp\left(\frac{\tau_D}{\tau_S}\right) \int_{\tau_D}^\infty \exp\left(-\frac{t(1 + s\tau_S)}{\tau_S}\right) dt \\ &= \frac{1}{\tau_S} \exp\left(\frac{\tau_D}{\tau_S}\right) \left[\exp\left(-\frac{t(1 + s\tau_S)}{\tau_S}\right) \right]_{t=\tau_D}^{t=\infty} = \frac{1}{\tau_S} \exp\left(\frac{\tau_D}{\tau_S}\right) \left[-\frac{\tau_S}{1 + s\tau_S} \exp\left(-\frac{t(1 + s\tau_S)}{\tau_S}\right) \right]_{t=\tau_D}^{t=\infty} \\ &= \frac{1}{\tau_S} \exp\left(\frac{\tau_D}{\tau_S}\right) \left[\frac{\tau_S}{1 + s\tau_S} \exp\left(-\frac{\tau_D(1 + s\tau_S)}{\tau_S}\right) \right] = \frac{1}{1 + s\tau_S} \exp\left(-\frac{\tau_D(1 + s\tau_S)}{\tau_S} + \frac{\tau_D}{\tau_S}\right) \\ &= \frac{1}{1 + s\tau_S} \exp(-\tau_D s) = \frac{1}{\tau_S} \frac{1}{s + \tau_S^{-1}} \exp(-\tau_D s) \end{aligned}$$

Then, the Laplace transform of Eq. (78) is

$$E_{UC}^\alpha(s) = \int_0^\infty \exp(-st) E_{UC}^\alpha(t) dt = \frac{\alpha}{\tau_S} \frac{1}{s + \tau_S^{-1}} \exp(-\tau_D s) + \frac{1 - \alpha}{\tau_F} \frac{1}{s + \tau_F^{-1}} \exp(-\tau_D s) \quad (79)$$

The RTD for 2 unit cells in series is given by the convolution

$$E_{2UC}^\alpha(t) = E_{UC}^\alpha(t) * E_{UC}^\alpha(t)$$

In the Laplace domain this gives

$$E_{2UC}^{\alpha}(s) = E_{UC}^{\alpha}(s) \cdot E_{UC}^{\alpha}(s) = \left[E_{UC}^{\alpha}(s) \right]^2 = \left[\frac{\alpha}{\tau_S} \frac{1}{s + \tau_S^{-1}} \exp(-\tau_D s) + \frac{1-\alpha}{\tau_F} \frac{1}{s + \tau_F^{-1}} \exp(-\tau_D s) \right]^2$$

$$= \left(\frac{\alpha}{\tau_S} \frac{1}{s + \tau_S^{-1}} + \frac{1-\alpha}{\tau_F} \frac{1}{s + \tau_F^{-1}} \right)^2 \exp(-2\tau_D s)$$

The RTD for n unit cells in series is given by the convolution

$$E_{nUC}^{\alpha}(t) = E_{(n-1)UC}^{\alpha}(t) * E_{UC}^{\alpha}(t)$$

In the Laplace domain this gives

$$E_{nUC}^{\alpha}(s) = \left[E_{UC}^{\alpha}(s) \right]^n = \left(\frac{\alpha}{\tau_S} \frac{1}{s + \tau_S^{-1}} + \frac{1-\alpha}{\tau_F} \frac{1}{s + \tau_F^{-1}} \right)^n \exp(-n\tau_D s) \quad (80)$$

For the PD model, it is $\alpha = 1$ and Eq. (80) simplifies to

$$E_{nUC}(s) = (1 + s\tau_S)^{-n} \exp(-n\tau_D s) = \frac{1}{\tau_S^n} \frac{1}{(s + \tau_S^{-1})^n} \exp(-n\tau_D s) \quad (81)$$

The backward transformation in the time domain of Eq. (81) is

$$E_{nUC}(t) = \frac{(t - n\tau_D)^{n-1}}{(n-1)! \tau_S^n} \exp\left(-\frac{t - n\tau_D}{\tau_S}\right) H(t - n\tau_D)$$

see ID 2 (delayed n th power with frequency shift) in the Table of selected Laplace transforms in the English Wikipedia web site on Laplace transformation (accessed June, 2009).

To determine the inverse of Eq. (80) we take advantage of the binomial theorem which reads

$$(a + b)^n = \sum_{k=0}^n \binom{n}{k} a^{n-k} b^k$$

In the present case n and k are positive integers. Then, for $n \geq k$ the binomial coefficients are given by

$$\binom{n}{k} = \frac{n!}{k!(n-k)!}$$

Introducing these results in Eq. (80) gives

$$\begin{aligned}
 E_{nUC}^\alpha(s) &= \left(\frac{\alpha}{\tau_S} \frac{1}{s + \tau_S^{-1}} + \frac{1-\alpha}{\tau_F} \frac{1}{s + \tau_F^{-1}} \right)^n \exp(-n\tau_D s) \\
 &= \sum_{k=0}^n \binom{n}{k} \left(\frac{\alpha}{\tau_S} \frac{1}{s + \tau_S^{-1}} \right)^{n-k} \left(\frac{1-\alpha}{\tau_F} \frac{1}{s + \tau_F^{-1}} \right)^k \exp(-n\tau_D s) \\
 &= \sum_{k=0}^n \frac{n!}{k!(n-k)!} \left(\frac{\alpha}{\tau_S} \right)^{n-k} \left(\frac{1-\alpha}{\tau_F} \right)^k \frac{1}{(s + \tau_S^{-1})^{n-k}} \frac{1}{(s + \tau_F^{-1})^k} \exp(-n\tau_D s)
 \end{aligned} \tag{82}$$

For $n = 1$ we have

$$\begin{aligned}
 E_{1UC}^\alpha(s) &= \sum_{k=0}^1 \frac{1}{k!(1-k)!} \left(\frac{\alpha}{\tau_S} \right)^{1-k} \left(\frac{1-\alpha}{\tau_F} \right)^k \frac{1}{(s + \tau_S^{-1})^{1-k}} \frac{1}{(s + \tau_F^{-1})^k} \exp(-\tau_D s) \\
 &= \frac{\alpha}{\tau_S} \frac{1}{s + \tau_S^{-1}} \exp(-\tau_D s) + \frac{1-\alpha}{\tau_F} \frac{1}{s + \tau_F^{-1}} \exp(-\tau_D s)
 \end{aligned}$$

which is equal to Eq. (79). For $n = 2$ Eq. (82) gives

$$\begin{aligned}
 E_{2UC}^\alpha(s) &= \sum_{k=0}^2 \frac{2}{k!(2-k)!} \left(\frac{\alpha}{\tau_S} \right)^{2-k} \left(\frac{1-\alpha}{\tau_F} \right)^k \frac{1}{(s + \tau_S^{-1})^{2-k}} \frac{1}{(s + \tau_F^{-1})^k} \exp(-2\tau_D s) \\
 &= \left(\frac{\alpha}{\tau_S} \right)^2 \frac{1}{(s + \tau_S^{-1})^2} \exp(-2\tau_D s) + 2 \frac{\alpha}{\tau_S} \frac{1-\alpha}{\tau_F} \frac{1}{s + \tau_S^{-1}} \frac{1}{s + \tau_F^{-1}} \exp(-2\tau_D s) \\
 &\quad + \left(\frac{1-\alpha}{\tau_F} \right)^2 \frac{1}{(s + \tau_F^{-1})^2} \exp(-2\tau_D s)
 \end{aligned}$$

For $n = 3$ Eq. (82) gives

$$\begin{aligned}
 E_{3UC}^\alpha(s) &= \sum_{k=0}^3 \frac{6}{k!(3-k)!} \left(\frac{\alpha}{\tau_S} \right)^{3-k} \left(\frac{1-\alpha}{\tau_F} \right)^k \frac{1}{(s + \tau_S^{-1})^{3-k}} \frac{1}{(s + \tau_F^{-1})^k} \exp(-3\tau_D s) \\
 &= \left(\frac{\alpha}{\tau_S} \right)^3 \frac{1}{(s + \tau_S^{-1})^3} \exp(-3\tau_D s) + 3 \left(\frac{\alpha}{\tau_S} \right)^2 \frac{1-\alpha}{\tau_F} \frac{1}{(s + \tau_S^{-1})^2} \frac{1}{s + \tau_F^{-1}} \exp(-3\tau_D s) \\
 &\quad + 3 \frac{\alpha}{\tau_S} \left(\frac{1-\alpha}{\tau_F} \right)^2 \frac{1}{s + \tau_S^{-1}} \frac{1}{(s + \tau_F^{-1})^2} \exp(-3\tau_D s) \\
 &\quad + \left(\frac{1-\alpha}{\tau_F} \right)^3 \frac{1}{(s + \tau_F^{-1})^3} \exp(-3\tau_D s)
 \end{aligned}$$

For $n = 4$ Eq. (82) gives

$$\begin{aligned}
 E_{4UC}^\alpha(s) &= \sum_{k=0}^n \frac{24}{k!(4-k)!} \left(\frac{\alpha}{\tau_S}\right)^{4-k} \left(\frac{1-\alpha}{\tau_F}\right)^k \frac{1}{(s+\tau_S^{-1})^{4-k}} \frac{1}{(s+\tau_F^{-1})^k} \exp(-4\tau_D s) \\
 &= \left(\frac{\alpha}{\tau_S}\right)^4 \frac{1}{(s+\tau_S^{-1})^4} \exp(-4\tau_D s) + 4 \left(\frac{\alpha}{\tau_S}\right)^3 \frac{1-\alpha}{\tau_F} \frac{1}{(s+\tau_S^{-1})^3} \frac{1}{s+\tau_F^{-1}} \exp(-4\tau_D s) \\
 &\quad + 6 \left(\frac{\alpha}{\tau_S}\right)^2 \left(\frac{1-\alpha}{\tau_F}\right)^2 \frac{1}{(s+\tau_S^{-1})^2} \frac{1}{(s+\tau_F^{-1})^2} \exp(-4\tau_D s) \\
 &\quad + 4 \frac{\alpha}{\tau_S} \left(\frac{1-\alpha}{\tau_F}\right)^3 \frac{1}{s+\tau_S^{-1}} \frac{1}{(s+\tau_F^{-1})^3} \exp(-4\tau_D s) + \left(\frac{1-\alpha}{\tau_F}\right)^4 \frac{1}{(s+\tau_F^{-1})^4} \exp(-4\tau_D s)
 \end{aligned}$$

To obtain the RTD for n unit cells in series in the time domain we have to perform the inverse Laplace transformation of Eq. (82). To simplify Eq. (82) we introduce the following abbreviations

$$\beta \equiv \frac{\alpha}{\tau_S}$$

$$\gamma \equiv \frac{1-\alpha}{\tau_F}$$

$$B_{n,k} \equiv \frac{n!}{k!(n-k)!}$$

$$F_{n,k}(s) \equiv \frac{1}{(s+\tau_S^{-1})^{n-k}} \frac{1}{(s+\tau_F^{-1})^k} = (s+\tau_S^{-1})^{-(n-k)} (s+\tau_F^{-1})^{-k}$$

The binomial coefficients $B_{n,k}$ and the functions $F_{n,k}(s)$ are given for $n=1-4$ and $k=0-4$ in Tab. 5 and Tab. 6, respectively.

Tab. 5: Binomial coefficients $B_{n,k}$ for $n=1-4$ and $k=0-4$.

	$k=0$	$k=1$	$k=2$	$k=3$	$k=4$
$n=1$	1	1	-	-	-
$n=2$	1	2	1	-	-
$n=3$	1	3	3	1	-
$n=4$	1	4	6	4	1

Tab. 6: Functions $F_{n,k}(s)$ for $n = 1 - 4$ and $k = 0 - 4$.

	$k = 0$	$k = 1$	$k = 2$	$k = 3$	$k = 4$
$n=1$	$(s + \tau_S^{-1})^{-1}$	$(s + \tau_F^{-1})^{-1}$	-	-	-
$n=2$	$(s + \tau_S^{-1})^{-2}$	$(s + \tau_S^{-1})^{-1}(s + \tau_F^{-1})^{-1}$	$(s + \tau_F^{-1})^{-2}$	-	-
$n=3$	$(s + \tau_S^{-1})^{-3}$	$(s + \tau_S^{-1})^{-2}(s + \tau_F^{-1})^{-1}$	$(s + \tau_S^{-1})^{-1}(s + \tau_F^{-1})^{-2}$	$(s + \tau_F^{-1})^{-3}$	-
$n=4$	$(s + \tau_S^{-1})^{-4}$	$(s + \tau_S^{-1})^{-3}(s + \tau_F^{-1})^{-1}$	$(s + \tau_S^{-1})^{-2}(s + \tau_F^{-1})^{-2}$	$(s + \tau_S^{-1})^{-1}(s + \tau_F^{-1})^{-3}$	$(s + \tau_F^{-1})^{-4}$

Then Eq. (82) can be written as

$$E_{nUC}^\alpha(s) = \sum_{k=0}^n B_{n,k} \beta^{n-k} \gamma^k F_{n,k}(s) \exp(-n\tau_D s) \quad (83)$$

The inverse of Eq. (83) is given by

$$E_{nUC}^\alpha(t) = \sum_{k=0}^n \mathcal{L}^{-1} \{ B_{n,k} \beta^{n-k} \gamma^k F_{n,k}(s) \exp(-n\tau_D s) \} = \sum_{k=0}^n B_{n,k} \beta^{n-k} \gamma^k \mathcal{L}^{-1} \{ F_{n,k}(s) \exp(-n\tau_D s) \} \quad (84)$$

Taking advantage of the following time shift property of the Laplace transform

$$\mathcal{L}^{-1} \{ F(s) \exp(-as) \} = f(t-a)H(t-a)$$

Eq. (84) simplifies to

$$E_{nUC}^\alpha(t) = H(t - n\tau_D) \sum_{k=0}^n B_{n,k} \beta^{n-k} \gamma^k f_{n,k}(t - n\tau_D) \quad (85)$$

where

$$f_{n,k}(t) \equiv \mathcal{L}^{-1} \{ F_{n,k}(s) \}$$

To determine the inverse Laplace transforms we take advantage of the relations listed in Tab. 7.

Tab. 7: Inverse Laplace transforms. In the reference column the numbers refer to those in McCollum and Brown (1965), CB, and Roberts and Kaufman (1966), RK, respectively.

$F(s)$	$f(t)$	Reference
$(s+a)^{-n}$	$\frac{t^{n-1} \exp(-at)}{(n-1)!}$	23 in CB
$(s+a)^{-1}(s+b)^{-1}$	$\frac{1}{b-a} [\exp(-at) - \exp(-bt)]$	14 in CB
$(s+a)^{-1}(s+b)^{-2}$	$\frac{1}{(a-b)^2} \{ \exp(-at) + [(a-b)t - 1] \exp(-bt) \}$	27 in CB
$(s+a)^{-2}(s+b)^{-2}$	$\frac{t \exp(-at)}{(b-a)^2} - \frac{2 \exp(-at)}{(b-a)^3} + \frac{t \exp(-bt)}{(a-b)^2} - \frac{2 \exp(-bt)}{(a-b)^3}$	33 in CB
$(s+a)^{-1}(s+b)^{-3}$	$\frac{1}{(a-b)^3} \left\{ \left[1 - (a-b)t + \frac{1}{2}(a-b)^2 t^2 \right] \exp(-bt) - \exp(-at) \right\}$	89 of section 2 in RK

With the above results, the inverse Laplace transforms of $F_{n,k}(s)$ for $n=1-4$ and $k=0-4$ are as follows

$$f_{1,0}(t) = \exp(-\tau_S^{-1}t)$$

$$f_{1,1}(t) = \exp(-\tau_F^{-1}t)$$

$$f_{2,0}(t) = t \exp(-\tau_S^{-1}t)$$

$$f_{2,1}(t) = \frac{1}{\tau_F^{-1} - \tau_S^{-1}} [\exp(-\tau_S^{-1}t) - \exp(-\tau_F^{-1}t)]$$

$$f_{2,2}(t) = t \exp(-\tau_F^{-1}t)$$

$$f_{3,0}(t) = \frac{t^2}{2} \exp(-\tau_S^{-1}t)$$

$$f_{3,1}(t) = \frac{\exp(-\tau_F^{-1}t)}{(\tau_F^{-1} - \tau_S^{-1})^2} + \frac{[(\tau_F^{-1} - \tau_S^{-1})t - 1] \exp(-\tau_S^{-1}t)}{(\tau_F^{-1} - \tau_S^{-1})^2}$$

$$f_{3,2}(t) = \frac{\exp(-\tau_S^{-1}t)}{(\tau_S^{-1} - \tau_F^{-1})^2} + \frac{[(\tau_S^{-1} - \tau_F^{-1})t - 1] \exp(-\tau_F^{-1}t)}{(\tau_S^{-1} - \tau_F^{-1})^2}$$

$$f_{3,3}(t) = \frac{t^2}{2} \exp(-\tau_F^{-1}t)$$

$$f_{4,0}(t) = \frac{t^3}{6} \exp(-\tau_S^{-1}t)$$

$$f_{4,1}(t) = \frac{1}{(\tau_F^{-1} - \tau_S^{-1})^3} \left\{ \left[1 - (\tau_F^{-1} - \tau_S^{-1})t + \frac{1}{2}(\tau_F^{-1} - \tau_S^{-1})^2 t^2 \right] \times \exp(-\tau_S^{-1}t) - \exp(-\tau_F^{-1}t) \right\}$$

$$f_{4,2}(t) = \frac{t \exp(-\tau_S^{-1}t)}{(\tau_F^{-1} - \tau_S^{-1})^2} - \frac{2 \exp(-\tau_S^{-1}t)}{(\tau_F^{-1} - \tau_S^{-1})^3} + \frac{t \exp(-\tau_F^{-1}t)}{(\tau_S^{-1} - \tau_F^{-1})^2} - \frac{2 \exp(-\tau_F^{-1}t)}{(\tau_S^{-1} - \tau_F^{-1})^3}$$

$$f_{4,3}(t) = \frac{1}{(\tau_S^{-1} - \tau_F^{-1})^3} \left\{ \left[1 - (\tau_S^{-1} - \tau_F^{-1})t + \frac{1}{2}(\tau_S^{-1} - \tau_F^{-1})^2 t^2 \right] \times \exp(-\tau_F^{-1}t) - \exp(-\tau_S^{-1}t) \right\}$$

$$f_{4,4}(t) = \frac{t^3}{6} \exp(-\tau_F^{-1}t)$$

With these results, we obtain the RTD of the PDD model for two and three unit cells from Eq. (85) as follows:

$$\begin{aligned} E_{2UC}^\alpha(t) &= H(t - 2\tau_D) \sum_{k=0}^2 B_{2,k} \beta^{2-k} \gamma^k f_{2,k}(t - 2\tau_D) \\ &= H(t - 2\tau_D) \left\{ B_{2,0} \beta^2 f_{2,0}(t - 2\tau_D) + B_{2,1} \beta \gamma f_{2,1}(t - 2\tau_D) + B_{2,2} \gamma^2 f_{2,2}(t - 2\tau_D) \right\} \\ &= H(t - 2\tau_D) \left\{ (t - 2\tau_D) \left[\left(\frac{\alpha}{\tau_S} \right)^2 \exp\left(-\frac{t - 2\tau_D}{\tau_S}\right) + \left(\frac{1 - \alpha}{\tau_F} \right)^2 \exp\left(-\frac{t - 2\tau_D}{\tau_F}\right) \right] \right. \\ &\quad \left. + \frac{2}{\tau_F^{-1} - \tau_S^{-1}} \frac{\alpha}{\tau_S} \frac{1 - \alpha}{\tau_F} \left[\exp\left(-\frac{t - 2\tau_D}{\tau_S}\right) - \exp\left(-\frac{t - 2\tau_D}{\tau_F}\right) \right] \right\} \end{aligned}$$

and

$$\begin{aligned}
E_{3\text{UC}}^\alpha(t) &= H(t-3\tau_D) \sum_{k=0}^3 B_{3,k} \beta^{3-k} \gamma^k f_{3,k}(t-3\tau_D) \\
&= H(t-3\tau_D) \left\{ B_{3,0} \beta^3 f_{3,0}(t-2\tau_D) + B_{3,1} \beta^2 \gamma f_{3,1}(t-3\tau_D) \right. \\
&\quad \left. + B_{3,2} \beta \gamma^2 f_{3,2}(t-3\tau_D) + B_{3,3} \gamma^3 f_{3,3}(t-2\tau_D) \right\} \\
&= H(t-3\tau_D) \left\{ \frac{(t-3\tau_D)^2}{2} \left(\frac{\alpha}{\tau_S} \right)^3 \exp\left(-\frac{t-3\tau_D}{\tau_S} \right) \right. \\
&\quad + \frac{3}{(\tau_F^{-1} - \tau_S^{-1})^2} \left(\frac{\alpha}{\tau_S} \right)^2 \frac{1-\alpha}{\tau_F} \left[\exp\left(-\frac{t-3\tau_D}{\tau_F} \right) + [(\tau_F^{-1} - \tau_S^{-1})(t-3\tau_D) - 1] \exp\left(-\frac{t-3\tau_D}{\tau_S} \right) \right] \\
&\quad + \frac{3}{(\tau_F^{-1} - \tau_S^{-1})^2} \frac{\alpha}{\tau_S} \left(\frac{1-\alpha}{\tau_F} \right)^2 \left[\exp\left(-\frac{t-3\tau_D}{\tau_S} \right) + [(\tau_S^{-1} - \tau_F^{-1})(t-3\tau_D) - 1] \exp\left(-\frac{t-3\tau_D}{\tau_F} \right) \right] \\
&\quad \left. + \frac{(t-3\tau_D)^2}{2} \left(\frac{1-\alpha}{\tau_F} \right)^3 \exp\left(-\frac{t-3\tau_D}{\tau_F} \right) \right\}
\end{aligned}$$

The expression for $E_{4\text{UC}}^\alpha(t)$ can also be obtained from the above results. However, due the complexity of the expression it is not explicitly given here.